Vulnerability of Short Range Wireless Technologies to Impulsive Noise in Electricity Substations

Shahzad Ahmed Bhatti

A thesis submitted in fulfilment of the requirement for the award of Doctor of Philosophy in Electronic and Electrical Engineering

Department of Electronic and Electrical Engineering,

University of Strathclyde, Glasgow, United Kingdom

2019

DEDICATION

I dedicate this work to my dear mother.

.

DECLARATION

I declare that this thesis embodies my own research work and that it was composed by me. I have referenced the work of others where appropriate throughout the thesis.

Shahzad Ahmed Bhatti

Date: 15/03/2019

ABSTRACT

The technical reliability and economic advantages of using sensors, communications and computing to more precisely monitor and control the state of electrical power systems are many. Implementing some of the communications functions wirelessly is cheaper, more flexible and more convenient than an implementation with their wired counterparts. Whilst wireless networks offer these obvious benefits over wired networks, concerns remain which need to be addressed. One such concern is the performance of wireless networks in the electromagnetically aggressive substation environment; an environment that is particularly rich in impulsive noise due to the presence of partial discharge, power electronics switching and other transient processes.

This thesis investigates the degree to which the dominantly impulsive noise environment of an electricity substation will degrade the performance of wireless technologies, primarily designed to operate in a Gaussian noise environment.

The electricity-substation noise environment is modelled as both a Middleton class-A process and a symmetric α-stable process. Values of model parameters are estimated from a database of impulsive noise measurements made in a 400/275/132 kV air-insulated substation. Computer simulations are then employed to evaluate the physical layer bit-error-ratio performance of the candidate wireless networking technologies including WLAN, Bluetooth and Zigbee.

All candidate technologies are shown to suffer a departure in performance degradation from that expected in a Gaussian noise environment.in the high SNR region whereas AWGN dominates in the low SNR region. In the high SNR region, there appears to be a noise floor which reduces the effect of an increase in SNR on the corresponding BER.

ACKNOWLEDGEMENTS

First, I would like to thank my supervisor, Prof Ian Andrew Glover, for his guidance and kind support at all stages of this work.

I am deeply indebted to my parents, siblings, friends and my wife Asmi for the wonderful support; I have received throughout the years.

.

TABLE OF CONTENTS

LIST OF FIGURES

LIST OF TABLES

GLOSSARY OF ACRONYMS

ACDF	Amplitude Cumulative Distribution Function
AIR	Air Insulated Substation
APD	Amplitude Probability Density
AWGN	Additive White Gaussian Noise
BB-IN	Broadband Impulsive Noise
BER	Bit Error Rate
BIC	Bayesian Information Criterion
BPSK	Binary Phase Shift Keying
CCK	Complementary Code Keying
CDF	Cumulative Distribution Function
CI	Communication Infrastructure
CLT	Central Limit Theorem
CPM	Continuous Phase Modulations
CRC	Cyclic Redundancy Check
DBPSK	Differential Binary Phase Shift Keying
DCS	Distributed Control System
DPSK	Differential Phase Shift Keying
DQPSK	Differential Quadrature Phase Shift Keying
DSO	Digital Storage Oscilloscope
DSSS	Direct Sequence Spread Spectrum
EM	Expectation Maximization
EOS	Extreme-Order Statistics
EPRI	Electric Power Research Institute
ERP	Extended Rate PHY
ETS	Electricity Transmission Substation
ETSI	European Telecommunications Standards Institute

FDMA	Frequency Division Multiple Access
FEC	Forward Error Correction
FFT	Fast Fourier Transform
FH	Frequency-Hopping
FHSS	Frequency-Hopping Spread Spectrum
FLOM	Fractional Lower Order Moments
FSK	Frequency Shift Keying
FT	Fourier Transform
G-CLT	Generalised Central Limit Theorem
G-SNR	Generalised Signal to Noise Ratio
GMSK	Gaussian Minimum Shift Keying
HI	Highly Impulsive
HMI	Human Machine Interface
HMM	Hidden Markov Model
HR DSSS	High Rate Direct Sequence Spread Spectrum
HV	High Voltage
IEC	International Electrotechnical Commission
IEEE	Institute of Electrical and Electronics Engineers
IF	Intermediate Frequency
IFFT	Inverse Fast Fourier Transform
IN	Impulsive Noise
ISI	Intersymbol Interference
ISM	Industrial, Scientific and Medical
LAN	Local Area Network
MAC	Medium Access Control
MI	Moderately Impulsive
MIMO	Multi-input Multi-output
MPDU	MAC Protocol Data Unit
MSDU	Medium Access Control Service Data Unit
MSK	Minimum Shift Keying
NAD	Noise Amplitude Distribution
NB-IN	Narrowband Impulsive Noise
O-QPSK	Orthogonal Quadrature Phase Shift Keying

OFDM	Orthogonal Frequency Division Multiplexing
OSI	Open System Interconnection
PAN	Personal Area Network
PBCC	Packet Binary Convolutional Code
PD	Partial Discharges
PDF	Probability Density Function
PHY	Physical Layer
PLCP	Physical Layer Convergence Protocol
PLCs	Programmable Logic Controllers
PMD	Physical Layer Dependent
PPDU	PHY Protocol Data Unit
PSDU	PHY Service Data Unit
QAM	Quadrature Amplitude Modulation
QPSK	Quadrature Phase Shift Keying
RF	Radio Frequency
RPP	Rayleigh Probability Presentation
RTU	Remote Terminal Unit
SCADA	Supervisory Control and Data Acquisition
SER	Symbol Error Rate
SFD	Start of Frame Delimiter
SIG	Special Interest Group
SNR	Signal to Noise Ratio
SαS	Symmetric α-Stable
TB	Time-Bandwidth
WGN	White Gaussian Noise
WLAN	Wireless Local Area Network
WPAN	Wireless Personal Area Network
WPT	Wavelet Packet Transformation
WSN	Wireless Sensor Network

LIST OF SYMBOLS

L_{ant}	Antenna Length
β_{ant}	Flare angle between antenna plates
α_{ant}	Azimuth angle of antenna plates
$\delta(m)$	Discrete-Time Unit Impulse
$\Delta(f)$	Fourier Transform of a Discrete-Time Unit Impulse
μ	Mean Value
σ^2	Variance
η_α	Electron Attachment Coefficient
Γ	Scale Factor of Class A Noise
α	Characteristic Exponent of SαS distribution
γ	Dispersion Parameter of SαS distribution
δ	Location Parameter of SαS distribution
A	Impulsive index of Class A Noise
C_e	Euler Constant
D	Gas-Density
E	Electric Field
$f(x)$	Amplitude Probability Density Function
$f_k(x)$	Noise Density Function

$I(t)$	Impulsive Noise
v_{rms}	Root Mean Square Voltage
P_N	Noise Power
$P_N(f)$	Spectral Density of Thermal Noise
$N(t)$	Auto-Correlation of White Noise
$w(z)$	Envelope PDF

CHAPTER 1 INTRODUCTION

Short range wireless technologies offer a number of monitoring, control, automation and surveillance applications in the future smart grids. The aim of this thesis is to assess the vulnerability of these wireless technologies to non-Gaussian impulsive noise, particularly electromagnetic noise found in an electricity substation environment.

This chapter describes the research motivation, organization of thesis, relevant publications and contributions to the scientific knowledge.

1.1 Research Motivation

The traditional power transmission paradigm is changing. The more efficient, complex, electricity grid of the future incorporating distributed generation using renewable energy sources, a disparate array of energy storage technologies and the active collaboration of consumers in load balancing via smart metering and demand-side management will require continuous grid monitoring and instant grid control.

Wireless technologies represent a convenient means of achieving the necessary communications connectivity in substations with significant flexibility and cost advantages when compared to fibre and copper cabling. Deployment of wireless communications equipment in electricity substations for monitoring, control and surveillance applications offers potential significant benefits over wired communications in terms of convenience, flexibility and cost [1, 2].

In industrial environments, Supervisory Control and Data Acquisition (SCADA) systems are becoming more sophisticated and more pervasive. These are computer

based monitoring systems which in many applications are complemented by a Distributed Control System (DCS). The principal components of a SCADA system are Remote Terminal Units (RTUs), the Human Machine Interface (HMI) and a Communication Infrastructure (CI). RTUs are connected to sensors, which send data to a control centre. In some more recent SCADA implementations, RTUs have been replaced with Programmable Logic Controllers (PLCs) which are more easily reconfigured than special purpose RTUs. The HMI presents the collected data to an operator who can supervise and manage the entire system. Alternatively, the system can be semi-automated by allowing computer programs to make control decisions. The CI connects the RTUs to the HMI and its reliability is critical. SCADA and DCS technologies are being increasingly used in the electricity supply industry and this trend is likely to accelerate with the implementation of the smart grid [3, 4]. RTUs can be widely scattered throughout electricity transmission substations and are traditionally connected by cables or optical fibre to the HMI [5]. Ethernet Local Area Network (LAN) implementations of such SCADA systems, which simplify the addition/reconfiguration of instrumentation and the coordination of protection systems, have been proposed and are already being evaluated [2, 6]. Significant flexibility and cost advantages over a wired LAN infrastructure would be gained, if signals could be routed around electricity substation compounds wirelessly. Furthermore, wireless communication technologies hold out the prospect of 'hot-line' sensors that can be deployed on energized High Voltage (HV) equipment without the inconvenience and costs associated with bridging the system's primary insulation.

Typically wireless receiver designs are based on the assumption that noise is Additive, White and Gaussian (AWG) and their applicability in a noise intensive electricity substation environment is not risk free [7, 8]. Major sources of impulsive noise (IN) in electricity substations are Partial Discharge (PD) and switching transients and, if the risks of deploying wireless communications equipment are to be properly assessed, the impact of such impulsive processes requires evaluation [9].

Wireless LAN (WLAN) technology is used extensively for networking computers with peripheral devices and is an obvious candidate for deployment in substations. Zigbee technology, based on the IEEE 802.15.4 standard, is another popular short range technology which has been used in many commercially available Wireless Sensor Network (WSN) solutions.

Whilst wireless networks have obvious benefits of cost and flexibility over wired networks, concerns remain which need to be addressed. One such concern is the practical performance that can be expected of commercially available wireless technologies in the unusual and challenging noise environment of electricity substations. This noise environment may be intensely impulsive in character due to PD, power electronic switching and other transient processes. The degree to which a dominantly IN environment might degrade the performance of wireless technologies, primarily designed to operate in a Gaussian noise environment, is an important consideration.

The primary objective of this research is to characterize the IN environment of electricity substations and evaluate the performance of short-range wireless technologies, and consider their suitability for their deployment in electricity substations.

1.2 List of Publications

1.2.1 Publications Directly Related to the Thesis

1. **S A Bhatti**, Shan Q, R Atkinson, I A Glover "Performance simulations of WLAN and Zigbee in electricity substation impulsive noise environments," *IEEE 3rd International Conference on Smart Grid Communications (SmartGridComm)*, Tainan, Taiwan, November 2012.

2. **S A Bhatti**, I Glover, "Performance Evaluation of IEEE 802.15.4 Receiver in the Presence of Broadband Impulsive Noise" *Student Application paper in IEEE Standards Education (E-magazine)*, July 2012.

3. **S A Bhatti**, Shan Q, R Atkinson, *M Vieira,* I A Glover: " Vulnerability of Zigbee to impulsive noise in electricity substations", *The XXX General Assembly and Scientific Symposium of International Union of Radio Science (URSI GASS)*, Istanbul, Turkey, August 2011.

4. **S A Bhatti**, Shan Q, I A Glover, R Atkinson, "On modeling of electricity substation impulsive noise environment", *International Conference on Statistical Methods of Signal and Data Processing (SMSDP), Kiev*, Ukraine, October 2010.

5. **S A Bhatti**, Shan Q, I A Glover, R Atkinson , P J Moore,I E Portugues , R Rutherford, "Vulnerability of Bluetooth to impulsive noise in electricity transmission substation*", IET International Conference on Wireless Sensor Network(IET-WSN),* Beijing, China, November 2010.

6. **S A Bhatti**, Shan Q, I A Glover, R Atkinson, P J Moore, I E Portugues, R Rutherford, "Impulsive Noise Modelling and Prediction of its Impact on the Performance of WLAN Receiver", 17th *European Signal Processing Conference(EUSIPCO 09)*, Glasgow, UK, August 2009.

7. Shan Q, I A Glover, R. Atkinson, **S A Bhatti**, I E Portugues, P J Moore, R Rutherford, M Vieira, A M Lima, B A De Souza, "Estimation of Impulsive Noise in an Electricity Substation," *IEEE Transaction on Electromagnetic Compatibility*, vol.53, no.3, pp.653,663, Aug. 2011.

8. Shan Q , **S A Bhatti** , I A Glover, R Atkinson, R Rutherford, "Detection of super-high-frequency partial discharge by using neural networks" , *Insight – Non-Destructive Testing and Condition Monitoring (The Journal of The British Institute of Non-Destructive Testing),* vol. 51, no. 8, pp.442-447, August 2009.

9. Shan Q, **S A Bhatti** , I A Glover, Atkinson R, Moore P J, Portugues I E, R Rutherford, "Noise amplitude distribution of impulsive noise from measurements in an electricity substation", *The 44th international Universities' Power Engineering Conference (UPEC)*, Glasgow, UK, September 2009.

10. Shan Q, **S A Bhatti**, I A Glover, R Atkinson , P J Moore ,I E Portugues , R Rutherford, "Characteristics of impulsive noise in electricity substations", *17th European Signal Processing Conference (EURSIP 09)*, Glasgow, UK, August 2009.

11. J M R Neto, E C T Macedo, J R Neto, E G Da Costa, **S A Bhatti**, I A Glover, "Partial discharge location using unsynchronized radiometer network for condition monitoring in HV substations – a proposed approach", Journal of Physics Conference Series, 2012.

12. E C T Macedo, D B Araújo, E G Da Costa, R C Freire, W T Lopes, I S Torres, J M Neto, **S A Bhatti**, I A Glover, "Wavelet transform processing applied to partial discharge evaluation", Journal of Physics Series, 2012..

13. Shan Q, I A Glover, R Atkinson, **S A Bhatti**, I E Portugues, P J Moore and R Rutherford, "Statistics of impulsive noise measured in an electricity substation"**,** *Tenth International Symposium on Communication Theory and Application(ISCTA 09),* Ambleside, UK, July 2009.

14. Shan Q, I A Glover, R Rutherford , **S A Bhatti**, R Atkinson, I E Portugues, P J Moore, "Detection of UWB impulsive noise in a 400 kV electricity substations", *20th International Conference on Electricity Distribution*, Prague, Czech Republic, June 2009.

15. Shan Q**, S A Bhatti**, I A Glover I A, R Atkinson, P J Moore , I E Portugues, R Rutherford, "Extraction of impulsive noise from measurements in a 400 kV electricity substation", *4th IASME/WSEAS- International Conference on Energy and Environment*, Cambridge, UK, February 2009.

16. Shan Q, I A Glover, P J Moore, I E Portugues, R Rutherford , R Atkinson , **S A Bhatti**, "Laboratory Assessment of WLAN Performance Degradation in the Presence of Impulsive Noise" , *International Wireless Communications and Mobile Computing Conference*, Crete, Greece, August 2008.

1.2.2 Seminars/Workshops

17. **S A Bhatti**, Shan Q, I A Glover, R Atkinson "Modelling of noise environment of an electricity transmission substation using symmetric alpha-stable distributions ", *2nd UK URSI Festival of Radio Science, Leicester*, UK, January 2011

18. **S A Bhatti**, Shan Q, I A Glover, R Atkinson, R Rutherford "Extraction of Middleton Noise Model Parameters from Measurement of the Noise Environment in an Electricity Substation", *URSI-Festival of Radio Science,* Birmingham, UK, December 2009.

1.3 Thesis Contributions

The work reported in this thesis can be grouped into two parts. The first part models the noise environment of Electricity Transmission Substations (ETS) and the second evaluates the Physical (PHY) layer bit error ratio (BER) of WLAN, Bluetooth and

Zigbee receivers in the presence of modelled IN. The thesis reports the following major contributions:

1. **Narrowband Impulsive Noise Model:** In the field of non-Gaussian noise modelling, the research work of Middleton is of paramount importance [10]. In this thesis, the assumptions made by Middleton are objectively analysed and their application and relationship to the substation noise environment are explored. A number of methods are reviewed to estimate the Class-A parameters from the measurements data and to tune it to represent the narrowband impulsive noise found in electricity substations.

2. **Broadband Impulsive Noise Model:** Discussion of impulsive noise modelling is further extended and a technical argument is presented to justify (i) that the impulsive noise environment of electricity substation can best be characterised by a broadband noise model and (ii) the use of Symmetric α-Stable (SαS) distributions to model the broadband impulsive noise phenomenon. Two methods are used to deal with the infinite variance of SαS, and to conclude a comparative account of the BER performance evaluation.

3. **Performance Evaluation of WLAN/WPAN:** PHY layer simulations of WLAN, Bluetooth and Zigbee standards are implemented (and/or adopted from the built-in MATLAB/Simulink libraries) and validated. BER performance of these technologies is evaluated in the presence of impulsive noise, modelled as both a narrowband and a broadband process.

1.4 Thesis Outline

An overview of the remaining six chapters of the thesis is given below.

Chapter 2 covers the background and state of the art including characteristics of the impulsive noise and stochastic nature of the underlying processes which make up the noise environment of an electricity substation.

Chapter 3 presents the details of the measurement campaign. It includes a description of the impulsive measurement and recording system, its deployment and an account of post-processing of the recorded data and extraction of impulse characteristics.

Chapter 4 examines several aspects of impulsive noise modelling. An account of the existing knowledge in this field is followed by a detailed description of the noise models and parameter estimation methds.

Chapter 5 details the implementation and validation of physical layer simulations of the candidate short-range wireless technologies.

Chapter 6 covers the performance assessment of the candidate short-range wireless technologies in the presence of impulsive noise.

Chapter 7 presents conclusions and suggests scope for the future research.

CHAPTER 2

BACKGROUND AND CONTEXT

2.1 Introduction

This chapter commences with a description of different types of noise processes, presents a detailed account of the noise profile of an electricity substation and state of the art for the deployment of wireless technologies in electricity substations. A paradigm for the performance evaluation of short range wireless technologies in the presence of non-Gaussian impulsive noise is given at the end of the chapter.

2.2 Background

The focus of this research is on the performance evaluation of short-range wireless technologies in the presence of non-Gaussian impulsive noise, found in electricity substations.

This section includes a classification and characteristics of different noise processes, noise profile of an electricity substation and a list of the candidate wireless technologies.

2.2.1 Noise

Noise is any unwanted signal that interferes with the information-bearing signal and degrades its quality. Noise is present in all environments, and its characteristics and extent depend on its physical source(s). Often, noise conveys information about the physical state of its sources and/or the environment in which it propagates [11]. For

example, noise originating from the insulation around HV cables can be used for insulation health monitoring and fault diagnosis.

In addition to noise, information signals become distorted because of non-linear characteristics of the communications channel. These distortions may arise, in part or in whole, from the multipath reflections and fading. The capacity of any communications or signal measurement system is limited by noise and signal distortions. Therefore, in the field of systems engineering, it is important to understand and model these two processes. This research work focusses solely on the noise process.

2.2.1.1 Noise Classification

In communication systems, noise is usually classified into two categories: internal and external. Internal noise refers to noise from inside the communications receiver and includes thermal noise, shot noise, flicker noise and burst noise, whereas external noise arises outside of the receiver and includes atmospheric, cosmic and electromagnetic emissions from electrical devices. Noise can also be classified based on its temporal characteristics and the frequency spectrum e.g. white noise, coloured noise, impulsive noise etc. Definitions of the several noise types are included in the thesis for the purpose of completeness. [11]

1. Thermal Noise

Thermal noise is intrinsic to all conductors and originates from movements of thermally energised charge carriers. Temperature is the measure of the mean kinetic energy of electrons. The power of thermal noise is therefore proportional to the

physical temperature. The mean square value of voltage due to thermal noise, across the terminals of a resistor of value R Ω, is given by:

$$\overline{v^2} = 4kTRB \qquad \text{(Equation 2.1)}$$

where $k = 1.381 \times 10^{-23}$ J/K is Boltzmann's constant, T is absolute temperature, and B is the bandwidth. The noise power dissipated in a matched load of resistance R Ω is:

$$P_N = \overline{i^2}R = \left(\frac{v_{rms}}{2R}\right)^2 R = \frac{\overline{v^2}}{4R} = kTB \ \ (W) \qquad \text{(Equation 2.2)}$$

where v_{rms} is the root mean square voltage. The spectral density of thermal noise per degree of freedom is given by:

$$P_N(f) = \frac{kT}{2} \ \ (\text{W/Hz}) \qquad \text{(Equation 2.3)}$$

This can be reconciled with Equation 2.2, by appreciating that the electromagnetic energy in an electrical circuit can exist in two orthogonal modes or degrees of freedom, e.g. at any one frequency, the voltage can either have a sinusoidal or cosinusoidal waveform.

The auto-correlation of the white noise, denoted by $N(t)$, can be written as:

$$R_{XX} = E[X(t)X(t+\tau)] = N_0\delta(\tau) \qquad \text{(Equation 2.4)}$$

This describes the noise where the samples are statistically independent. The baseband equivalent of a thermal noise process, often used in computer simulations, has complex values and comprises an in-phase $N_I(t)$ component and a quadrature $N_Q(t)$ component which are modelled as independent baseband random variables with Gaussian Probability Density Function (PDF). The value of the auto-correlation $R_{XX}(\tau)$ for each component is $(N_0/2)\ \delta(\tau)$. The thermal noise is white and Gaussian, as illustrated in Figure 2.1. Since the distribution of the samples is Gaussian, the amplitude PDF is given by:

$$f(x) = \frac{1}{\sqrt{2\pi\sigma^2}}\, e^{-\frac{(x-\mu)^2}{2\sigma^2}} \qquad \text{(Equation 2.5)}$$

It has two parameters. μ (mean value) and σ2 (variance), where the variance is a measure of the spread of samples around mean value. The term white implies that it has contant noise spectral density over all frequencies i.e. $G_N(f) = N_0$ (as is shown in Figure 2.1. The thermal noise samples follow a Gaussian distribution as is expected from the Central Limit Theorem (CLT)[1][12].

2. Shot Noise

Shot noise is intrinsic to current flow and originates from the random motion of carriers across a potential barrier. While thermal noise depends on temperature, shot noise, being determined by the movement of charged particles, solely depends on the current magnitude [13].

[1] The Central Limit Theorem (CLT) states that the sampling distribution of the mean of any independent, random variable will be normal or nearly normal, if the sample size is large enough.

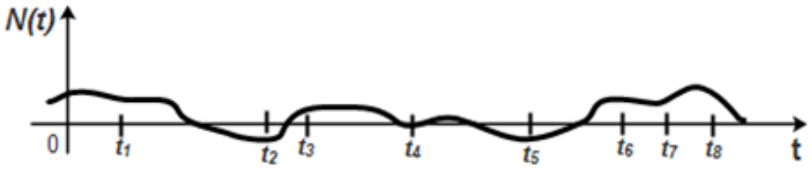

Schematic illustration of thermal noise time series

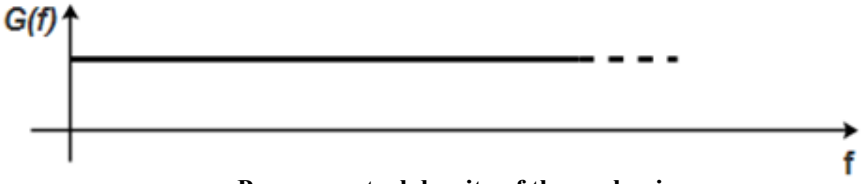

Power spectral density of thermal noise

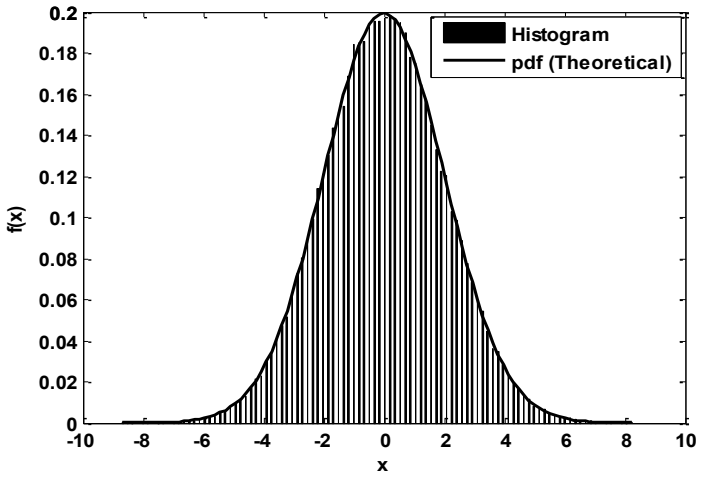

Theoretical PDF and histogram of white noise (Generated from 10^5 samples and 100 bins)

Figure 2.1 Thermal noise characteristics

3. Flicker Noise

Flicker noise is the result of a number of effects in electronic devices, such as impurities in a conductor channel and recombination noise in a transistor due to the base current [11].

4. Burst Noise

Burst noise consists of step transitions in voltage, as high as several hundred millivolts, at random times and for random durations [14].

5. White Noise

White noise is a random process with a flat power spectral density. Theoretically, it contains all frequencies, but it is not realisable in practice since any white noise process would carry infinite power. Thermal noise is a good example of white noise, which, at room temperatures, has constant spectral density up to the terahertz region. The precise bandwidth of (unfiltered) thermal noise is determined by quantum mechanical considerations and depends on temperature.

6. Coloured Noise

Strictly speaking, any noise process which has a frequency dependent power spectral density could be classified as a coloured noise.

2.2.1.2 Impulsive Noise

Impulsive noise is a non-stationary stochastic process which consists of random occurrences of voltage or current pulses with random amplitudes. In this section, a mathematical definition of the impulse function and spectra of ideal and short duration pulses are discussed.

2.2.1.2.1 Theoretical Impulse

A continuous-time unit impulse function or dirac delta is defined as a function that is zero for all values of $t \neq 0$ and yet its integral is nonzero, as is shown in Equations 2.6 and 2.7 and plotted in Figure 2.2. The frequency domain representation of a continuous-time unit impulse is given in Equation 2.8 [15].

$$\delta(t) = 0 \ \ for\ all\ t \neq 0 \qquad \text{(Equation 2.6)}$$

$$\int_{-\infty}^{\infty} \delta(t) = 1 \qquad \text{(Equation 2.7)}$$

$$\Delta(f) = \int_{-\infty}^{\infty} \delta(t) e^{-j2\pi f t} dt = 1 \qquad \text{(Equation 2.8)}$$

A discrete-time unit impulse can be defined as

$$\delta(m) = \begin{cases} 1 & if\ m = 0 \\ 0 & otherwise \end{cases} \qquad \text{(Equation 2.9)}$$

and the Fourier Transform (FT) of a discrete-time unit impulse is given by

$$\Delta(f) = \sum_{m=-\infty}^{\infty} \delta(m) e^{-j2\pi f m} = 1.0 \qquad for\ -\infty < f < \infty \qquad \text{(Equation 2.10)}$$

2.2.1.2.2 Real Impulse

In contrast to the ideal impulse where the pulse width tends to zero, a real impulse has a duration longer than one sample and impulsive noise is characterized by a train of short duration pulses with different amplitudes and inter-arrival times. Spectra of an ideal impulse and two short-duration pulses are shown in Figure 2.3.

The literature of communications theory has traditionally been dominated by the Gaussian noise models (justified by the CLT) which simplifies design and analysis of the receiver structures. An important class of non-Gaussian noise processes, encountered in practice, can best be characterized as impulsive.

The features which differentiate an impulsive process from a typical Gaussian noise process are:

a) Impulsive noise has a higher probability of producing high-amplitude excursions from the mean value.

(b) Impulsive noise exhibits sharp spikes or occasional bursts of outlying observations.

(c) The tails of impulsive noise density functions decay slowly compared to Gaussian.

The topic of impulsive noise is revisited in Chapter 4, where different aspects of its characterization and modelling are discussed.

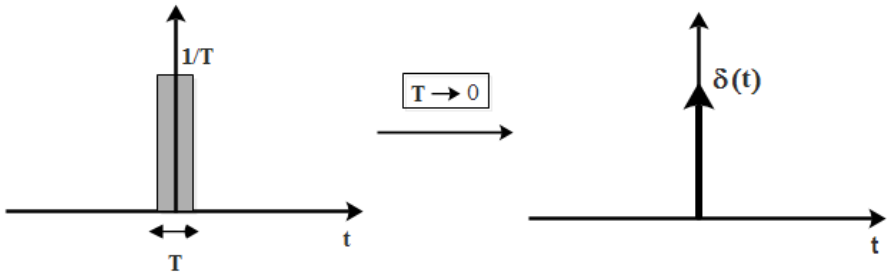

Figure 2.2 Unit impulse function.

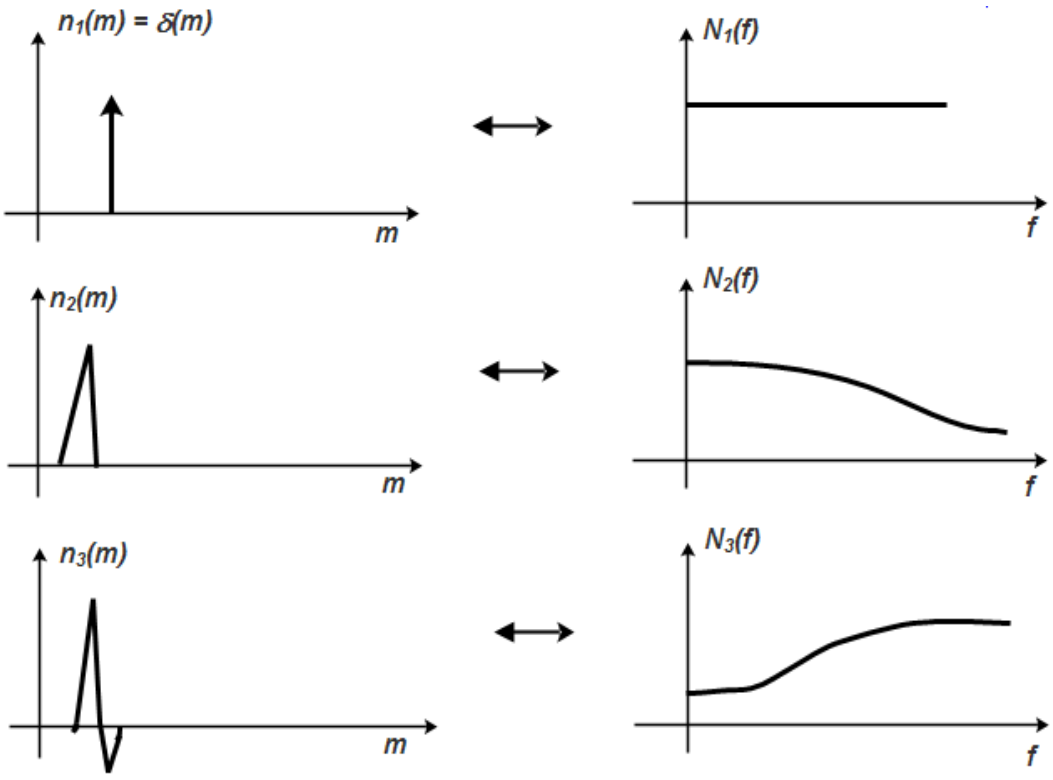

Figure 2.3 Spectra of an impulse and short duration pulses [11].

2.2.2 Substations

Substations are an integral part of power generation, transmission and distribution systems. The components of a substation are HV transformers, cables, switchgears, busbars, protective relays, voltage regulators, capacitors, and surge arrestors. In

addition to these components, there are a number of control, protection and measurement instruments, scattered throughout the substation. Typical functions of a substation are transmission lines connection, voltage levels transformation, fault isolation and power factor correction.

Traditionally, control and monitoring signals are connected to SCADA (Supervisory Control and Data Acquisition) systems using cables or optical fibres. SCADA systems provide a centralized solution for control and monitoring of a substation or a number of substations.

The HV substation equipment is a high-energy source of the unwanted radio frequency emissions. Partial Discharges (PD) and switching transients are the major noise sources in an electricity substation. [16].

2.2.3 PD and Switching Transients

Electrical insulations suffer from imperfections because of manufacturing faults, ageing (i.e. chemical or physical changes), and mechanical damage. Often such imperfections are represented initially by microscopic voids or cracks. When the potential difference across a void crosses a certain threshold, the air inside the void becomes ionized and this process releases energy in the form of heat, smoke, light, sound and electromagnetic radiation. This phenomenon is called a PD and is defined as a discharge that does not bridge the space between the conductors supporting the potential that causes it. The energy released in a PD erodes the internal surface of the void and makes the void grow large. If this process continues the result may be the breakdown of the electrical insulation.

The origins of PD are voids in solid dielectrics and gas filled spaces on the dielectric-conductor interfaces. Corona is a special case of PD which occurs around air-insulated conductors and is usually accompanied by visible light. Some of the causes of PD are metal contaminants, air bubbles, voids in epoxy castings and polluted/cracked insulations. Examples of internal and external PD occurrences are shown in Figures 2.4 - 2.7.

The IEC International Standard 60270 for PD measurements defines PD as "*a localized electrical discharge that only partially bridges the insulation between conductors and which can or cannot occur adjacent to a conductor*".

The necessary condition for a PD to occur, inside a void containing electro-negative gas, is:

$$(E/D) > (E/D)_c$$

where (E/D) is the electric field to gas-density ratio and $(E/D)_c$ is the critical value at which coefficient (α_i) is equal to the electron attachment coefficient (η_α) [17]. Moreover, if n_e is the number of electrons generated during this process then:

1. For $n_e < 10^8$, PD can simply be considered as an electron avalanche with a mean value of n_e, given by:

$$\overline{n_e} = \exp\left[\int_0^l [\alpha_i(x) - \eta_\alpha(x) d\acute{l}(x)\right] \qquad \text{(Equation 2.11)}$$

   where l is the path followed by the electron avalanche inside the void, and $d\acute{l}(x)$ is an element of path length. This is the state when the total charge generated from the ionization is not sufficient to disturb the externally applied electric field.

2. For $n_e \sim 10^8$, the electric field produced by electron avalanche becomes comparable to the externally applied electric field and transforms into a self-propagating phenomenon. This self-propagating phenomenon is often referred to as a streamer and results in the generation of a series of current pulses [18].

The energy released from an individual PD is usually very small (of order 1 μJ) and does not start the process of insulation degradation. During a continuous PD process, however, a small number of high-energy electrons are released and it is believed that most of the insulation degradation, directly or indirectly, is initiated by the bombardment of these high-energy electrons. These high-energy electrons have energies of order 10 eV and can potentially disrupt insulation molecules since the strengths of typical bonds e.g. C-H and C=H is much lower than 10 eV [19].

Moreover, production of reactive species such as OH, O and O3 can cause chemical transformation of the insulator and accelerates the PD activity.

PD phenomenon is inherently pulse-like and is the result of many underlying physical processes whose behaviour can best be explained statistically.

Figure 2.4 Internal PD

Figure 2.5 External PD

A current transformer (on left) and its sectioned part (on right) to show the damage caused by PD

It shows the tracking across the surface of the insulation.

Figure 2.6 Transformer PD damage

Figure 2.7 Tracking on epoxy resin busbar.

Figure 2.4 & 2.5 – (EA Technology, available at www.eatechnology.com)

Figure 2.6 & 2.7 – (Hoestar Inspection International, available at www.hoestarinsp.com)

The statistical variability of properties of PD pulses, such as amplitude, shape and duration, results in a very complex deterministic description of the process. Field induced emissions of electrons from a discharge prone surface are governed by quantum mechanics and are, therefore, inherently probabilistic [20]. Similarly, electron-molecule collision processes, which determine PD growth, are explained in terms of collision cross-section probabilities. The stochastic nature of the PD phenomena can be described empirically by observing the pulse statistics of different types of PD, which occur when different insulation materials experience electrical stresses of varying strengths and time durations. In practical systems, the stochastic behaviour of PD becomes more complex due to the presence of many PD sources e.g. in transformers, capacitors, circuit breakers and cables etc.

The noise environment of electricity substation is particularly complex since it comprises PD generated because of electron avalanches, high-energy streamers and corona from a number of sources.

In addition to PD, switching transients also contribute to the noise profile of a substation and these are of particular interest. Switching transients are significantly important as the switching process is the occasion when control and protection equipment is required to work reliably. Switching transients result in sporadic impulses of large amplitudes and very small durations. The nature of radiated impulses from PD and switching transients depends on the rate of current during the insulation breakdown process or the switching event. [16].

2.2.4 Candidate Wireless Technologies

The candidate short range wireless technologies for deployment in electricity substation are WLAN, Bluetooth and Zigbee. A comparison in terms of data rates and operating frequency is given in Table 2.1 and detailed specifications are covered in Chapter 5.

Table 2.1: Candidate wireless technologies

Technology	Data Rate	Operating Frequency
WLAN	1-54 Mbps	2.4 and 5 GHz
Bluetooth	1 Mbps	2.4 GHz
Zigbee	20-250 kbps	900 MHz and 2.4 GHz

2.3 Literature Review – Wireless Technologies in Substations

2.3.1 Applications

Wireless technology has been used in electricity substations for decades, mainly for the applications which are not safety critical. The potential of wireless technologies for control, monitoring and protection has been investigated by the Electric Power Research Institute (EPRI) of USA and P1777 – Wireless Working Group of the IEEE, and it has been suggested that the incorporation of wireless technologies in future substation control systems is inevitable [21-23].

Successful demonstrations of the use of WLAN for line differential protection applications in a laboratory environment and monitoring of air-core inductors in a substation environment have been reported by Abdel-Latif et. al.[24] and Brown et. al. [25] respectively. A number of applications of wireless technologies have been reported for future smart grids [26-29].

The research and development of robust wireless transceivers have been initiated by a number of power utilities manufacturers e.g. RuggedCom, Tropos GridCom and Carlson Wireless [30].

2.3.2 Substation Noise

A number of studies have been conducted to characterize the substation noise profile but most of them have used narrowband equipment and have not explored the full spectral extent of the electromagnetic radiations [31, 32].

There are only a few substation measurements, reported in the literature, which have used broadband equipment e.g. Moore et. al. [33] has conducted PD measurements using a broadband system (~1GHz) and has reported that the discharges from SF6 have significant spectral energy up to 800 MHz.

In another study, substation noise measurements have been conducted for the 900 MHz and 2.4 GHz frequency bands and it has been reported that there are noticeable changes in the RF noise profile up to 2.4 GHz [1, 34]. Q. Shan et.al. [35, 36] have reported substation measurements in a 400 kV Air Insulated Substation (AIS) using an ultra-wideband equipment for the 2.4 and 5 GHz frequency bands.

2.3.3 Performance Evaluation in non-Gaussian Impulsive Noise

The performance evaluation of different modulation and error coding techniques, in the presence of non-Gaussian impulsive noise has been reported in a number of studies.

The performance evaluation of a Quadrature Amplitude Modulation (QAM) system, in the presence of Class A[2] noise, has been reported to degrade significantly [37, 38]. The BER performance of Minimum Shift Keying (MSK) and Gaussian MSK (GMSK) in Class A noise has been shown to degrade at high SNR values[39]. A comparative study of a Direct Sequence Spread Spectrum (DSSS) with and without error coding has been undertaken. The results show that overall performance differs significantly and it is advantageous to use error coding [40].

Jia and Meng [41] have investigated the performance of ZigBee systems at 915 MHz and 2.4 GHz bands, in the presence of PD noise and have reported that it is advantageous to use 2.4 GHz compared to 915 MHz. In another study, the performance of a Zigbee based sensor has been shown to degrade. Further research was proposed into the noise immunity of the Zigbee sensors [42].

2.4 Scope of the Research

The scope of this research is to evaluate physical layer BER performance of the candidate short range wireless technologies in the presence of non-Gaussian impulsive noise, found in electricity substations, using computer simulations.

An overview of the performance evaluation work is shown in Figure 2.8 illustrating the tasks and the sequence, in which, they have been carried out.

[2] Class A is a narrowband impulsive noise model. Details are given Chapter 4.

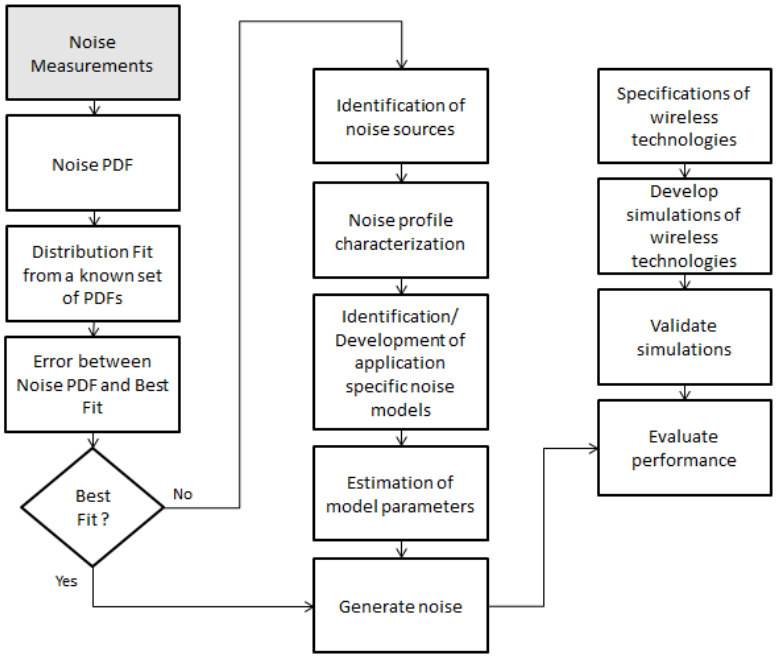

Figure 2.8: Performance evaluation overview

2.5 Summary

This chapter has covered the characteristics of different types of electromagnetic noise and the stochastic nature of the underlying processes that make up the noise environment of an electricity substation. State of the art of substation noise measurements and performance evaluation of wireless technologies in substation noise environment has also been explored.

CHAPTER 3

RF NOISE MEASUREMENTS

3.1 Introduction

This chapter covers the details of substation noise measurements including the design of measurement system, measurement campaign, analysis of recorded data and process of impulsive noise extraction from RF measurements.

3.2 Measurement System

An ultra-wideband detection system has been developed for the detection and recording of impulsive noise as part of the EPSRC funded project [43]. Since the potential interfering effects of impulsive noise will not only depend on power spectral density but also on the time-domain waveform, it is important that generic measurements should retain pulse shape information as far as possible. It will allow the effects of arbitrary filtering (introduced by commercial receivers) to be properly emulated when assessing performance impact. In view of this, the measurement system has been designed not only to have wide bandwidth but also to have good impulse response [36].

A block diagram of the measurement system is shown in Figure 3.1 [35]. It comprises three antennas, a LeCroy SDA9000 4-channel digital storage oscilloscope (DSO), an external 1 TB Hard Disk Drive (HDD) and a laptop computer for data logging and data pre-processing.

The DSO sampling rate is 20 GS/s per channel and its analogue channel bandwidth is ~6 GHz. The antennas are connected directly to the DSO. Direct sampling is used to

minimize signal distortion [44]. Interconnection is with 18 GHz, 50 Ω, coaxial cables. The time-series is recorded using conventional amplitude triggering. Duration of each recorded time-series is 2.5 ms which is the longest possible using the available DSO RAM. The recorded signals are transferred to the external HDD which is connected to the DSO via a USB interface.

Two quasi-TEM half-horns, a high-band (HB) horn and low-band (LB) horn, have

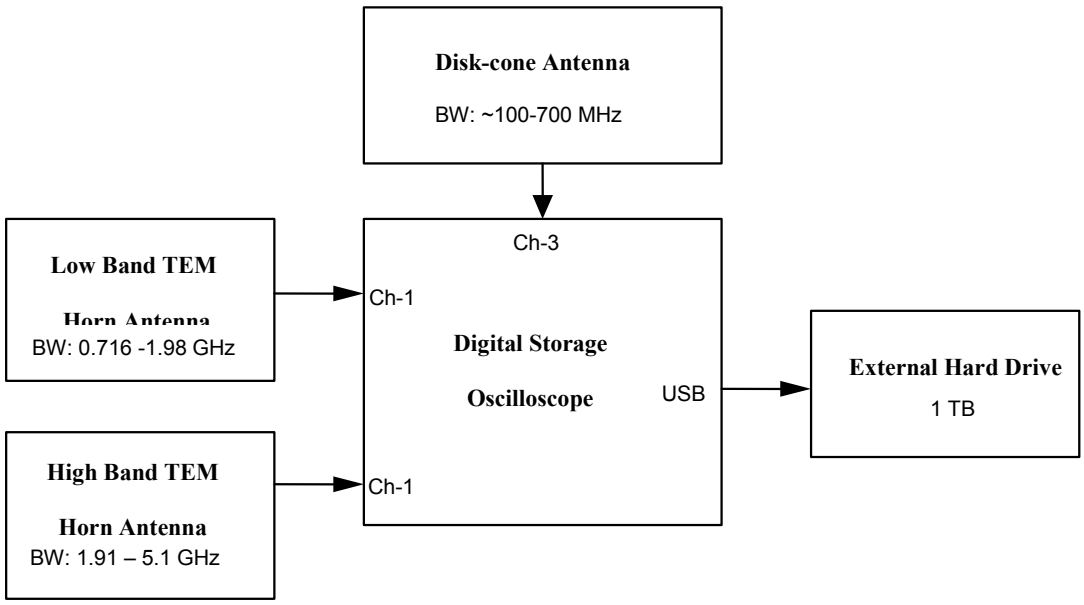

Figure 3.1 Impulsive noise detection and recording system[35]

been designed to cover the previously unexplored frequency range above 700 MHz [36]. Quasi-TEM horns were selected for the frequency bands of greatest interest due to their wide bandwidth, linear phase response and, thus, excellent impulse characteristics. Two horn antennas were used since a single antenna covering the

entire band was found to be impractical without compromising the phase characteristic.

The LB horn covers the range 0.7 – 2 GHz and the HB horn covers the range 2 – 6 GHz. The third antenna is a Discone which is used to extend data collection below 700 MHz, i.e. into the bands already investigated in the context of PD [45].

The TEM horn, in its basic form, consists of two isosceles conducting plates. The apexes of the plates form the antenna feed-point. The sides of each plate opposite to the apex are parallel and form the antenna aperture. The flare angle, apex angle and plate length are chosen such that the characteristic impedance at the feed-point is equal to that of the feeding transmission line and the impedance at the aperture is equal to the plane-wave impedance of free space.

The three principal design parameters are the length of the antenna (L_{ant}), the azimuth angle of the antenna plates (α_{ant}), and the flare angle between the antenna plates (β_{ant}). L_{ant} determines the lower end of the antenna frequency response and it must be at least one half-wavelength at the lowest frequency of interest. The upper end of the frequency response is inversely proportional to the separation between the plates at the feed point. The TEM half-horn comprises a single triangular plate mounted above a ground plane. Schematic diagrams of TEM-horn and disk-cone are shown in Figure 3.2 and Figure 3.3 respectively.

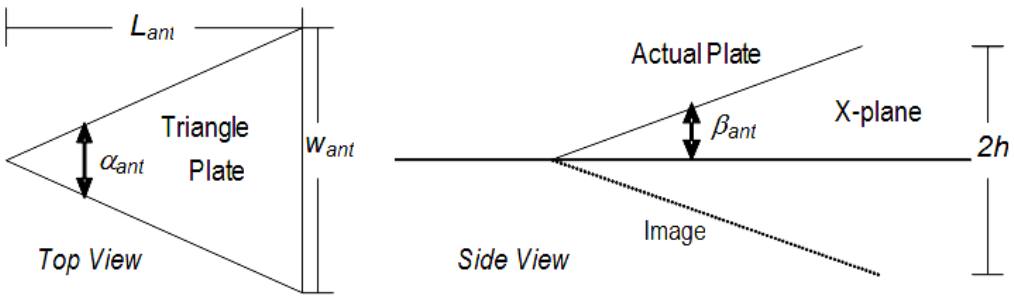

Figure 3.2: Schematic diagram of TEM horn antenna

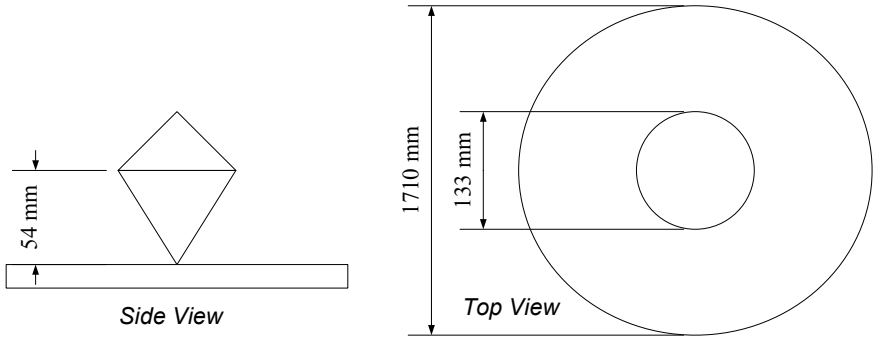

Figure 3.3: Schematic diagram of Disk-cone antenna

A summary of the antennas design parameters is given below:

LB Horn: The LB horn is constructed from a triangular aluminium plate and a 122 cm × 122 cm aluminium ground plane. The width (w) of the triangular plate at the aperture is 65.1 cm, its length (L) is 84 cm, and its aperture height measured from the ground plane (h) is 20.1 cm. The antenna feed is a 50 Ω SMA connector with its flange in electrical contact with the ground plane and its centre-conductor connected to the triangular plate apex. The amplitude response, measured using a network

analyzer, shows the 3dB bandwidth of a pair of identical cascaded horns (transmit and receive) to be 1.264 GHz covering the frequency range 716 MHz - 1.98 GHz. The peak value of the amplitude response occurs at 1.068 GHz. A picture of LB Horn antenna is shown below (Figure 3.4)

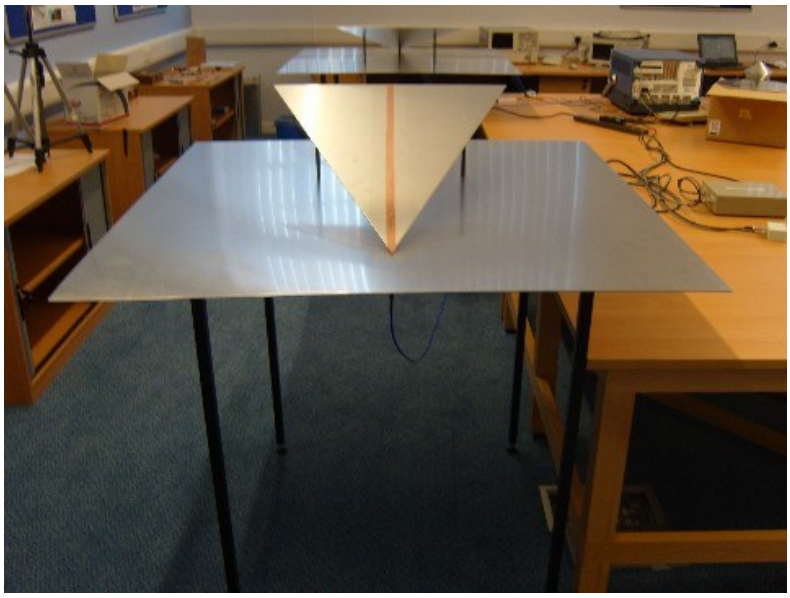

Figure 3.4: LB TEM Horn Antenna

HB Horn: The HB horn triangular flange is constructed from a printed circuit board. The flange width (w) at the aperture is 21.7 cm and its length (L) is 28 cm. The aperture height (h) is 6.7 cm. The feed structure and ground plane are identical to those of the LB horn. The 3dB bandwidth of a cascaded pair (transmit and receive) is 3.195 GHz (1.905 to 5.1 GHz) and the peak value of the amplitude response occurs at 2.13 GHz. A picture of HB Horn antenna is shown in Figure 3.5

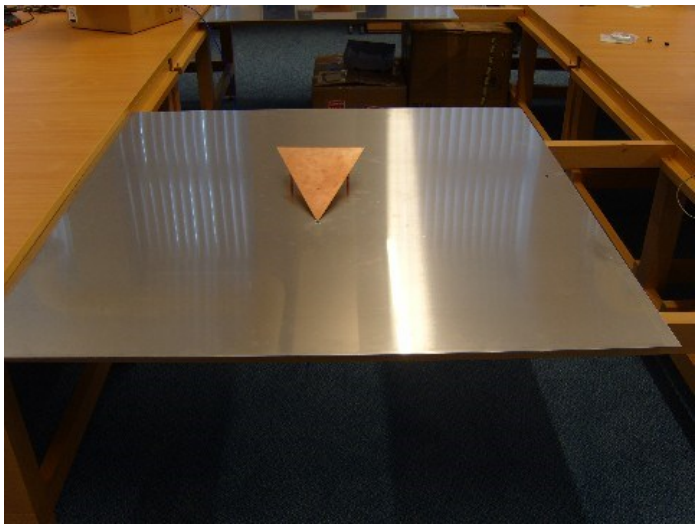

Figure 3.5: HB TEM Horn Antenna

Disk-cone Antenna: The disk-cone antenna consists of an inverted right circular cone over a circular ground plane. The ground plane is 17.1 cm in diameter and is constructed from aluminium plate. The cone was machined from solid aluminium. It has a base diameter of 13.3 cm and a height of 5.4 cm. A non-inverted cone with equal base diameter sits on top of the inverted cone. Its height is 4.9 cm. A picture of Disk-cone antenna is shown in Figure 3.6

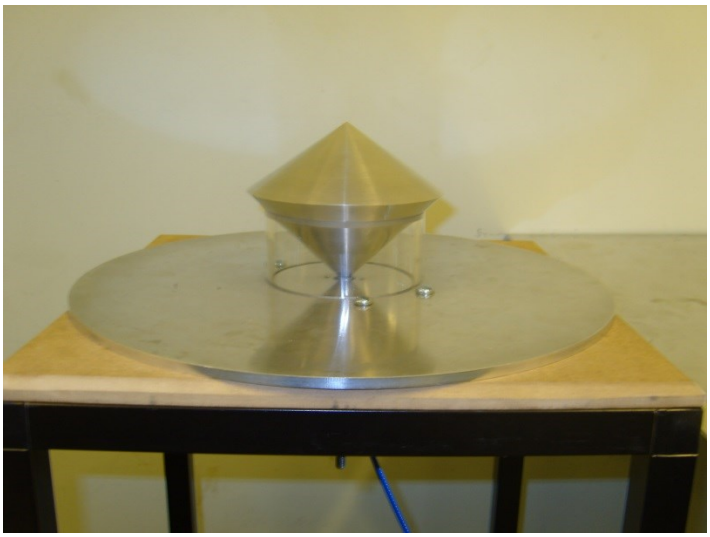

Figure 3.6: Disk-cone antenna

3.3 Measurement Campaign

The measurement site is Strathaven 400/275/132 kV air-insulated substation in the UK, owned by Scottish Power Limited. The geographical location of the site is illustrated in Figure 3.7.

The measurement system was deployed in 400 kV and 275 kV control rooms and the locations of the control rooms inside the substation are shown in Figure 3.8. The control rooms are located close to the centre of the substation.

All antennas were deployed with vertical polarization. The deployment of measurement systems inside the control room is shown in Figure 3.9, whereas Figures 3.10, 3.11 and 3.12 show the composite images of 400 kV, 275 kV and 132 kV compounds, respectively.

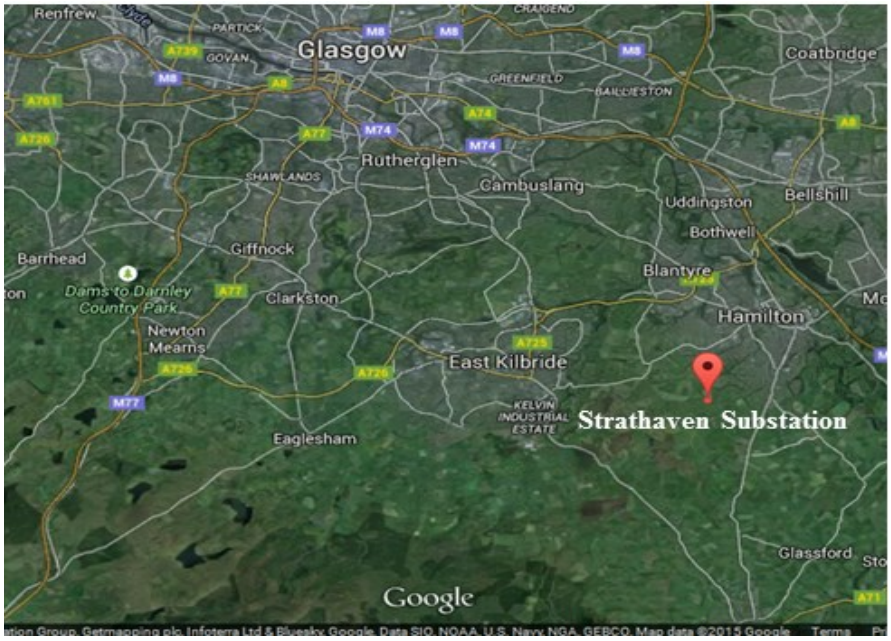

Figure 3.7: Geographical location of Strathaven Substation

Figure 3.8: Location of the measurement system in the substation.

(A) 400 kV control room, (B) 275 kV control room.

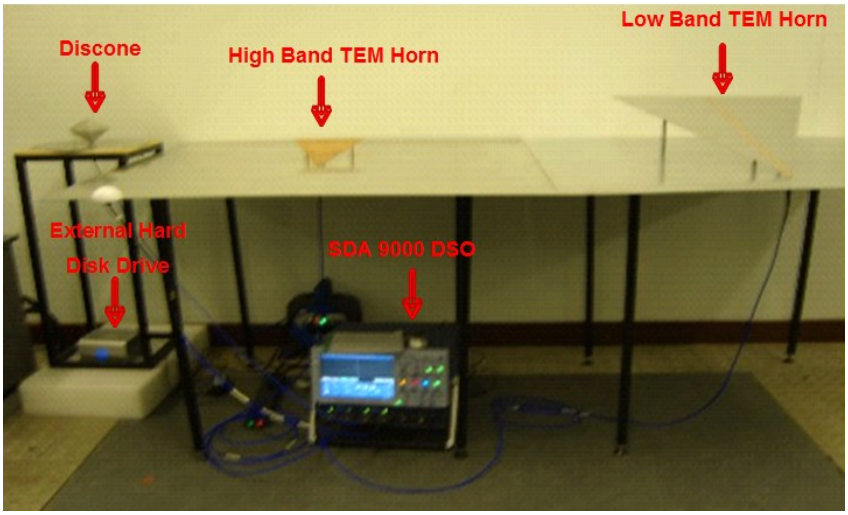

Figure 3.9: Impulsive noise detection and recording system deployment

.

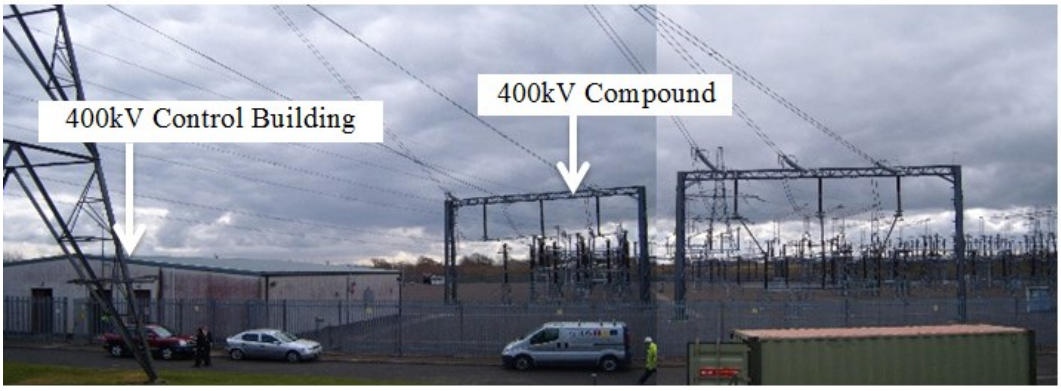

Figure 3.10 Measurement site: 400kV compound

Figure 3.11 Measurement site: 275kV compound

Figure 3.12 Measurement site: 132kV compound

3.4 Data Analysis

The duration of the measurement campaign was from January 2008 to April 2009. However, only datasets recorded between August 2008 and Feb 2009 by HB horn antenna are used for the noise modelling and performance evaluation work.

Table 3.1 shows the number of datasets captured in each month. Each dataset comprises $50x10^6$ samples, representing a 2.5 ms time window, and sampled at 20 GS/s.

A snapshot of raw sample data recorded in the substation is shown in Figure 3.13. This figure, showing a $50x10^3$ samples dataset (250 μs), is produced here for illustration purpose as one can see that any particular effects from PD and switching are hidden by noise from other sources. It also shows that what a broadband measurement system has picked up when it was triggered to capture a PD or a switching transient

Table 3.1: Time-series datasets

Month	Number of Datasets
August 2008	51
September 2008	68
October 2008	22
November 2008	47
December 2008	76
January 2009	45
February 2009	30

The recorded signal is a mixture of unwanted signals and noise including interference from other broadcast radio/tv communications and radar signals. A Fast Fourier Transform (FFT) of one recorded time-series dataset (2.5 ms) is shown in Figure 3.14, where the strong spectral peaks are labelled by comparing, in part, with the OFCOM's radio frequency allocation table [46]. A mapping of spectral peaks in FFT of time-series dataset and potential external interference sources is shown in Table 3.2.

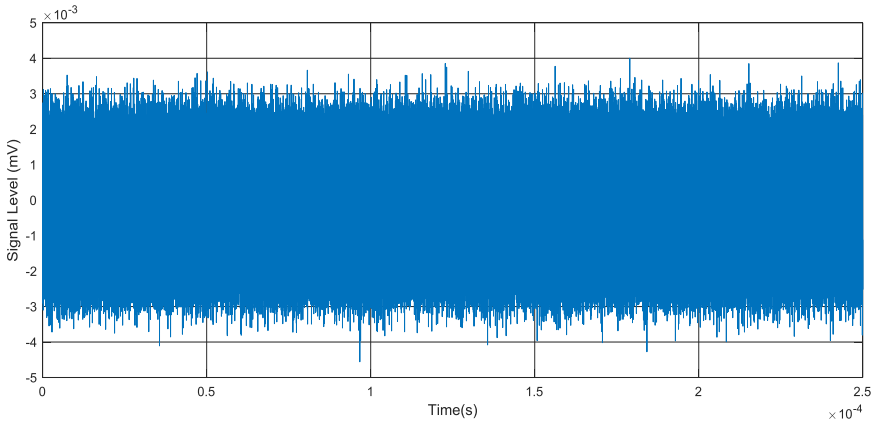

Figure 3.13: An example of raw sample data

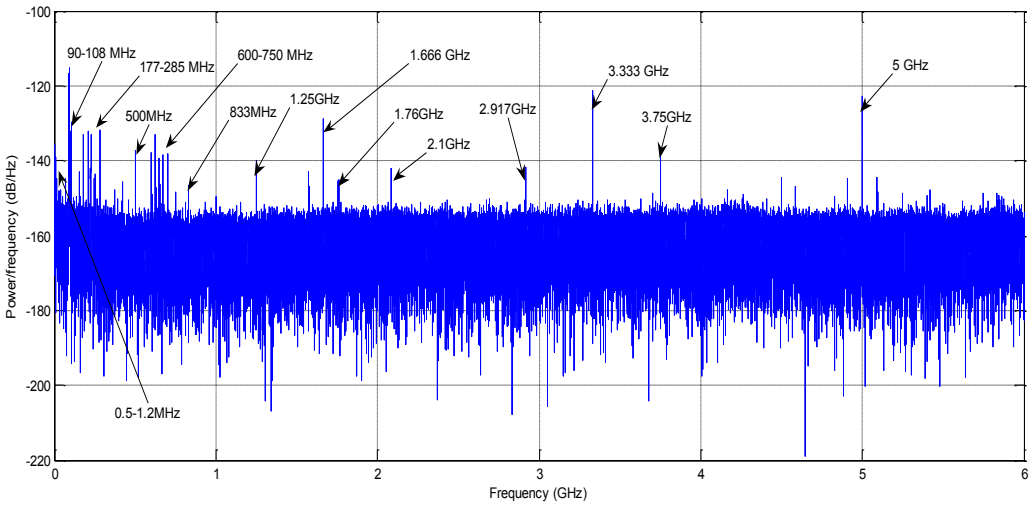

Figure 3.14: FFT of a recorded substation noise dataset [35]

The noise from PD and switching transients has been obscured by these broadcast, radar and communications signals and thus there is no obvious sign of impulsive noise in Figure 3.13.

Table 3.2 Description of the frequency spectrum of recorded noise data

Spectral Peaks of Recorded Data	Potential Sources
0.5 - 1.2 MHz	MW AM broadcast
90 – 108 MHz	FM radio band
177 – 285 MHz	Public Access Mobile Radio
500 MHz	TV broadcast
600 – 750 MHz	TV broadcast
833 MHz	TV broadcast
1.25 GHz	Civil airport radar band
1.76 GHz	GSM 1800
2.1 GHz	3G
2.917 GHz	Civil maritime, air traffic control and range safety radars
3.333 GHz	Maritime mobile band
3.75 GHz	C-Band satellite TV
5 GHz	Civil landing system signals

3.5 Extraction of Impulsive Noise

The measured data have been 'de-noised' using a Wavelet Packet Transformation (WPT) algorithm, to extract the impulsive noise buried in mixed unwanted noise processes and external interference [47].

The use of WPT for de-noising was encouraged by existing literature on the topic, where it has been reported to be an efficient method for the extraction of PD from RF noise measurements [48-50].

The application of WPT based de-noising algorithm to one time-series record has the following steps [47]:

Step – 1: Read the 10 M samples from the time-series record.

Step -2: Divide each 10 M samples block into 50 sub-datasets each with ~200,000 samples.

Step - 3: Compute the wavelet packet decomposition of both the approximation and detail, up to 12 levels using symlet-6.

Step - 4: Compute the optimal wavelet packet tree using an entropy function.

Stein's Unbiased Risk Estimate (SURE) entropy function was used. The entropy measures signal energy spread over a particular basis. Lower entropy means that fewer basis vectors are needed for representing the energy spread, and thus results in a more efficient decomposition.

SURE works well if a signal is normalized in such a way that the data fits the model x(t) = f(t) + e(t), where e(t) is a Gaussian white noise process with zero mean and unit variance. The SURE is defined by [47]:

$$SURE = \sqrt{2\ln(n\log_2(n))} \qquad \text{(Equation 3.1)}$$

where n is the number of signal samples.

Step - 6: Apply thresholding.

Hard thresholding was applied that removes all detail coefficients with a value lower than the threshold level.

Step - 7: Reconstruct the signal at each level using the original approximation coefficients and modified detail coefficients.

Repeat the steps 1 to 7 five times to complete de-noising of one time-series dataset.The five sub-datasets (10 M samples each) of a time-series dataset (50 M samples) and their corresponding de-noised or WPT processed datasets are shown in Figures 3.15 – 3.24. The presence of an impulsive process can be observed in the de-noised datasets.

An impulsive noise database has been compiled by applying the WPT based de-noising algorithm to time-series datasets recorded between August 2008 and February 2009 (Table 3.1). This compiled impulsive noise database has been used for noise modelling which will be described in Chapter 4.

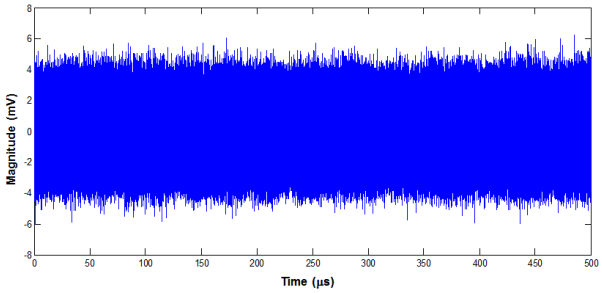

Figure 3.15: Sub-dataset 1 - Raw sample data

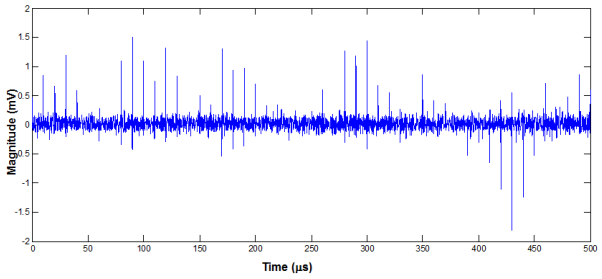

Figure 3.16: Sub-dataset 1 - De-noised data

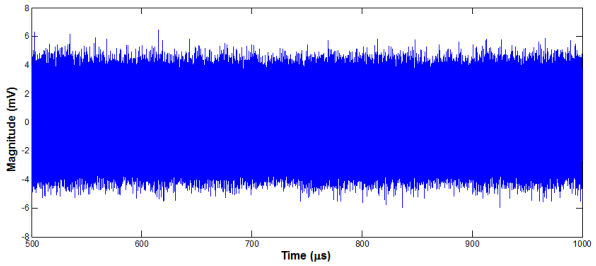

Figure 3.17: Sub-dataset 2 - Raw sample data

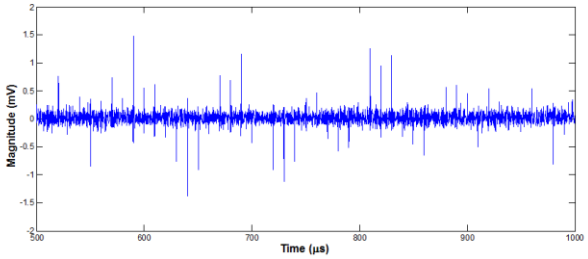

Figure 3.18: Sub-dataset 2 - De-noised data

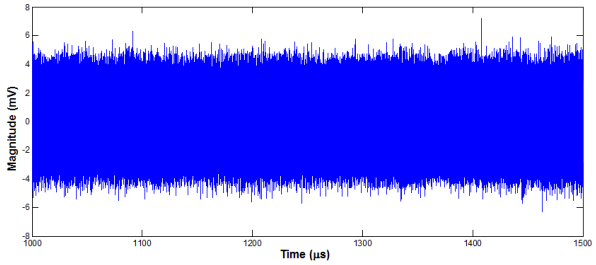

Figure 3.19: Sub-dataset 3 - Raw sample data

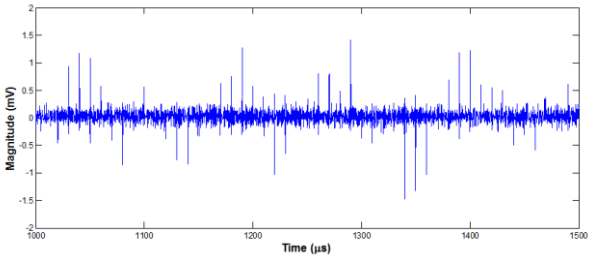

Figure 3.20: Sub-dataset 3 - De-noised data

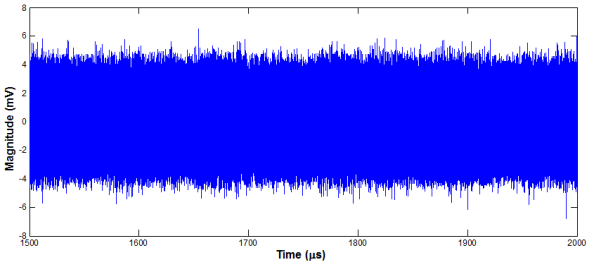

Figure 3.21: Sub-dataset 4 - Raw sample data

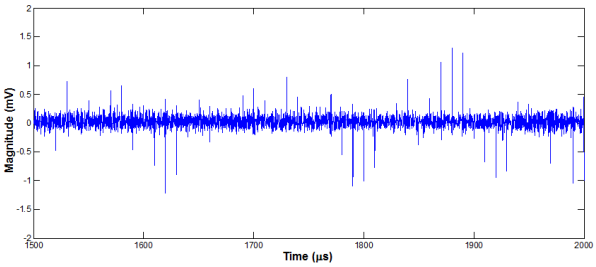

Figure 3.22: Sub-dataset 4 - De-noised data

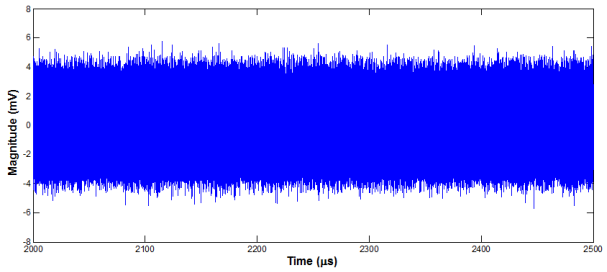

Figure 3.23: Sub-dataset 5 - Raw sample data

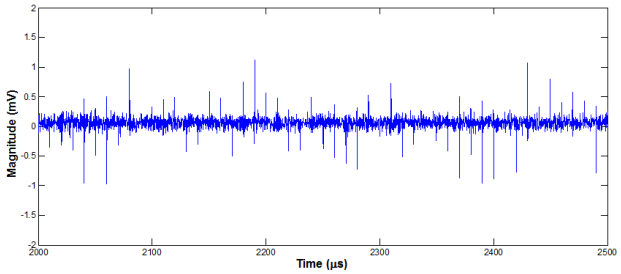

Figure 3.24: Sub-dataset 5 - De-noised data

3.6 Summary

The details of the noise measurements and extraction of impulsive noise from measurement data have been presented in this chapter. An impulsive noise database has been compiled which is used in Chapter 4.

CHAPTER 4

IMPULSIVE NOISE MODELLING

4.1 Introduction

An important source of electromagnetic noise in electricity substations is PD which radiates from the flaws in the insulation materials used in the electrical equipment. The PD phenomenon is described in detail in Chapter 2, Section 2.4. This chapter builds on the discussion of the nature of PD and explores potential mathematical and statistical techniques that can be used to model such phenomena.

Section 4.2 outlines the mathematical basis of impulsive noise modelling. This is followed in section 4.3 by a detailed account of Middleton's seminal work and description of the Class-A and Class-B models.

Section 4.4 provides a description of α-stable distributions and the characteristics that make them potential techniques for modelling broadband impulsive noise.

The model selection criteria and justification of adopting Middleton's Class-A and Symmetric α-Stable (SαS) to model the PD noise environment of the electricity substations are given in section 4.5.

Section 4.6 describes the parameter estimation methods and provides validation by comparing the noise amplitude distributions of both the recorded and generated noise data.

4.2 Impulsive Noise Models

The noise which originates from the PD is impulsive. It can be characterised by bursts of short duration pulses with random amplitude and random time of occurrence. Mathematically PD noise can be described as a summation of individual pulses or summation of pulse trains (if we consider that each PD results in a pulse train). The resulting noise process is non-stationary i.e. its statistical parameters (including mean and variance) vary with time.

If a non-stationary process has a well-defined Markovian structure then a Hidden Markov Model (HMM) can be used to statistically characterize the time-varying behaviour of the noise [51]. HMM is essentially a finite state Markov chain where each state corresponds to a stationary sub-process. The number of states in the HMM depends on the character of the noise[3].

Figure 4.1 shows a binary state Markov model, which can be used to model impulsive noise. State-1 corresponds to the absence of the impulsive noise and state-2 to the presence of impulsive noise [14]. This is the simplest model to describe the time-varying nature of the impulsive noise. It has limited applications to representing the complex noise encountered in industrial environments such as electricity substations.

[3] Markov process is a stochastic process whose future behaviour is independent of past behaviour, and can be determined by present state only. Markov (1856-1922) proposed this process, when he was working on the generalisation of the Central Limit Theorem (CLT).

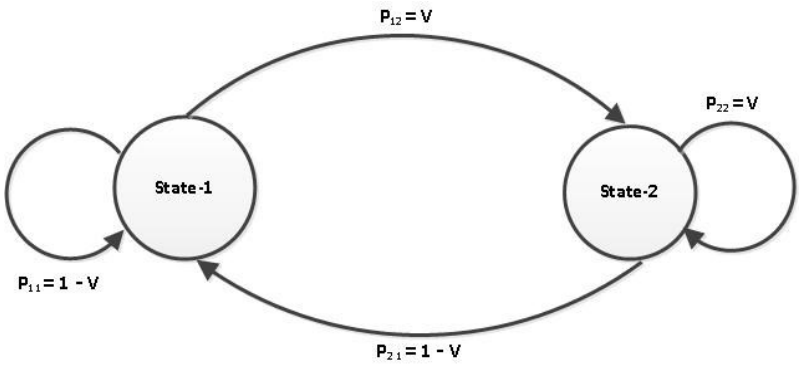

Figure 4.1 Markov Binary state noise model

If a noise process does not have a well-defined Markovian structure then Gaussian mixture distributions offer an alternative approach. This alternative approach is particularly useful for impulsive processes [52].

There have been many characterizations of submarine acoustic noise, man-made urban radio frequency (RF) noise, and low-frequency atmospheric noise. For such noise environments, it is well-established that the simple Gaussian noise model, although mathematically very appealing, is not appropriate [53-56]. The probability of occurrence of large-magnitude observations is high in these environments and the resultant noise process does not converge to a Gaussian distribution.

The presence of impulsive noise results in a non-Gaussian noise profile whose density function tails decay at a lower rate than a Gaussian density function. To model this noise process, the tail behaviour of the Gaussian distribution function, therefore, needs to be adjusted. One approach is to generalize the Gaussian density function and allow its exponential decay to become a free parameter. A second approach is to control the algebraic decay in the tails of a Cauchy density function by introducing free parameters. Thus in both cases (generalized Gaussian and

generalized Cauchy), the behaviour of the tails can be controlled and a variety of different density shapes, which are appropriate for modelling different non-Gaussian noise profiles, can be achieved.

The presence of PD is a root cause of the non-Gaussian nature of the noise originating from an ETS.

Algazi and Learner [57] have reported that certain types of atmospheric impulsive noise can be modelled with a generalized Gaussian density function, in which the rate of exponential decay parameter $k = 0.5$. The noise density function for parameter k and variance σ^2 is defined as:

$$f_k(x) = \frac{k}{2\,A(k)\,\Gamma\left(\frac{1}{k}\right)}\, e^{-\left[\frac{|z|}{A(k)}\right]^k} \qquad \text{(Equation 4.1)}$$

where

$$A(k) = \left[\sigma^2 \frac{\Gamma\left(\frac{1}{k}\right)}{\Gamma\left(\frac{3}{k}\right)}\right]^{\frac{1}{2}} \qquad \text{(Equation 4.2)}$$

and Γ is the gamma function:

$$\Gamma(\alpha) = \int_0^\infty x^{a-1} e^{-x}\, dx \qquad \text{(Equation 4.3)}$$

In a similar way, Mertz [58] modelled the amplitude distribution of impulsive noise found in digital communication systems using a higher-order hyperbolic distribution which, with the assumption that noise density is symmetric and $k = 1$, reduces to the generalized Cauchy distribution and can be written in terms of three parameters σ^2, k and v as:

$$f_{k,v}(x) = \frac{B(k,v)}{[1 + \frac{1}{v}\left[\frac{|x|}{A(k)}\right]^{k}]^{v+1/k}} \qquad \text{(Equation 4.4)}$$

where

$$B(k,v) = \frac{k\, v^{-\frac{1}{k}}\, \Gamma\left(\mathrm{v} + \frac{1}{\mathrm{k}}\right)}{2\, A\,(k)\, \Gamma(\mathrm{v})\, \Gamma\left(\frac{1}{\mathrm{k}}\right)} \qquad \text{(Equation 4.5)}$$

and *A(k)* is defined by Equation 4.2. The density function $f_{k,v}(x)$ has algebraic rather than exponential decay in the tails. This generalization of the Cauchy distribution is explained later in the context of Symmetric α-Stable (SαS) distributions.

Another perspective on modelling non-Gaussian impulsive process is to use the mixed density function, which can be written as:

$$f(x) = (1 - \varepsilon)G(x) + \epsilon\, I(x) \qquad \text{(Equation 4.6)}$$

where ε is a constant in the range [0,1]. *G(x)* can be a Gaussian density and *I(x)* is some other density function with heavier tails than Gaussian. In this density function, for small values of *x*, Gaussian behaviour dominates, and for large values *I(x)* dominates. The sum results in a heavy-tailed density function appropriate to impulsive noise. A mixture Rayleigh density function can be used to fit radar clutter, which also has heavier tails than a Gaussian density function [59].

The impulsive noise can be considered to be a Poisson point process with i.i.d. amplitude values. It can be written as:

$$I(t) = \sum_{k=-\infty}^{\infty} A_k \, p(t - t_k) \qquad \text{(Equation 4.7)}$$

where 'p' is the pulse shape and is determined by the receiver's impulse response, A_k is amplitude values and t_k is Poisson distributed. If we suppose 'v' is a rate parameter of the Poisson process and T_p is the width of the pulse then for $vT_p << 1$, the density function of *I(t)* is given in Equation 4.8 [60, 61].

$$f_I(x) = \left(1 - vT_p\right)\delta(x) + vT_p \, I(x) \qquad \text{(Equation 4.8)}$$

In Equation 4.8, the density function *I(x)* depends on the shape and amplitude distribution of the pulse. The quantity 1 - vT_p corresponds to the probability of no impulsive noise being present. If $f_I(x)$ is convolved with background (Gaussian) noise, this relationship results in the density function *f(x)* [Equation 4.6], where ε is replaced with vT_p .

The seminal work of Middleton [62], described in the next section, generalizes the concept of mixture noise.

4.3 Middleton Noise Models

Man-made interference can be either categorised as intelligent when the interfering signal carries meaningful information or unintelligent when the interfering signal carries no (conventional) information. The latter includes partial discharge (PD), switching transients and combustion engine ignition noise etc. When sufficiently close to a PD source, unintelligent impulsive interference will dominate.

The realization of a tractable analytical model for combined man-made and natural radio noise serves a number of purposes [10, 62]:

a. It provides a realistic and quantitative description of man-made and natural electromagnetic interference.

b. It provides a framework for experimental protocols for the measurement of such interference.

c. It can be used to assess the comparative performance of competing communication systems in realistic noise environments.

Middleton's three models (class A, B and C) are statistical physical models which include the non-Gaussian components of natural and man-made noise. These models are canonical in nature, i.e. their mathematical form is independent of the physical environment. The distinction between the three models is based on the relative bandwidth of noise and the receiver. The class A model is suitable for narrowband noise (relative to receiver front-end bandwidth) and the class B model is suitable for broadband impulsive noise (relative to receiver front-end bandwidth). Class C refers to the noise environment when both Class A and Class B interferers are present. The Class C model has limited practical applications and is not extensively developed in the literature.

Middleton considered a set of impulsive noise sources distributed around a receiver as illustrated in Figure 4.2. These sources can be categorized as weak when their effect is benign, due to large distances between the source and receiver or simply low radiated power. It is assumed that electromagnetic radiation from the sources is Poisson distributed. The received signals from a large number of sources overlap allowing the application of the Central Limit Theorem (CLT). The noise distribution (for weak sources) therefore tends to a Gaussian shape. An environment with a large

number of independent weak noise sources, therefore, does not impose any performance degradation to the receiver designed to perform optimally in the Gaussian noise.

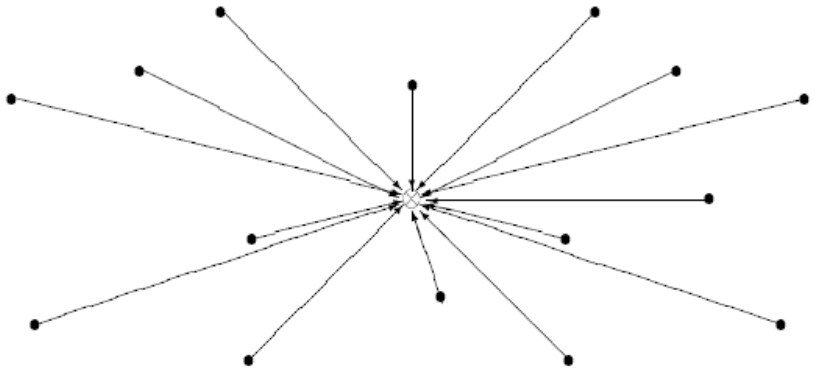

Figure 4.2 Middleton Noise Models – Depiction of multiple weak sources

In addition to weak sources which superpose and lose their individual characteristics, there is a second category of fewer but stronger, noise sources (illustrated in Figure 4.3) These may be strong either because of their short distance from the receiver or their relatively high level of radiated power. Such strong sources do not overlap sufficiently to lose their individual characteristics. The inclusion of the strong sources thickens the tails of the density function. For a noise environment with both strong and weak sources, the models proposed by Middleton represent good statistical tools.

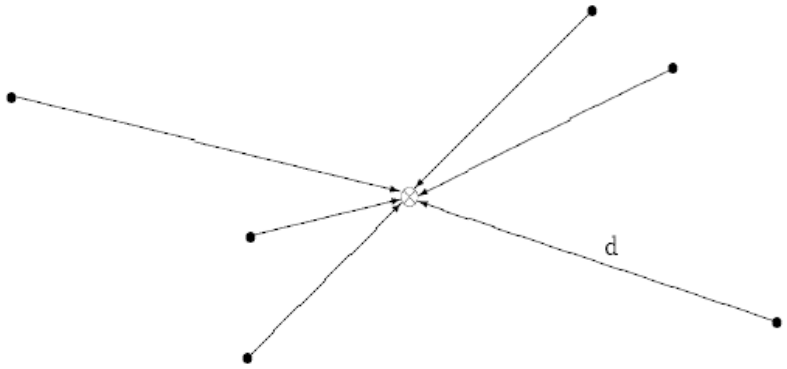

Figure 4.3 Middleton Noise Models – Depiction of strong noise sources

The same description of weak and strong sources can be extended to the noise environment of an electricity substation in which PD and switching/fault transients are the major, non-Gaussian, impulsive, noise sources. The inclusion of electromagnetic radiation from PD and switching/fault transients in the noise characterization modifies the overall distribution of the noise and invalidates a Gaussian distribution assumption.

Middleton noise models are based on the location and distribution of noise sources and their radiated power. The parameters of the noise models have physical meaning and provide better stochastic behaviour when compared to other non-Gaussian noise models.

There are a number of key assumptions made in the derivation of the Middleton noise models. These assumptions are:

1. There are two independent components (a) a small number of strong sources Poisson distributed (in time and space) and (b) zero-mean Gaussian noise which accounts for internal receiver noise and any external noise sources (including

large numbers of weak sources) which tend to a Gaussian distribution in accordance with the central limit theorem.

2. Phases uniformly distributed over 0-2π.
3. Far-field (Fraunhofer) condition.
4. Minimal relative motion between sources and the receiver (i.e. negligible Doppler effects).

Note that the above assumptions do not require the noise sources or the receiving antenna to be omnidirectional.

Middleton has used the Rayleigh Probability Presentation (RPP) for the representation of densities of the noise models [63]. RPP is a log-log representation of the amplitude exceedance probability. In an RPP plot, thermal noise appears as a straight line with a gradient of -0.5. The ordinate shows the rms voltage envelope and the abscissa displays the time fraction that the envelope exceeds the ordinate. The difference between Class-A and Class-B noise models and the significance of RPP are now addressed.

4.3.1 Middleton Class-A Noise Model

Class-A noise represents impulsive noise with a spectrum that is narrow compared to the receiver bandwidth and includes all pulses which do not produce transients in the receiver's RF and IF stages [10]. Thus, the receiver filter passes the impulsive components and the parameters of the model can be interpreted in terms of physical mechanisms which are generating this noise. Its PDF [11]is given by:

$$f(x) = e^{-A} \sum_{m=0}^{m=\infty} \frac{A^m}{m!\sqrt{2\pi\sigma_m^2}} e^{-\frac{x^2}{2\sigma_m^2}} \qquad \text{(Equation 4.9)}$$

where

$$\sigma_m^2 = \frac{\frac{m}{A} + \Gamma'}{1 + \Gamma'} \qquad \text{(Equation 4.10)}$$

The density function, given in Equation 4.9, for Middleton Class A noise, is obtained as an infinite sum of weighted Gaussian densities of different variances, where the weights decrease with increasing variance. For a variety of non-Gaussian noise environments, two or three terms of parameter *m* are sufficient where *m* determines the number of Gaussian densities to be included [64, 65]. The difference between the truncated Class A envelope distribution with *m* = 2 and 3 and the true envelope distributions is negligible for the expected range of the other Class A noise model parameter values [65]. Class-A noise has the following two parameters:

1) Impulsive index (*A*): which is the product of mean impulse rate and impulse duration and is similar to *vTp* discussed in Section 4.2. The density function of class-A noise has a Gaussian noise component and an impulsive, Poisson distributed noise component. The lower the value of *A* the more impulsive is the noise.

2) Scale Factor (*Γ'*): which is the ratio of power in the Gaussian noise component and the power in the impulsive noise component.

$$\Gamma' = \frac{(X_G^2)}{(X_I^2)} \qquad \text{(Equation 4.11)}$$

Figure 4.4 and 4.5 show the PDF of Class-A noise with a fixed value of Γ' ($\Gamma' = 0.001$) and four values of A. $\Gamma = 0.001$ corresponds to highly impulsive noise. Class-A noise model has been used to evaluate a wide variety of modulation and error control coding techniques for communication systems operating in impulsive noise environments [66-70].

The values of these parameters are estimated from the impulsive noise database compiled from the measurements made in the Strathaven electricity substation.

4.3.2 Middleton Class-B Noise Model

Class-B noise refers to impulsive noise, which is wideband when compared to the receiver bandwidth and can produce transients in the receiver front end. Its practical applications are limited because of its mathematical complexity. It requires the estimation of five parameters and an inflection point, which needs to be arrived at empirically. A practical alternative is to use Symmetric α-Stable (SαS) distributions. The resultant probability density function of the summation of zero-mean Gaussian noise and SαS (for $0 < \alpha < 2$) converges to the Class-B probability density function [71]. In this work, SαS process is used to model the broadband impulsive noise.

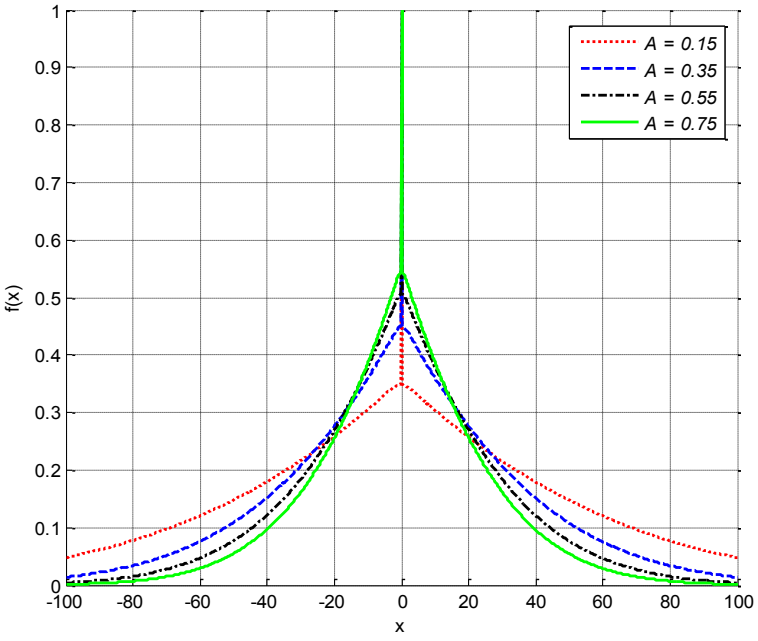

Figure 4.4 PDF of the Class-A noise model, for different values of A and Γ' = 0.001

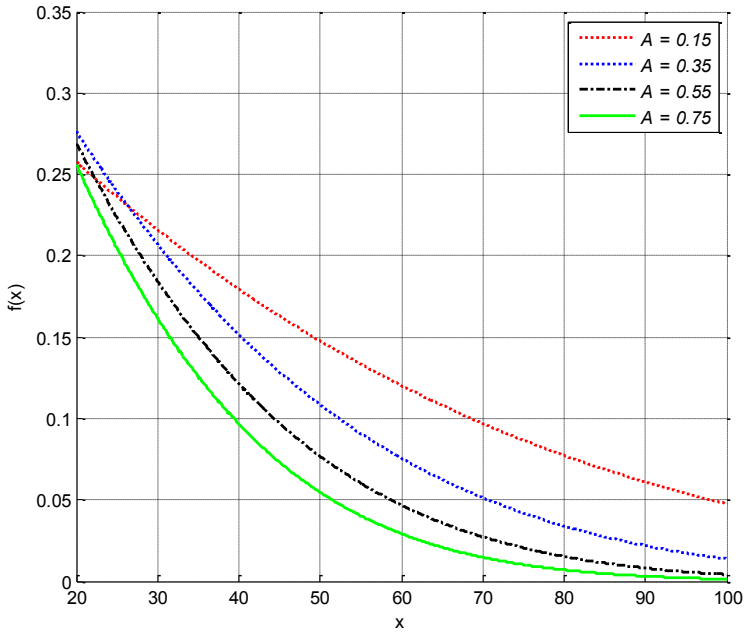

Figure 4.5 Tails of the density function of Middleton Class A noise model, for different values of A and Γ' = 0.001

4.4 Symmetric α-Stable (SαS) Noise Model

Stable random variables can be used to model a wide range of impulsive phenomena [72]. Some of their desirable properties for modelling impulsive phenomena are:

1. They conform to Generalized Central Limit Theorem (G-CLT) which states that '*if the sum of independent and identically distributed (i.i.d) random variables with or without finite variance converges to a distribution by increasing the number of variables, the limit distribution must belong to the family of stable laws'*.

   The Central Limit Theorem (CLT) describes the convergence of infinitely many independent i.i.d. random variables with a finite variance to a Gaussian distribution whereas the G-CLT describes the convergence of random variables with an infinite variance to non-Gaussian stable distributions.[12] [73].
2. Their PDF tails decay slower than the Gaussian PDF. This property makes them suitable for modelling impulsive phenomena as it is evident from the empirical data that impulsive phenomena have heavier tails [74, 75].

The SαS distribution is characterised by three parameters; α (the characteristic exponent), γ (the dispersion parameter) and δ (the location parameter). The SαS distribution includes the Gaussian distribution as a limiting case (when the characteristic exponent α = 2):

$$f(w) = e^{j\delta w - \gamma |w|^{\alpha}} \qquad \text{(Equation 4.12)}$$

where $0 < \alpha < 2$, $\gamma > 0$ and $-\infty < \delta < \infty$. Its PDF is given by:

$$f(x) = \frac{1}{2\pi} \int_{-\infty}^{\infty} e^{(j\delta w - \gamma |w|^{\alpha})} e^{-jwx} dw \qquad \text{(Equation 4.13)}$$

The characteristic exponent or shape parameter α controls the decay gradient of the PDF tails. For small values of α, the tails decay slowly corresponding to a highly impulsive process. For α = 2, the SαS distribution reduces to the Gaussian distribution while, for $\alpha = 1$, it reduces to the Cauchy distribution.

The dispersion parameter γ controls the spread of the distribution around its location (determined by δ). It can have any positive value and has a similar role to the variance in a Gaussian distribution. (For $\alpha = 2$, the Gaussian case, γ is equal to half of the variance).

The location parameter is the point of symmetry of the SαS PDF. It is equal to the mean of the distribution when $1 \leq \alpha \leq 2$.

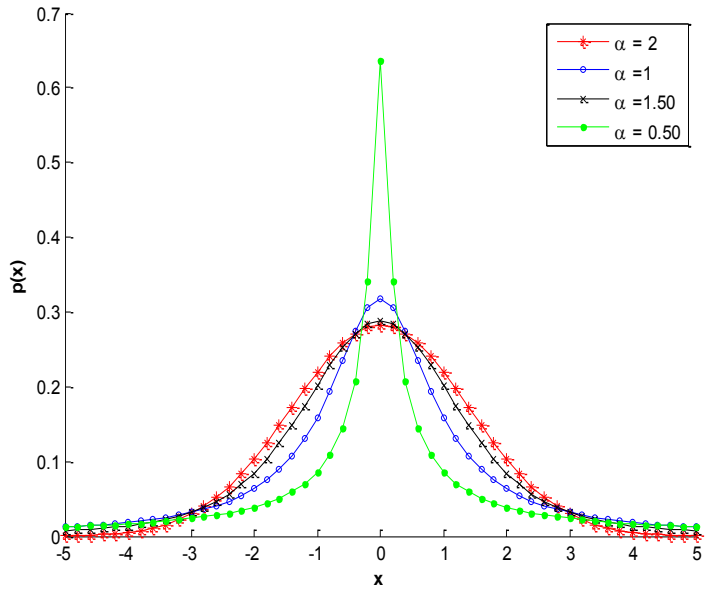

Figure 4.6 SαS PDF curves for different value of the characteristic exponent (α)

General closed-form expressions for the SαS density and distribution functions are not known, apart from the special cases of Gaussian ($\alpha = 2$) and Cauchy ($\alpha = 1$). Its density function can, however, be expanded as a convergent power series [76]. The standard SαS density function is given by Equation 4.14.

$$f(x) = \begin{cases} \frac{1}{\pi x}\sum_{k=1}^{\infty}\frac{(-1)^{k-1}}{k!}\Gamma(\alpha k+1)x^{-\alpha k}\sin(\frac{k\alpha\pi}{2}) & \text{for } 0<\alpha<1 \\ \frac{1}{\pi(x^2+1)} & \text{for } \alpha = 1 \\ \frac{1}{\pi\alpha}\sum_{k=0}^{\infty}\frac{(-1)^{k}}{2k!}\Gamma(\frac{2k+1}{\alpha})x^{2k} & \text{for } 1<\alpha<2 \\ \frac{1}{2\sqrt{\pi}}\exp[-\frac{x^2}{4}] & \text{for } \alpha = 2 \end{cases} \quad (4.14)$$

where Γ( ) is the gamma function:

$$\Gamma(x) = \int_0^{\infty} t^{-1}e^{-t}dt \quad \text{(Equation 4.15)}$$

The PDF curves of the SαS for different values of the characteristic exponent α are shown in Figure 4.6 to illustrate the impact of the value of α on the shape of the PDF curves.

4.5 Selection of Models

The most common impulsive noise models used in the literature are Middleton's Class-A and Class-B as described in the previous section [10]. In addition to Middleton models, a variety of impulsive noise models based on the statistical description of measured data have been used for modelling non-Gaussian noise

processes [77, 78]. These models are environment specific thus cannot be generalised or applied to other impulsive noise environments.

Given the complexity of ETS noise environment, properties of Middleton Class-B noise model, and its mathematically convenient and equivalent SαS based model, is suggested to be a good choice to model this type of noise environment [72]. This model selection is based on the following points:

1. PD results in the generation of a series of current pulses which contribute to the impulsive noise component of the overall ETS noise profile. The technical literature, e.g. [10] encourages the use of Middleton Class-B noise model which is implemented in this work as an equivalent SαS based model.
2. Amplitude distribution based models for impulsive noise, e.g. higher order hyperbolic, Weibull, Pareto, exponential, log-normal, and Rayleigh have been proposed [58, 75, 79, 80]. However, none of these offers a good fit for the ETS data. A statistical comparison of the best four representative distributions is shown in Figure 4.7 and Table 4.1.

   The plot in Figure 4.7 includes the CDF of ETS noise amplitude data (recorded over the month of August 2008) and the top four representative distributions. The ranking is based on the goodness of distribution-fit that is evaluated using the Bayesian Information Criterion (BIC). The BIC is a log-likelihood based distribution (or model) selection criterion which selects the best-fit distribution from a set of potential distributions. The distribution set which is used for model selection includes normal, higher order hyperbolic (Mertz [58]), t-Location Scale,

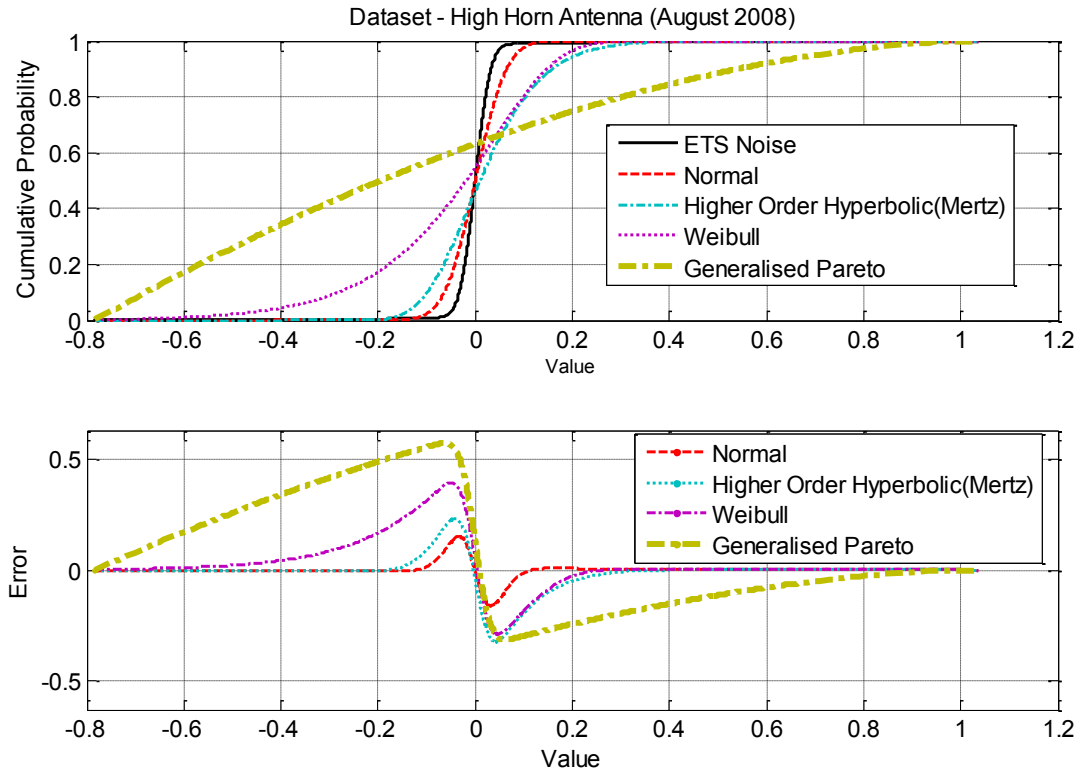

Figure 4.7 CDF comparison of candidate heavy-tailed distributions for impulsive noise modelling.

Extreme Value, Generalised Pareto, Weibull, and Logistic. BIC can be defined as:

$$BIC = 2\ln(\hat{L}) + k\ln(n) \qquad \text{(Equation 4.16)}$$

where n is the dataset size, k is the number of free parameters to be estimated and $\hat{L}$ is the maximum likelihood of a model selected from the distribution set. The smaller the BIC value is, the better is the model.

Table 4.1 Goodness of fit comparison of top three candidate heavy-tailed distributions for impulsive noise modelling (Dataset – August 2008).

Distribution	**Goodness of Fit Metric** (BIC - Bayesian Information Criterion)
Normal	-4.5256e+005
Higher Order Hyperbolic (Mertz)	-3.3571e+005
Weibull	-2.1427e+005
Generalised Pareto	1.3359e+005

3. Noise measurements are detailed in Chapter 3 and statistics of the recorded data have been reported in [81]. A comparison of the data generated from a model built from the statistics of measurement data and estimated statistics of the measured data shows the weakness of a model based on the set of well-known set of distributions. The weakness of this model lies in the statistical variation among data sets recorded on different days/time. As is stated earlier, this approach lacks generalisation and leads to a model which can fit a certain dataset (recorded on a certain time and date) but fails when used to fit different datasets. Table 4.2 shows a comparison of datasets from seven months (August 2008 to February 2009). It includes a first best-fit distribution and corresponding BIC score. It is apparent that none of the distributions from the selected set of heavy-tailed distributions fits the data.

Table 4.2 Best-fit distribution comparison of all measurement datasets

Dataset	Best-Fit Distribution	Goodness of Fit Metric (BIC - Bayesian Information Criterion)
August 2008	Normal	-4.5256e+005
September 2008	Normal	-1.5663e+005
October 2008	Extreme value	-4.0590e+005
November 2008	Normal	-4.5624e+005
December 2008	t-location scale	-4.3963e+005
January 2009	Logistic	-1.2693e+005
February 2009	Normal	-1.8734e+005

4.6 Model Parameter Estimation

In this section, some of the parameter estimation techniques for the Middleton Class A and SαS models are introduced.

4.6.1 Class A Estimation Techniques

The parameter estimation challenge for the Class-A noise model has been the focus of research in many studies and a number of estimation methods have been derived [63, 64, 82-86].

Middleton has proposed two parameter estimation methods for the Class-A model. The first is based on an empirical approximation of the distribution function and the second is based on the moments of the data [82]. Middleton's empirical approximation estimation method has been extended by Zabin and Poor and they have derived an efficient threshold comparison estimation method [83].

A typical Class-A envelope distribution for parameter values of A = [0.10, 0.20, 0.30] and, Γ' = 0.001, is shown in Figure 4.8 [83] and it can be seen that the distribution function curve has the following three distinct regions:

1. Gaussian region: the region of lower values of the distribution function corresponding to the background Gaussian noise or the measurement values where the Gaussian noise component is dominant.
2. Null region: the middle region of distribution function where the probability $P(Z > z_0)$ has insignificant variation.
3. Impulsive region: the region of higher values of the distribution function where the impulsive noise component is dominant. A threshold value can be set to mark the point where the distribution function departs from the straight-line.

In the threshold comparison method, the estimated parameters are A and K instead of A and Γ, where K is an approximate product of A and Γ. The estimation process can be described as follows:

Step 1: Divide the ETS measurements dataset (Z) into two sub-datasets, based on the threshold (T_{IB}). The sub-dataset, which has values above the threshold, represents impulsive noise component (denoted as Z_I) and the dataset, which has values below the threshold, represents the background noise (denoted as Z_B).

Step 2: Estimate the value of A from these two datasets using:

$$\bar{A} = \frac{n_I}{n} \qquad \text{(Equation 4.17)}$$

where n_I is the length[4] of impulsive sub-dataset (Z_I) and n is the length of the measurements dataset (Z).

Step 3: Estimate K as the ratio of average energy in the background and impulsive noise datasets, which can be written as:

$$\overline{K} = \left(\frac{1}{n_B}\sum_{i=1}^{n_B} Z_B(i)\right)^2 \Big/ \left(\frac{1}{n_I}\sum_{i=1}^{n_I} Z_I(i)\right)^2 \qquad \text{(Equation 4.18)}$$

For $A \geq 10^{-1}$; $\Gamma \leq 10^{-3}$, the estimated value of A is the value on the abscissa, corresponding to the start of the sharp increase in the distribution function or the point where the distribution function starts to depart from the straight-line behaviour [83].

An envelope distribution curve for the ETS measurements data[5] has also been included in Figure 4.8 and it can be observed from figure labels that the values of threshold (T_{IB}) and A are -15 dB (~0.178) and ~0.25 respectively.

The second parameter estimation method, derived by Middleton for Class-A, is based on the higher moments of the measurements data. The values of parameters A and Γ can be estimated using Equation 4.19 and 4.20 respectively [82].

[4] Length in terms of number of values in the dataset

[5] The measurement data is the PD noise recorded using HB TEM horn antenna, over the period from the August 2008 to February 2009. The total number of datasets used is 345 where each dataset has approximately 300 observations.

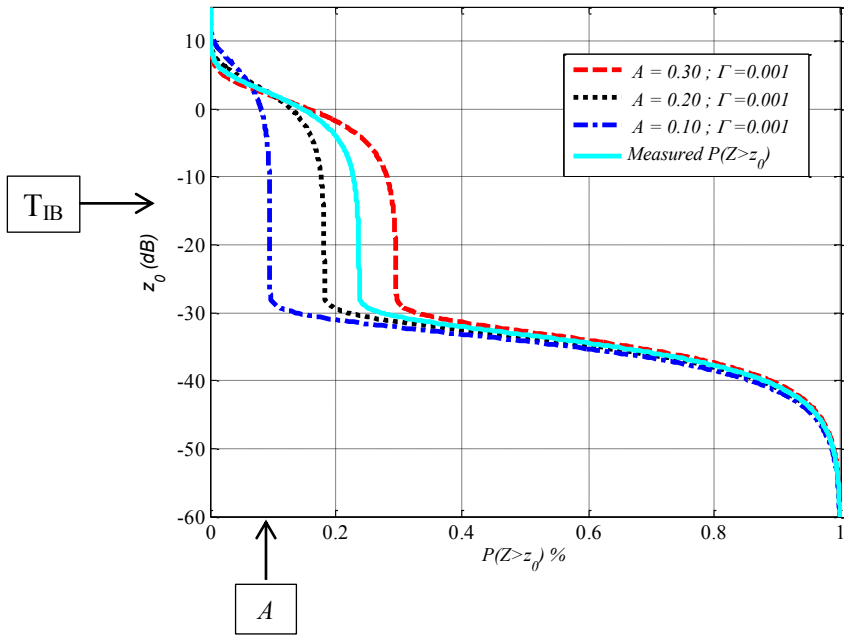

Figure 4.8 Envelope probability distribution [*P (Z > z_0)*] of Class-A and ETS noise.

$$\bar{A} = 9(e_4 - 2e_2^3)^3 \,/\, 2(e_6 - 12e_2^3 - 9e_2e_4)^2 \qquad \text{(Equation 4.19)}$$

$$\bar{\Gamma} = (2e_6 + 12e_2^3 - 9e_2e_4) \,/\, 3(e_4 - 2e_2^2)^3 \qquad \text{(Equation 4.20)}$$

where e_2, e_4 and e_6 denote second, fourth and sixth moments of the ETS measurements data.

Zabin and Poor developed another parameter estimation method for the Class-A noise model, based on the Expectation Maximization (EM) algorithm [84]. In this method, the envelope pdf of Class-A model has been described in the form of a sum of weighted probability densities. If Θ is the set of parameters A and K (where $K = A\Gamma$), then the envelope pdf can be written as:

$$w(z) = \sum_{j=1}^{\infty} \pi_j(A) h_j(z, \Theta) \qquad \text{(Equation 4.21)}$$

The envelope pdf of the Class-A model after Equation 4.9 is:

$$w(z) = \left\{ 2e^{-A} \sum_{m=0}^{\infty} \frac{A^m}{m!\,\sigma_m^2} z e^{-\frac{z^2}{\sigma_m^2}} \right. \quad \text{(Equation 4.22)}$$

then the $\pi_j(A)$ and $h_j(z, \Theta)$ for Class-A model can be written as:

$$\pi_j(A) = \frac{e^{-A}\, A^{(j-1)}}{(j-1)!}$$

$$h_j(z, \Theta) = 2z \left(\frac{A+K}{(j-1+K} \right) e^{-z^2 \frac{A+K}{j-1+K}} \quad \text{(Equation 4.23)}$$

The EM algorithm is a two-step process where step-1 is an evaluation of the expected value of log-likelihood function $Q(\Theta|\Theta^{(p)})$. For the Class-A model, this is given by Equation 4.24 [84].

$$Q(\Theta|\Theta^p) = \sum_{i=1}^{N-1} \sum_{j=1}^{\infty} a_{ij}[-A + (j-1)\ln(A) - \ln(j-1)\,!]$$

$$+ \sum_{i=1}^{N-1} \sum_{j=1}^{\infty} a_{ij} \left[\ln(2z_i) + ln\left(\frac{A+K}{j-1+K}\right) - z_i^2 \left(\frac{A+K}{j-1+K}\right) \right] \quad (4.24)$$

where, using Equation 4.23, a_{ij} is

$$a_{ij} = \frac{\pi_j(A) h_j(z_i, \Theta^p)}{\sum_{j=1}^{\infty} \pi_j(A) h_j(z_i, \Theta^p)} \quad \text{(Equation 4.25)}$$

Step-2 of the EM algorithm is to determine $\Theta = \Theta^{(p+1)}$ to maximize $Q(\Theta|\Theta^{(p)})$. This is an iterative process. First, the value of *K* is fixed to maximize *A,* and then the value of *A* is fixed to maximise *K.* The value of parameters estimated using the method of moments are used to initialize the EM algorithm.

The estimated Class A parameters for ETS noise are given in Table 4.3. These parameter values are used in Chapter 6 for generation of the narrowband impulsive noise.

Table 4.3: Estimated Class A Model Parameters for ETS Noise

Method	Parameter Value	
	A	Γ
Envelope distribution method	0.253	0.2408
Method of moments	0.132	0.2931
EM based method	0.141	0.2291

4.6.1.1 Validation

The accuracy of the parameter estimation techniques is validated using the following two test cases. The validation process is illustrated in Figure 4.9.

4.6.1.1.1 Test Case 1

Class A noise datasets are generated using a known set of parameters and three estimation techniques are applied to estimate the parameters. The estimated parameters are compared against the known parameters.

The estimation results of the parameters A and Γ are shown in Figure 4.10 and Figure 4.11 respectively. It can be seen that the EM based estimation method has better overall performance as it gives the minimum estimation error (the difference between the actual and estimated value) among the three estimation techniques.

4.6.1.1.2 Test Case 2

The three estimation techniques are applied to the ETS measurement dataset and the estimated parameters are used to generate a Class A noise dataset. For validation,

Amplitude Cumulative Distribution (ACDF) curves are compared for the both real and Class A noise datasets generated using the estimated parameters.

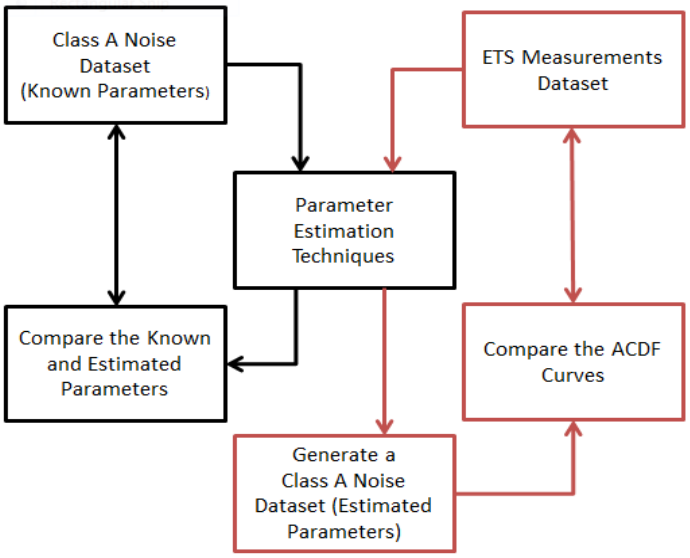

Figure 4.9: Illustration of parameter estimation validation

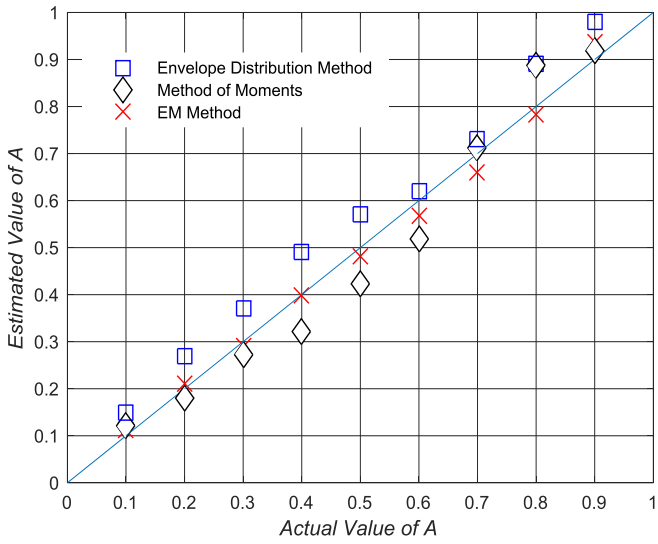

Figure 4.10: Test Case 1 – Estimation of the parameter A when $\Gamma = 0.005$.

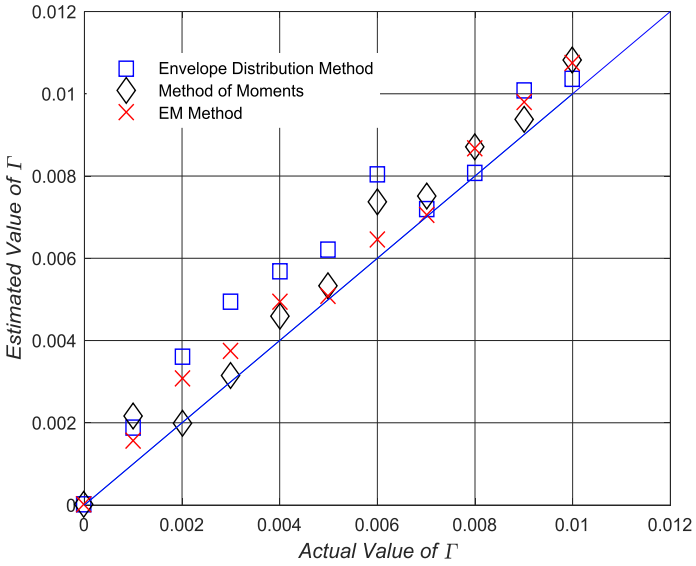

Figure 4.11: Test Case 1 – Estimation of the parameter Γ when $A = 0.35$.

The results of ACDF comparison are shown in Figure 4.12. The comparison shows the similarity between the ETS measurements dataset and the Class-A noise dataset, with the parameters, estimated from the envelope distribution, moments and EM based methods. It is apparent that either the Method of moments or the EM based method can be used for the parameter estimation.

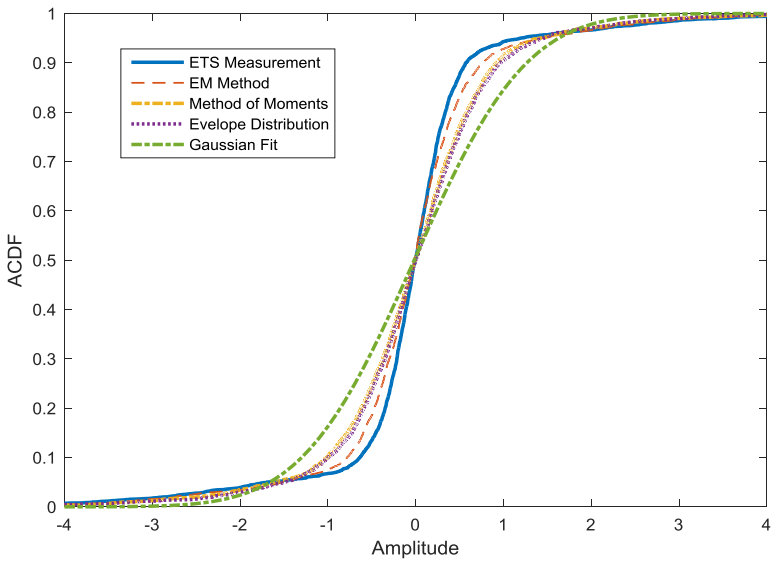

Figure 4.12 Comparison of the ETS ACDF and Class-A ACDF

4.6.2 SαS Model Estimation Techniques

The challenge of SαS parameter estimation has been addressed by many authors over the past four decades and the proposed estimation techniques are based on either the quantile of the dataset or the Fractional Lower Order Moments (FLOM).

Fama and Roll [87] have proposed a quantile-based parameter estimation technique, where the p^{th} quantile of a dataset is defined as the value of x_p for which $f_x(p) = p$. The disadvantages of this technique are that it limits the value of characteristic exponent (α) to be greater than 1 and the estimated parameters are biased, even when

measurements are within the valid range. McCulloch [88] suggested another quantile-based technique which removed the asymptotic estimate biasing and allows the range of α to be ($0.5 \leq \alpha \leq 2$).

The FLOM is a property of SαS and there is a one-to-one relationship between the SαS parameters and FLOMs i.e. each set of distribution parameters has a unique set of FLOMs. It is defined as:

$$E(|Z|^p) < \infty \ for \ p < \alpha \qquad \text{(Equation 4.26)}$$

Note that the parameter α controls the tails of the PDF and thus it can control the moments of the distribution. The FLOM can be estimated empirically [72, 89] as:

$$E|Z|^p = C(p,\alpha)\gamma^{\frac{p}{\alpha}} \qquad \text{(Equation 4.27)}$$

where

$$C(p,\alpha) = \frac{2^{p+1}\Gamma\left(\frac{p+1}{2}\right)\Gamma\left(\frac{-p}{\alpha}\right)}{\alpha\sqrt{\pi}\,\Gamma\left(\frac{-p}{2}\right)} \qquad \text{(Equation 4.28)}$$

There are two popular FLOM based estimation techniques. The first uses Log-FLOM [90, 91] and the second uses the asymptotic behaviour of the Extreme-Order Statistics (EOS) [76].

The first Log-FLOM technique uses the definition of the FLOM i.e. $E(e^{px})$ for $-1 < p < \alpha$ and the parameters can be estimated using:

$$E(Z) = C_e\left(\frac{1}{\alpha} - 1\right) + \frac{1}{\alpha}\log(\gamma) \qquad \text{(Equation 4.29)}$$

$$Var(Z) = \frac{\pi^2}{6\alpha^2} \qquad \text{(Equation 4.30)}$$

where C_e is the Euler constant.

The second EOS based technique estimates all three parameters and involves relatively simple computations. A description of this technique is as follows:

Let $X_1, X_2, \ldots, X_N$ be a measured series of independent samples from an SαS random variable with unknown values of α, γ and δ. The estimation procedure includes three algorithms. The first algorithm estimates δ. It does not need knowledge of α or γ. The second algorithm estimates α, using the estimated value of δ. The third algorithm estimates γ, using the estimates of α and δ.

The estimate of the location parameter is the sample median of the measurement series:

$$\hat{\delta} = median\{X_1, X_2, X_3, \ldots, X_N\} \qquad \text{(Equation 4.31)}$$

The estimate of the characteristic exponent α is calculated using three steps.

1. The centred data series is divided into L non-overlapping segments of equal length.

$$\{X_1 - \hat{\delta}, X_2 - \hat{\delta},, X_3 - \hat{\delta}, \ldots, X_N - \hat{\delta}\} = \{X(1), X(2), X(3), \ldots., X(L)\} \quad (4.32)$$

2. If $X_{(l,\,max)}$ and $X_{(l,\,min)}$ are the maximum and minimum of the l^{th} data segment and the $\overline{X}_l$ and $\underline{X}_l$ are:

$$\overline{X}_l = \log\left(X_{(l,max)}\right) \; and \; \underline{X}_l = \log\left(X_{(l,min)}\right) \qquad \text{(Equation 4.33)}$$

The standard deviations of $\overline{X}_l$ and $\underline{X_l}$ are calculated in the usual way:

$$\overline{s} = \sqrt{\frac{1}{(L-1)}} \sum_{i=1}^{l} (\overline{X}_l - \overline{X})^2 \qquad \text{(Equation 4.34)}$$

$$\underline{s} = \sqrt{\frac{1}{(L-1)}} \sum_{i=1}^{l} (\underline{X_l} - \underline{X})^2 \qquad \text{(Equation 4.35)}$$

where

$$\overline{X} = \frac{1}{L} \sum_{l=1}^{L} \overline{X}_l \;\; and \;\; \underline{X} = \frac{1}{L} \sum_{l=1}^{L} \underline{X_l}$$

3. Finally, the estimate of the characteristic exponent (α) is calculated using:

$$\hat{\alpha} = \frac{\pi}{2\sqrt{6}} \left(\frac{1}{\overline{s}} + \frac{1}{\underline{s}} \right) \qquad \text{(Equation 4.36)}$$

4. The estimation of the dispersion (γ) parameter based on the theory of fractional lower order moments [17] is calculated from:

$$\hat{\gamma} = \left[\frac{\frac{1}{N} \sum_{k=1}^{N} \left| X_k - \hat{\delta} \right|^p}{C(p, \hat{\alpha})} \right]^{\frac{\hat{\alpha}}{p}} \qquad \text{(Equation 4.37)}$$

where $C(p, \hat{\alpha})$ is given by Equation 4.25 and the recommended order of fractional moment p is 1/3 of the estimated value of the characteristic exponent (α).

$$C(p, \hat{\alpha}) = \frac{\Gamma\left(1 - \frac{p}{\hat{\alpha}}\right)}{\cos\left(\frac{\pi}{2} p\right) \Gamma(1-p)} \qquad \text{(Equation 4.38)}$$

These two FLOM based techniques are used in this work for the estimation of the SαS model.

4.6.2.1 Validation

A similar validation process to that previously illustrated in Figure 4.9 is adopted in order to evaluate the accuracy of the two FLOM methods.

4.6.2.1.1 Test Case 1

SαS datasets are generated using a known set of parameters and the two FLOM based estimation techniques are applied to estimate the parameters. The estimated parameters are compared against the known parameters.

The estimation results are shown in Figure 4.13 and Figure 4.14. The performance of the EOS-FLOM technique is satisfactory whereas Log-FLOM under-estimates the value of α by 10%. Since the same dataset is used (α is estimated first and the estimated value used to compute γ) for the estimation of γ, an over-estimation of γ by roughly the same amount can be seen in Figure 4.14.

4.6.2.1.2 Test Case 2

The two estimation techniques, Log-FLOM and EOS-FLOM, are applied to the ETS measurements dataset and the estimated parameters are used to generate an SαS dataset. For validation Amplitude Cumulative Distribution Function (ACDF) curves are compared for both the real ETS data and the emulated SαS dataset, generated using the estimated parameters.

The results of ACDF comparison are shown in Figure 4.15. The comparison shows that the parameters estimated using EOS-FLOM provide the best fit CDF curve.

The estimated parameter values of the ETS measurement data sets are recorded in Table 4.4. These parameters are used in Chapter 6, for the generation of the broadband impulsive noise.

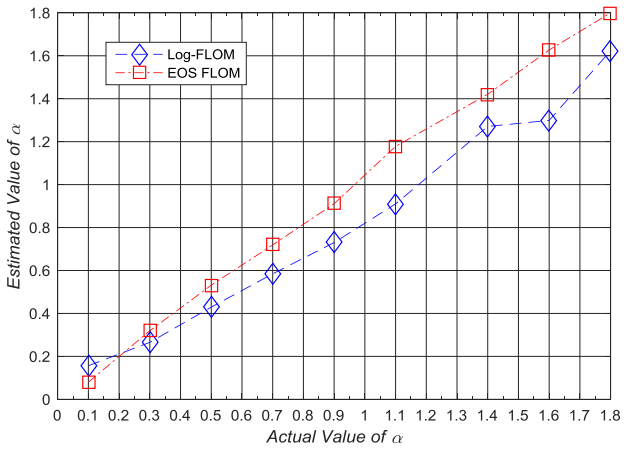

Figure 4.13: Estimation of α when γ = 0.0015 and δ = 0

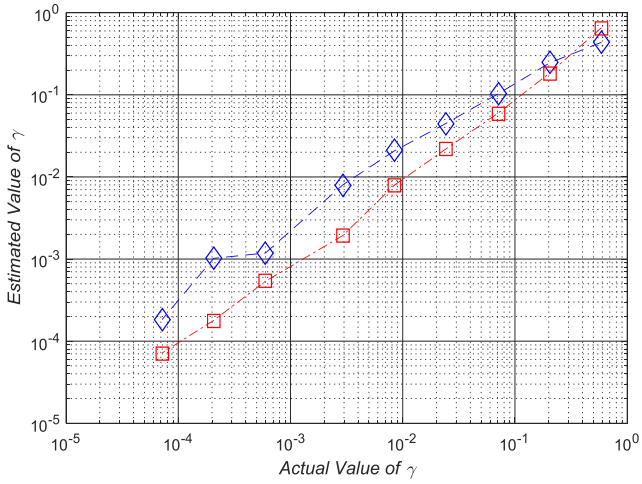

Figure 4.14: Estimation of γ when α = [0.1 (0.2) 0.8] and δ = 0

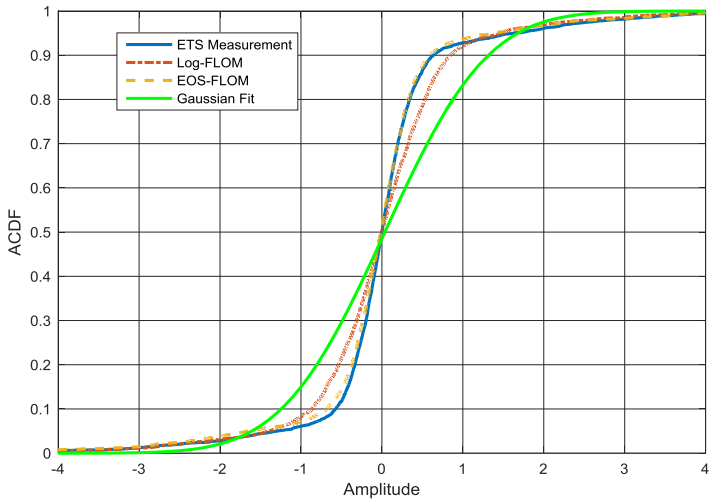

Figure 4.15 Comparison of the ACDF of ETS measurements noise dataset and ACDF of the SαS dataset generated using the estimated parameters

Table 4.4: Estimated parameters of SαS broadband impulsive noise model for electricity transmission substations

Parameters	Estimated Value
Location Parameter (δ)	1.1805E-7
Characteristic Exponent (α)	1.4130
Dispersion (γ)	6.3422E-7

4.7 Summary

Impulsive noise modelling, not restricted to but including the seminal work of Middleton, has been reviewed. The practicality of applying Middleton's models has been discussed and the use of a Symmetric α-Stable (SαS) distribution as a

mathematically-tractable alternative to Middleton's Class-B model for application to electricity substations noise environment has been proposed.

Parameter estimation techniques for both Middleton Class A and SαS noise models are detailed and their performance is evaluated. The parameters for the ETS measurements data are computed for both narrowband (Class A) and broadband (SαS) impulsive noise models to be used in the performance assessment of candidate short-range wireless technologies in Chapter 6.

CHAPTER 5

PHYSICAL LAYER MODELS AND SIMULATIONS

5.1 Introduction

Computer simulations are an effective tool for the design and validation of electronic systems. They serve as a first step in the prototyping of a system. In communication systems, information is processed at the transmitter prior to be sent to the receiver through a noisy medium or channel. The objective of the processing at the transmitter is, in part, to make the signal resilient to additive noise, system non-linearities and channel variations. The receiver is designed to mitigate the effects of the channel, reverse the transmitter processing and thus retrieve the source information.

Traditionally communication systems are designed using analytic expressions for noise characteristics, system non-linearities and channel effects. This design process provides insight into the effects of only a relatively restricted set of noise and interference environments.

Computer simulations provide an alternative that allows communication system performance to be assessed against a greater range of system parameters, noise characteristics and channel impairments [92]. Modelling of a communication system using simulation tools typically employs a modular approach in which each signal processing task is implemented as a block. Parameters of each block are variable. MATLAB and Simulink are widely-used digital modelling tools for communication

systems and they have a number of built-in functions which can be used or tailored to perform different signal processing tasks; e.g. generation of random numbers, coding, modulation, and filtering.

Simulink has a wide range of blocks for the implementation of Physical (PHY) layer communication protocols. While Omnet and NS3 might be software packages of choice for simulation of the Network and higher layers, Simulink might be considered especially appropriate for the simulation of PHY layer communication protocols [93]. It is flexible and allows incorporation of the blocks designed by the user. Algorithms and procedures can be implemented (coded as s-functions) in MATLAB and used in Simulink with the built-in blocks. S-functions make the basis of Simulink blocks and can be written in C or MATLAB.

The three short-range wireless technologies which are evaluated in this work, for their deployment in noise intensive environment of an electricity substation, are WLAN, Bluetooth and Zigbee. The PHY models of these wireless technologies are implemented using MATLAB and Simulink. The validation of these PHY models has been carried out by comparing the theoretically expected and computed Bit Error Rates (BER). The details of implementation and validation are presented in this chapter. The structure of the work described in this chapter is illustrated in Figure 5.1.

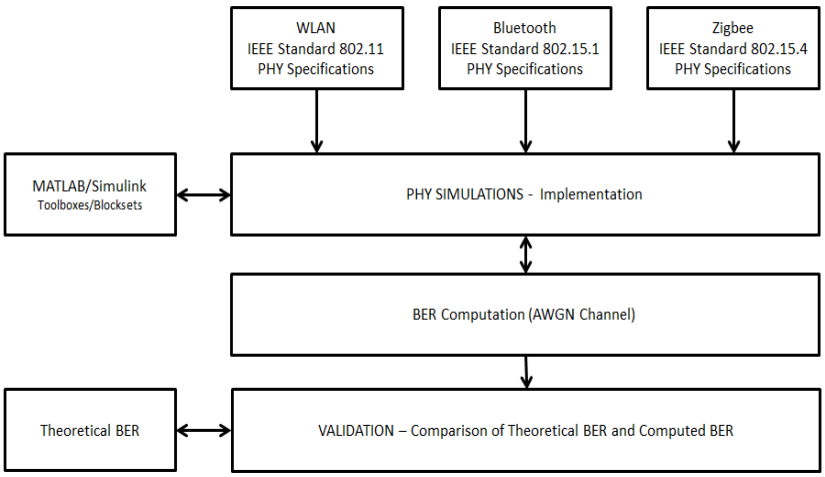

Figure 5.1: Overview of the PHY Layer Simulations

The rest of the chapter is organised as follows: Section 5.2 covers the three IEEE 802.11 PHY Layer variants of a WLAN whereas sections 5.3 and 5.4 provide a detailed description and validation of Bluetooth and ZigBee PHYs.

5.2 WLAN

The base standard for WLAN is IEEE 802.11 which was released in 1997. It standardised the two bottom layers of the seven-layer Open Systems Interconnection model (OSI) for WLAN communications The lowest two layers of the OSI model are PHY and Medium Access Control (MAC) [94, 95].

PHY layer provides the interface between the MAC and the wireless media through following two functional entities:

1. Physical Layer Convergence Protocol (PLCP) adds a PHY header to the MAC protocol data unit (MPDU). The MPDU is composed of data units passed down from higher layers e.g. Network and Transport.
2. Physical Medium Dependent (PMD) performs the necessary signal processing (modulation, spreading, error coding, pulse shaping etc.) before transmitting the signal over the wireless medium.

The IEEE 802.11 base standard operates in the 2.4 GHz frequency band and supports data rates of 1 and 2 Mbps. It employs Differential Phase Shift Keying (D-PSK) modulation and Direct Sequence Spread Spectrum (DSSS).[94].

The following four PHY extensions of the base standard have been released since 1997:

1. IEEE 802.11b, which employs Complementary Code Keying (CCK) modulation, supports data rates of 5.5 and 11Mbps and operates in the 2.4 GHz frequency band.
2. IEEE 802.11a which employs Orthogonal Frequency Division Multiplexing (OFDM) modulation and convolutional Forward Error Correction (FEC), supports data rates of up to 54 Mbps and operates in the 5 GHz frequency band [96].
3. IEEE 802.11g which uses CCK and OFDM modulations, supports data rates of up to 54 Mbps, operates in the 2.4 GHz frequency band and has three operational modes. These are (1) legacy mode – which is backward compatible with IEEE 802.11b CCK (2) mixed mode – in which the transceiver can switch between IEEE 802.11b CCK and IEEE 802.11a OFDM (3) New mode – in which all devices in the network are IEEE 802.11g enabled. The achieved data rate and

throughput are very comparable to the IEEE 802.11a OFDM devices operating at 5 GHz.

4. IEEE 802.11n which employs antenna arrays for transmission and reception and uses space diversity to achieve the high rates of up to 600 Mbps and operates in the 2.4 and 5 GHz frequency bands. Support for the operation at 5 GHz is optional. IEEE 802.11n is not assessed in this thesis due primarily to the need to restrict its scope to the time and resource available[6].

A comparison of the specifications of the four IEEE 802.11 PHY extensions and the base standard is shown in Table 5.1.

Table 5.1: Specifications of the IEEE 802.11 PHY Extensions

Release year	PHY Extensions	Frequency Band (GHz)
1997	Base standard (IEEE 802.11)	2.4
1999	OFDM PHY (IEEE 802.11a)	5
1999	HR DSSS PHY (IEEE 802.11b	2.4
2003	IEEE 802.11g	2.4
2009	IEEE 802.11n	2.4 and 5

5.2.1 WLAN DSSS PHY

The DSSS PHY is one of the three PHYs which were introduced in the base standard and the remaining two PHYs are Frequency Hopping Spread Spectrum (FHSS PHY) and Infrared PHY (IR PHY). Given the limited applications of IR PHY and inclusion of an FHSS based Bluetooth receiver in this work, only DSSS PHY has been

[6] The research can be extended in future and impulsive noise models employed to assess the performance of MIMO systems. IEEE 802.11n is one example of MIMO where antenna arrays are used for the transmission and reception.

included in the performance evaluation work. The description of DSSS PHY is structured into three subsections which are Framing, Modulation and Spreading.

5.2.1.1 PHY Framing

The PHY protocol data unit (PPDU) comprises 144-bit PLCP preamble,

48-bit PLCP header and a PHY service data unit (PSDU) of variable length. The length of PSDU is dependent on the data rate. The composition of the PPDU is shown in Table 5.2.

The PLCP preamble consists of SYNC (128 bit) and SFD (16 bit) fields. SYNC sequence is a string of 1s which is scrambled before transmission and is used by the receiver to synchronise its carrier tracking and timing. SFD (Start of Frame Delimiter) indicates the end of PLCP header. It is common to use hexadecimal word 'F3A0' for SFD in all DSSS receivers.

The PLCP header consists of SIGNAL (8 bit), SERVICE (8 bit), LENGTH (16 bit) and CRC (16 bit) fields. SIGNAL is an indicator of the modulation technique to be used for the transmission and reception. The bit-by-bit functionality of the SERVICE field is shown in Table 5.3. LENGTH field carries the time in microseconds to transmit the PSDU. The SIGNAL, SERVICE and LENGTH fields are protected by CRC-16 frame check sequence. Equation 5.1 shows the representative polynomial for the CRC-16 algorithm.

$$G(x) = x^{16} + x^{12} + x^5 + 1 \qquad \text{(Equation 5.1)}$$

The receiver computes a CRC based on the SIGNAL, SERVICE and LENGTH fields and compares it with the value in the CRC field. This error detection and the

subsequent decision for retransmission or termination of the frame lies with the MAC layer.

Table 5.2: PLCP PPDU format

SYNC (128 bits)	**SFD** (16 bits)	**SIGNAL** (8 bits)	**SERVICE** (8 bits)	**LENGTH** (16 bits)	**CRC** (16 bits)	**PSDU** (variable length)
PLCP Preamble (144 bits)		PLCP Header (48 bits)				PSDU (variable length)
PPDU						

Table 5.3: SERVICE field definitions

B0	**B1**	**B2**	**B3**	**B4**	**B5**	**B6**	**B7**
Reserved	Reserved	Locked Clock bit 0-Not 1-Locked	Mod Selection bit 1-CCK 0-PBCC	Reserved	Reserved	Reserved	Length extension bit

5.2.1.2 Modulation

The Differential Binary Phase Shift Keying (DBPSK) and the Differential Quadrature Phase Shift Keying (DQPSK) are employed for 1 and 2 Mbps data rates respectively. The PLCP header and preamble is modulated using DBPSK at 1 Mbps whereas the PSDU is modulated using either of DBPSK or DQPSK to achieve the required data rate.

DBPSK is a variant of BPSK. In BPSK the phase of a constant amplitude carrier switches between 0° and 180°. In DBPSK, information is carried as the phase difference between the consecutive bits. For example, if the phases of the current bit

(b_k) and a previous bit (b_{k-1}) are φ_k and φ_{k-1} respectively, the DBPSK phase assignment can be written in the form of Equation 5.2 [97].

$$\varphi_k = \varphi_{k-1} \qquad if\ b_k = 1$$
$$\varphi_k = \varphi_{k-1} + \pi \qquad if\ b_k = 0 \qquad \text{(Equation 5.2)}$$

The implementation of a DBPSK modulator involves differential encoding of the binary data prior to BPSK modulation and the rule for differential encoding is:

$$d_k = \overline{b_k \oplus d_{k-1}} \qquad \text{(Equation 5.3)}$$

DQPSK is a variant of QPSK. In QPSK, the signal moves among four phases which are 90° apart and has four states on an I/Q diagram. Both I and Q components can carry binary digits enabling a QPSK symbol to carry two bits. It is equivalent to the transmission of two DBPSK symbols, one on each of the I and Q components.

The signal constellations (I/Q diagrams) of DBPSK and DQPSK are shown in Figure 5.2 and Figure 5.3 respectively.

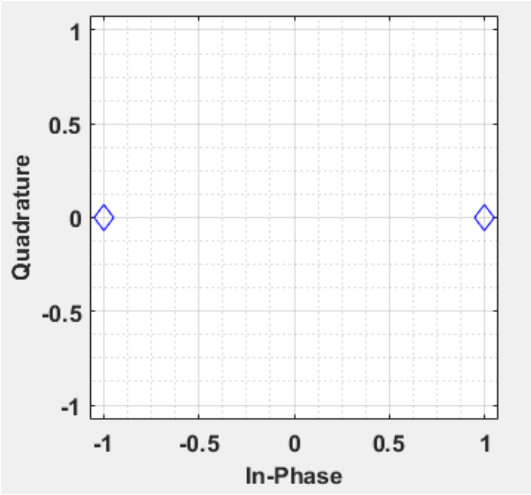

Figure 5.2 DBPSK signal constellation

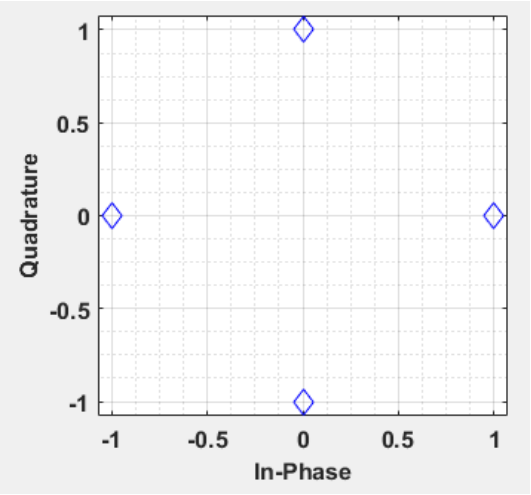

Figure 5.3 DQPSK signal constellation

5.2.1.3 PHY Spreading

Spreading is a technique where signal energy is spread over a wider bandwidth compared to the bandwidth of the information signal. In DSSS PHY, a Barker sequence, where each information bit is converted to an 11 digit Barker code, is used for the spreading. The Barker word used in DSSS is [+1.-1,+1,+1,-1,+1,+1,+1,-1,-1,-1] and has optimally low correlation at all offsets except zero. The autocorrelation of this Barker word is 11 at 0 offset and it is 0 or -1 at all other offsets [98].

The Barker word is passed through a Modulo-2 adder together with each information bit at the transmitter. This spreading process increases the number of physical pulses (referred to as chips) by a factor of 11. In the frequency domain, the signal is spread over a wider bandwidth with a lower RF power spectral density.

At the receiver, the signal is correlated with the same 11-chip Barker word to recover the information bits. In-band interference is spread such that much of its energy then falls outside the collapsed signal bandwidth and, thus, is removed.

The ratio of spread bandwidth and de-spread bandwidth is called processing gain:

$$P_{(gain)} = 10log_{10}(Chip\ rate/Bit\ rate) \qquad \text{(Equation 5.4)}$$

5.2.1.4 PHY Simulation Model

A block diagram of DSSS PHY transmitter and receiver showing the functional blocks of both the transmitter and receiver is given in Figure 5.4. Simulink/MATLAB was used to implement[7] this model and values of all the parameters of functional blocks are derived from the IEEE 802.11 base standard.

In Mode-1[8] transmitter, the *Random Integer* block generates frame-based binary data where *samples per frame* (or frame size) is 1024, symbol time period is 1μs and *sample time* is set for achieving a data rate of 1 Mbps. The *DBPSK* block is a differential binary phase shift keying baseband modulator from *Communications System Toolbox* with a *phase rotation* of zero. The output of *DBPSK* is converted to a row vector prior to spreading using an 11-chip Barker code. The Barker chips are passed through *Tx Pulse Shaping Filter* before their transmission through AWGN channel. The *Tx Pulse Shaping Filter* is a root raised cosine filter where values of the *roll-off factor*, *filter order* and *Oversampling factor* are 0.3, 84 and 8 respectively.

In the receiver data are passed through the *Rx Pulse Shaping filter, despreading* and *DBPSK demodulator* blocks. Bit Error Rate (BER) is computed using the *Error Rate Calculation* block from the *Communications System Toolbox.*

[7] It was built in the early 2008 when it was not available as a demo as part of the MATLAB documentation.
[8] Mode-1 is 1 Mbps data rate mode of WLAN DSSS PHY.

In the simulation of the Mode-2[9], a DQPSK modulator and demodulator are used instead of the DBPSK modulator and the *symbol time* is changed alongside computational and receive delays.

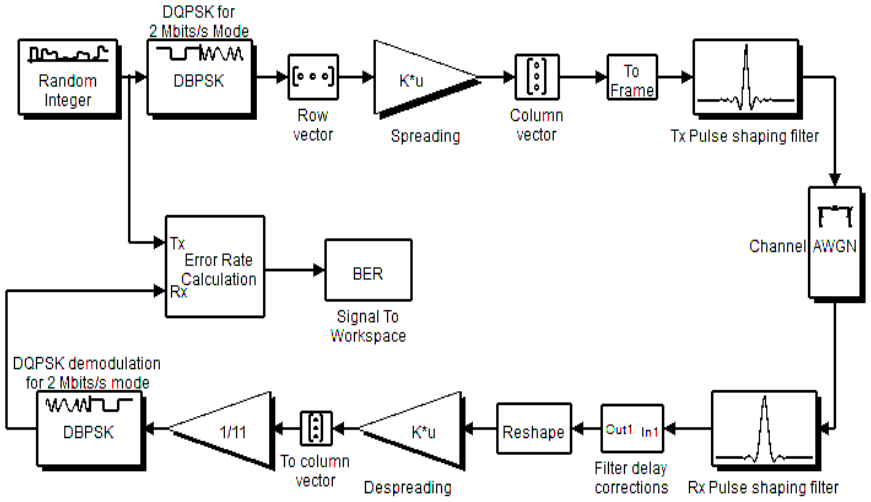

Figure 5.4 IEEE 802.11b - DSSS PHY (Mode1 and Mode 2) transceiver

5.2.1.5 Validation

The validation of the DSSS PHY simulation is carried out by a comparison between the theoretically expected and simulated BER. The theoretical BERs of the DBPSK and DQPSK are given by Equations 5.5 and 5.6 respectively [99].

$$P_b = \frac{1}{2}\exp\left(-\frac{E_b}{N_0}\right) \qquad \text{(Equation 5.5)}$$

$$P_b = Q_1(a,b) - \frac{1}{2}I_0(a,b)\exp\left(-\frac{1}{2}(a^2+b^2)\right) \qquad \text{(Equation 5.6)}$$

[9] Mode-2 is 2 Mbps data rate mode of WLAN DSSS PHY.

where

$$a = \sqrt{\frac{2E_b}{N_0}\left(1 - \frac{1}{\sqrt{2}}\right)} \; and \; b = \sqrt{\frac{2E_b}{N_0}\left(1 + \frac{1}{\sqrt{2}}\right)} \qquad \text{(Equation 5.7)}$$

and $Q_1(a,b)$ and $I_0(a,b)$ are Marcum Q-function and the modified Bessel function respectively [100].

For the BER computation, simulations are run to process 100 bit errors or 10^6 bits, whichever is reached first. The channel is AWGN and the results are averaged over 50 simulation runs.

The validation of the DSSS-PHY is shown in Figure 5.5 where the theoretical BER of the DBPSK and DQPSK are compared with the BER computed from the simulations for Modes 1 and 2. This validates the PHY simulation.

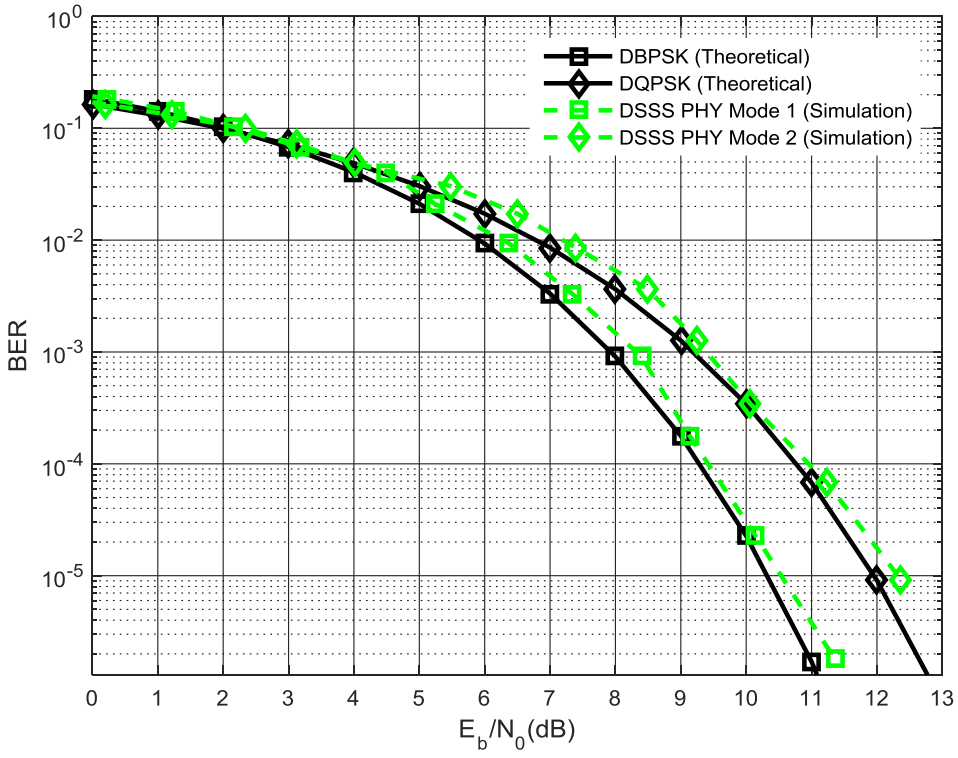

Figure 5.5: DSSS PHY validation - Comparison of theoretical and simulated BER

5.2.2 WLAN OFDM PHY

The OFDM PHY extension was released in 1999, as IEEE 802.11a. One motivation, among several, was the release of 300 MHz of spectrum by FCC in January 1997 in the 5 GHz band. It uses Orthogonal Frequency Modulation (OFDM) and Forward Error Correction (FEC) codes, operates at 5 GHz and supports several data rates ranging from 6 Mbps to 54 Mbps.

The description of OFDM PHY is divided into three parts; the frame composition, modulation techniques, structure and parameters of OFDM.

5.2.2.1 PHY Framing

The OFDM PHY frame (also called PPDU frame) comprises a PLCP preamble, a Signal field and a Data field.

The Signal field is 24 bits long which includes 4 bits to command data rate, 11 bits for the PSDU length, 1 parity bit and 6 tail bits. Both PLCP preamble and PLCP header are BPSK-OFDM modulated, encoded using convolutional encoding rate of R = ½ and transmitted at a data rate of 6 Mbit/s. The PLCP preamble is used to obtain the transmitted OFDM signal at the receiver and synchronize/train the demodulator. The PLCP preamble comprises 10 short and 2 long symbols; short symbols are used to acquire coarse channel estimation and long symbols to refine the estimate.

The Data field comprises a 16-bit service field, variable length PSDU, and tail and pad fields of 6 bits each. The length of the Data field is the product of the number of OFDM symbols (*Nsym*) and number of data bits per OFDM symbol (*Ndbps*).

5.2.2.2 Modulations and Coding

OFDM is a block modulation scheme where a block of N serial data symbols are converted to N parallel data symbols. This process of serial to parallel conversion increases the duration of each symbol by a factor of N. For example if T_s is the duration of each symbol before 'serial to parallel conversion', then after conversion it will become NT_s. Such an increase in symbol duration reduces the impact of Intersymbol Interference (ISI) and improves resilience in the presence of multipath propagation. Each symbol is used to modulate a separate sub-carrier from a large set of orthogonal subcarriers. Orthogonality is achieved by using subcarriers which are integer multiples of the base or first subcarrier. All the sub-carriers are transmitted as a segregated sum (grouped together and transmitted in parallel).

Forward error correction coding is used to detect and correct the errors induced by the channel. Convolutional coding with a standard coding rate of ½ is used for the lowest data rate mode (Mode 1, see Table 5.4 for details of modes), with a constraint length of 7 and generator polynomials (133,171). For the higher data rate modes (Modes 2-8), puncturing is used to generate the higher coding rates of ⅔ and ¾.

5.2.2.2.1 OFDM – A Mathematical Description

An OFDM symbol can be written in the form of a summation of complex waveforms as shown in Equation 5.8 where each complex waveform represents a single subcarrier.

$$S(t)_{OFDM} = \frac{1}{N}\sum_{n=0}^{N-1} A_n e^{j[\omega_n t + \phi_n(t)]} \qquad \text{(Equation 5.8)}$$

In Equation 5.8, $\omega_n = \omega_0 + n\Delta\omega$. When this summation is considered over one symbol period, A_n and ϕ_n are constant values. The discrete time or sampled version can be written in the form of Equation 5.9, given that the sampling period is ΔT_s.

$$S_{OFDM}(k\Delta T_s) = \frac{1}{N}\sum_{n=0}^{N-1} A_n e^{j[(\omega_0 + n\Delta\omega t)kT_s + \phi_n]} \qquad \text{(Equation 5.9)}$$

In this sampled signal representation, N samples represent one symbol and if the sampling rate is ΔT_s, then the duration of a symbol (T_s) is $N\Delta T_s$. Equation 5.9 can be written in the form of Equation 5.10, by letting $\omega_0 = 0$.

$$S_{OFDM}(k\Delta T_s) = \frac{1}{N}\sum_{n=0}^{N-1} A_n e^{j\phi_n} e^{j(n\Delta\omega)kT_s} \qquad \text{(Equation 5.10)}$$

The general form of the Inverse Fast Fourier Transform (IFFT) is shown in Equation 5.11 and a comparison with Equation 5.9 shows why IFFT is used for the generation of OFDM symbols.

$$g(kT_s) = \frac{1}{N}\sum_{n=1}^{N-1} G\left(\frac{n}{N\Delta T_s}\right) e^{\frac{j2\pi nk}{N}} \qquad \text{(Equation 5.11)}$$

In Equation 5.11, $G(\frac{n}{N\Delta T_s})$ is the frequency domain representation of the discrete time domain signal $g(kT_s)$ whereas in Equation 5.9, $A_n e^{j\phi_n}$ is the definition of signal $S(k\Delta T_s)$ sampled in the frequency domain. The condition for the equivalence of Equation 5.8 and 5.10 is:

$$\Delta f = \frac{\Delta\omega}{2\pi} = \frac{1}{N\Delta T_s} = \frac{1}{T_s} \qquad \text{(Equation 5.12)}$$

The condition of orthogonality in OFDM thus allows the use of IFFT for the generation of the OFDM symbols.

5.2.3 PHY Parameters

The IEEE 802.11a standard defines 52 non-zero subcarriers comprising 48 data subcarriers and 4 pilot subcarriers for the OFDM PHY and supports a range of data rates, which are achieved using different signal constellations and error coding rates. Data rates supported by OFDM PHY and their corresponding parameters are given in Table 5.4. Inverse Fast Fourier Transform (IFFT) and Fast Fourier Transform (FFT) are used for implementing the modulator and demodulator banks respectively.

Table 5.5 details the time-related OFDM parameters and their values.

Table 5.4 Data rate dependent OFDM PHY parameters [96]

Mode	Data rate (Mbps)	Modulation	Coding rate (R)	Coded bits per subcarrier (N_{BPSC})	Coded bits per OFDM symbol (N_{CBPS})	Data bits per OFDM symbol (N_{DBPS})
1	6	BPSK	½	1	48	24
2	9	BPSK	¾	1	48	36
3	12	QPSK	½	2	96	48
4	18	QPSK	¾	2	96	72
5	24	16 QAM	½	4	192	96
6	36	16 QAM	¾	4	192	144
7	48	64 QAM	⅔	6	288	192
8	54	64 QAM	¾	6	288	216

Table 5.5 Values of OFDM parameter [96]

Parameter	Value
N_{SD} (Number of data subcarriers)	48
N_{SP} (Number of pilot subcarriers)	4
N_{ST} (Total number of subcarriers)	52 ($N_{SD} + N_{SP}$)
Δ_F (Subcarrier frequency spacing)	0.3125 MHz (= 20 MHz/64)
T_{FFT} (IFFT/FFT period)	3.2 µs ($1/\Delta_F$)
$T_{PREAMBLE}$ (PLCP preamble duration)	16 µs ($T_{SHORT} + T_{LONG}$)
T_{SIGNAL} (Duration of the SIGNAL BPSK-OFDM symbol)	4.0 µs ($T_{GI} + T_{FFT}$)
T_{GI} (GI duration)	0.8 µs ($T_{FFT}/4$)
T_{GI2} (Training symbol GI duration)	1.6 µs ($T_{FFT}/2$)
T_{SYM} (Symbol interval)	4 µs ($T_{GI} + T_{FFT}$)
T_{SHORT} (Short training sequence duration)	8 µs (10 x $T_{FFT}/4$)
T_{LONG} (Long training sequence duration)	8 µs ($T_{GI2} + 2xT_{FFT}$)

5.2.4 PHY Simulation Model

A block diagram of the Simulink implementation of OFDM PHY transceiver is shown in Figure 5.6. The description of the functional blocks of the OFDM PHY simulation is given below:

1. **Mode Selector:** takes an integer input in the range of 1-8 to set the mode of operation. Mode 1 corresponds to 6 Mbps and Mode 8 corresponds to 54 Mbps.

In addition to setting the data rate, this input selects the corresponding modulator/encoder and demodulation/decoder from the Modulator and Demodulator bank.

2. **Data Source**: is a binary random data source and implemented using the *Random Source* block. The generated random data follows uniform distribution and data-rate is dependent on the mode selected using Mode Selector.
3. **Modulator Bank:** includes an implementation of all 8 combinations of modulator/channel encoder. Its underlying structure is shown in Figure 5.6. A trellis structure is passed to the convolutional encoder that determines the encoding code to be used. The trellis structure is formed using MATLAB function *poly2trellis* and its inputs are constraint length and a pair of octal numbers.
4. **OFDM symbol**: reshapes/group the data into OFDM symbol.
5. **Assemble OFDM Frames**: pads the pilot and training sequence to the OFDM symbol and generates an OFDM frame. The pilot is generated using a *PN Sequence Generator* and *Unipolar to Bipolar* Simulink blocks.
6. **IFFT**: The underlying functionality of this block is based on the Simulink block *IFFT*. The input to IFFT is 52 source symbols and the output is 52 orthogonal sinusoids. The IFFT is applied to output complex time-domain samples that represent the combined OFDM subcarrier waveforms.
7. **Append Cyclic Prefix:** fills in the guard interval by adding a copy of the end of the symbol to its start, which further improves the immunity of the OFDM symbol against inter-symbol interference (ISI) and also provides protection against time offset.

8. **Multiplex OFDM Frames:** a parallel to serial converter which transmits the OFDM symbols one by one.
9. **AWGN**: a standard Simulink block which adds Gaussian noise to the input signal.
10. **De-multiplex OFDM Frames:** a serial to parallel converter which receives each time domain OFDM symbol and constructs a parallel OFDM frame.
11. **Removed Cyclic Prefix:** removes the cyclic prefix from each symbol.
12. **FFT:** converts the OFDM symbols back to the frequency domain so that each frequency bin can be decoded independently.
13. **Frequency Domain Equalizer:** The OFDM signal is affected by frequency selective fading and this block is a one-tap zero-forcing equaliser that is applied to each subcarrier to compensate for multipath fading. It does not have any effect for AWGN.
14. **Disassemble OFDM Frames:** unpacks the OFDM frame i.e. serialises the OFDM symbol and passes symbols individually to the *Demodulator Bank* block.
15. **Demodulator Bank:** performs demodulation and decoding. After demodulation, the values are passed onto a *Viterbi decoder block* where decoding decisions are based on the Hamming distance (as un-quantised option is selected in the decision type menu in *Viterbi decode block*). The value of *Traceback depth* parameter in the *Viterbi decoder block* is the length of the decoder delay and should be six times the constraint length of the code.

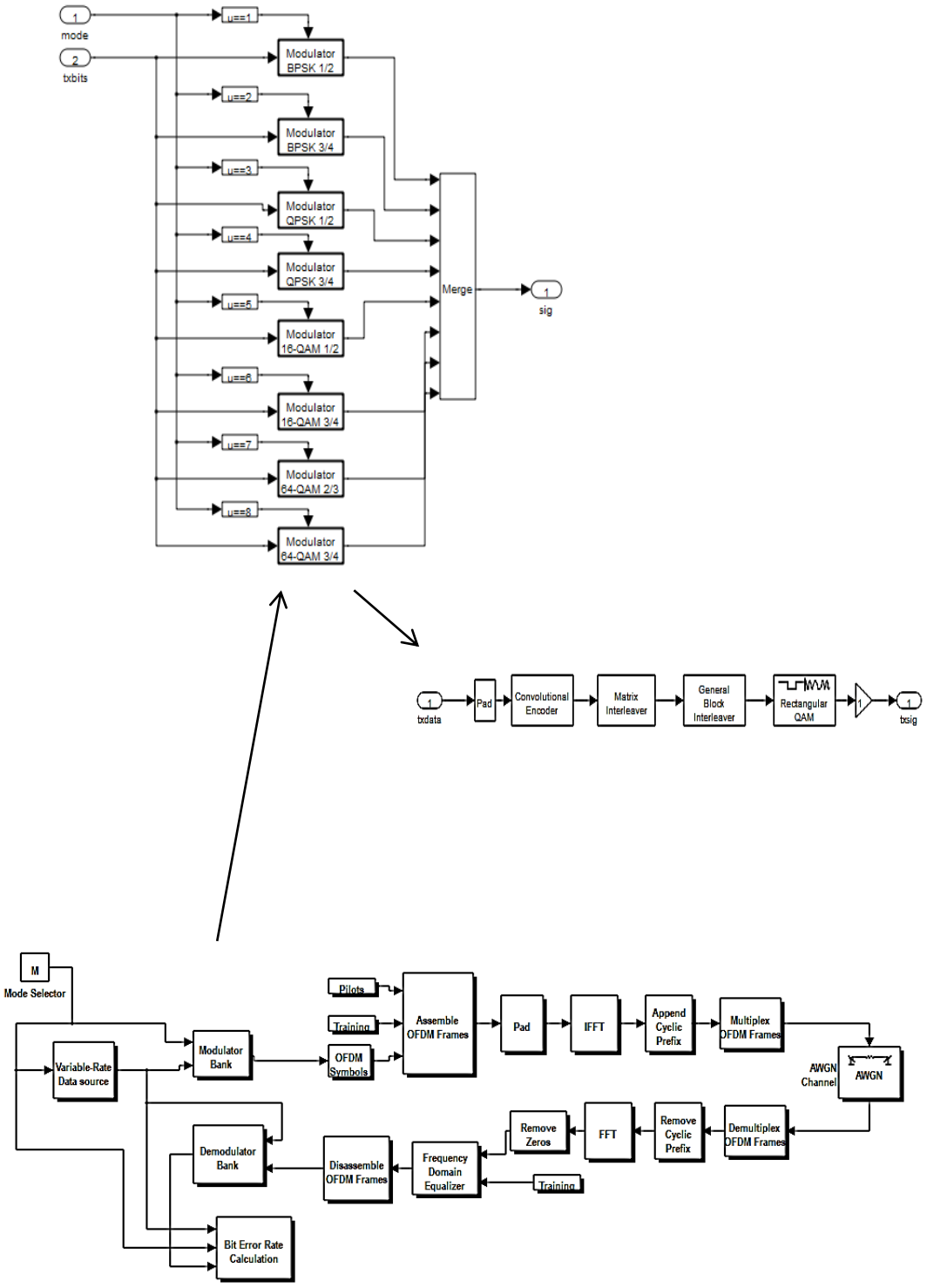

Figure 5.6: OFDM PHY Simulink block diagram

16. Bit Error Calculation: The inputs to this block are, a range of E_b/N_0 values, recieve delay and conditions to stop the simulation when a certain number of bit-errors or a number-of-received-bits have been reached. Receive delay is computed using the traceback path depth, and delays introduced by buffers in the simulation.

The end condition for the simulation is when either 100 bit errors or 10^7 message bits have been processed.

5.2.5 Validation

The validation of OFDM PHY is carried out by the comparison of theoretical and simulation-computed BER.

5.2.5.1 Modes 1-4

The theoretical AWGN channel BER for BPSK and QPSK is [101]:

$$BER = \frac{1}{2} erfc\left(\sqrt{\frac{E_b}{N_0}}\right) \quad \text{(Equation 5.13)}$$

where erfc(.) is the complementary error function.

The validation results are shown in Figure 5.7, where the theoretical BER of BPSK[10] is compared with the BER computed from the OFDM PHY layer simulation modes 1-4.

The coding gain is apparent in the result and its upper bound can be evaluated using Equation 5.14 where R is coding rate and d_f is free distance of the code [102].

$$r \leq 10log_{10}(R.d_f) \quad \text{(Equation 5.14)}$$

[10]Theoretical BERs of BPSK and QPSK are equal.

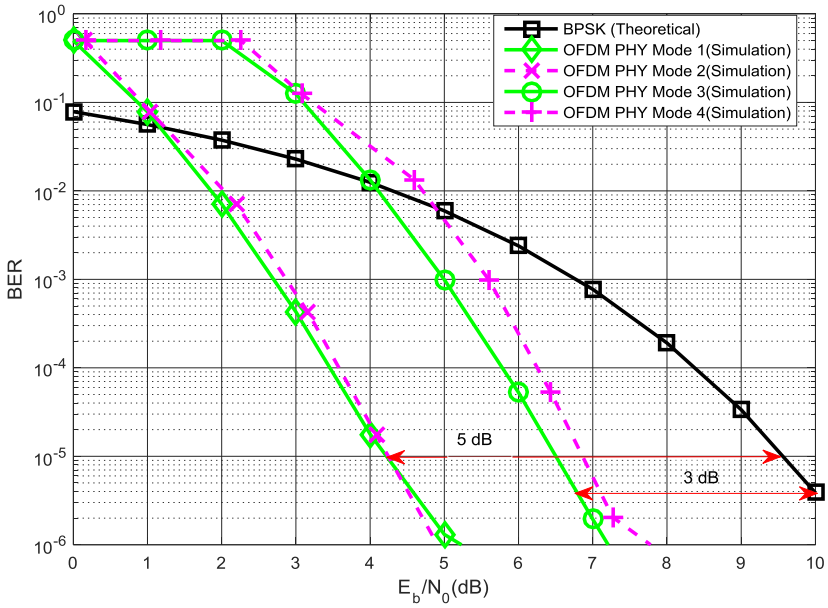

Figure 5.7 Validation of WLAN OFDM PHY Modes 1-4

The minimum free distance (d_f) for convolutional codes is the minimum Hamming distance between two codewords. The difference between simulated and theoretical results is because of coding gain which follows the upper bound stated in Equation 5.14 [103].

The coding gain of modes 1 and 2 is ~5 dB for BER < 10^{-5}, where the difference between the two modes, is the application of the puncturing in mode 2 for achieving the higher data rate.

The coding gain of modes 3 and 4 is ~3 dB for BER < 10^{-5}, where the difference between the two modes is, use of the puncturing in mode 4 for achieving the higher data rate. The effect of the puncturing (Modes 2 and 4) is small (<1 dB) on the BER performance when compared against modes 1 and 3 which do not use puncturing [104].

5.2.5.2 Modes 5-8

Symbol Error Rate (SER) and BER for a square M-QAM can be written in the form of Equation 5.15 and Equation 5.16 respectively [105, 106]

$$SER = 4\frac{\sqrt{M}-1}{\sqrt{M}}Q\left(\sqrt{\frac{3}{M-1}\frac{kE_b}{N_0}}\right) - 4\left(\frac{\sqrt{M}-1}{\sqrt{M}}\right)^2 Q^2\left(\sqrt{\frac{3}{M-1}\frac{kE_b}{N_0}}\right) \quad \text{(Equation 5.15)}$$

$$BER = \frac{2}{\sqrt{M}\,log_2\sqrt{M}}\,X$$

$$\sum_{k=1}^{log_2\sqrt{M}}\sum_{i=0}^{(1-2)\sqrt{M}-1}\left\{(-1)^{\left\lfloor\frac{i2^{k-1}}{\sqrt{M}}\right\rfloor}\left(2^{k-1}-\left\lfloor\frac{i2^{k-1}}{\sqrt{M}}+\frac{1}{2}\right\rfloor\right)\left(Q(2i+1)\sqrt{\frac{6log_2M}{2(M-1)}\frac{E_b}{N_0}}\right)\right\}$$

(Equation 5.16)

where $k = log_2 M$

The validation results are shown in Figure 5.8, where the theoretical BERs of 16 and 64 QAM are compared with the BERs computed from the OFDM PHY layer modes 5-8 simulation. The coding gain is apparent in the result and its upper bound is given by Equation 5.14

The coding gains of modes 5-6 and 7-8 are ~4dB and 3dB respectively, for a BER of ~ 10^{-5}, where modes 6 and 8 use puncturing for achieving the higher data rates and again the effect of puncturing on BER performance is small [104].

In Figures 5.7 and 5.8, the difference between the theoretical and simulated BER is explained in terms of the coding rate and the theoretically expected upper bound on the coding gain.

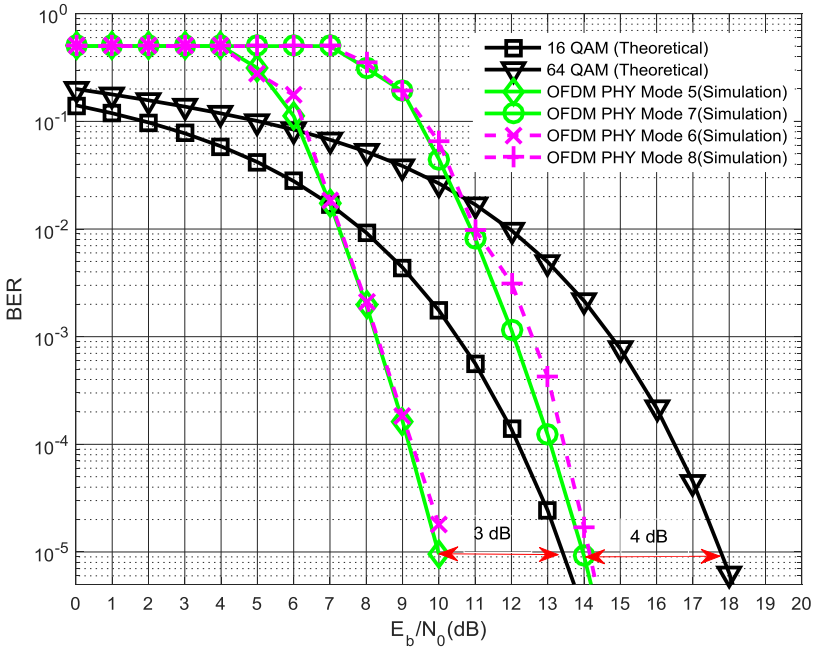

Figure 5.8 Validation of WLAN OFDM PHY Modes 5-

In order to further establish the validity of the simulations, channel coding is disabled and the BER of Modes 1, 5 and 7 is evaluated from the simulation and compared with the theoretical BER of BPSK, 16 and 64 QAM. The results are compared in Figure 5.9 and it can be noticed that there is a very little difference between the two BERs. The remaining modes 2, 6 and 8 use the same modulation schemes as modes 1, 5 and 7 but employ puncturing to achieve the higher data rates.

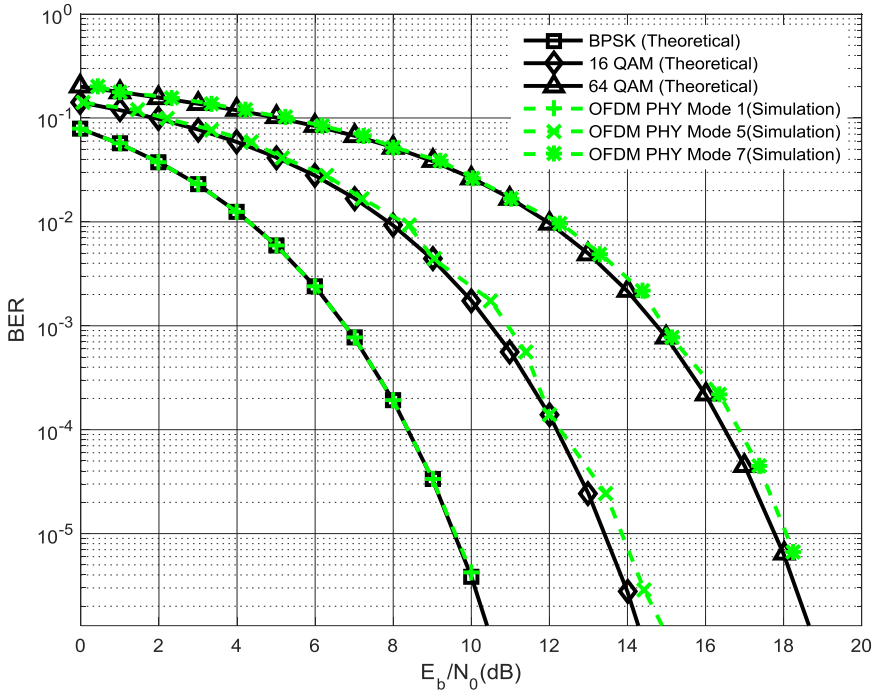

Figure 5.9: Validation of WLAN OFDM PHY without channel coding

5.2.6 HR DSSS PHY

The HR-DSSS PHY operates at 2.4 GHz in the license-free ISM frequency band and has 14 channels with centre frequency separation of 5 MHz and an overall channel bandwidth of 22 MHz. ETSI regulations allow using channels 1-13 in the EU. Not all channels can be used at the same time and data rates of 5 and 11 Mbps in addition to the 1 and 2 Mbps are supported by the base standard. A mechanism has also been included for shifting back to low data rates to support the legacy IEEE 802.11 base standard.

5.2.6.1 PHY Framing

A long and short preamble are supported. The description of the long preamble has already been given in the DSSS PHY section. The length of the short preamble is 72

bits comprising 56-bit short SYNC and 16-bit short SFD. The short preamble is transmitted at a data rate of 1 Mbps using DBPSK.

The short header consists of SIGNAL (8 bits), SERVICE (8 bits), LENGTH (16 bit) and CRC (16 bits) fields, and is transmitted at a data rate of 2 Mbps using DQPSK. Further details of the functionality and implementation of all PLCP fields can be found in the IEEE 802.11 standard [107].

5.2.6.2 Modulation and Spreading

In the HR-DSSS PHY, Complementary Code Keying (CCK) is employed to support the high data rates. CCK is a variation of an M-ary orthogonal keying modulation and provides interoperability with the base standards by maintaining the same bandwidth and support for existing PLCP preamble and PLCP header.

In the CCK modulation, polyphase complementary codes are used for bandwidth spreading where the length of the spreading sequence is 8 and chip rate is 11Mchip/s. The CCK code for mode 2 (11 Mbit/s mode) is given in Equation 5.17, and a subset of this code is used for mode 1 (5.5 Mbps). The data symbols are represented by 4 and 8 bits in modes 1 and 2 respectively.

Equation 5.17 has four phases. One provides the QPSK rotation to the entire code vector. The other three modulate every odd pair and every odd quad of the chips. Also, every 4^{th} and 7^{th} term are rotated counter-clockwise by 180^{o}.

$$c = \left\{ \begin{matrix} e^{j(\varphi_1+\varphi_2+\varphi_3+\varphi_4)}, e^{j(\varphi_1+\varphi_3+\varphi_4)}, e^{j(\varphi_1+\varphi_2+\varphi_4)}, -e^{j(\varphi_1+\varphi_4)}, e^{j(\varphi_1+\varphi_2+\varphi_3)}, \\ e^{j(\varphi_1+\varphi_3)}, e^{j(\varphi_1+\varphi_2)}, e^{j(\varphi_1)} \end{matrix} \right\}$$

(Equation 5.17)

The spreading rate is kept at 11 Mbps so that the CCK spectra are the same as the base standard. The symbol rate is increased to 1.375 Msymbol/s to support the higher data rates.

In 5.5 Mbps mode, PPDU bits are grouped into four bits (nibbles). Two bits are used to select the spreading function and the remaining two, modulate the signal using QPSK. The selected spreading sequence then drives the I/Q modulators and DQPSK modulates the symbol.

In 11Mbps mode, PPDU bits are split into groups of six and two bits. The six bits determine the spreading sequence while the two bits DQPSK modulate the entire symbol. CCK implementation is adapted from Simulink built-in libraries. The implementation is shown in Figure 5.10. Details of the complementary properties of codes used in HR DSSS PHY can be found in [108].

5.2.6.3 PHY Simulation Model

A Simulink implementation of the HR-DSSS PHY which supports four modes with data payloads of 5.5 and 11 Mbps is shown in Figure 5.11.

In the simulation, *Random Integer* and *Integer to Bit converter* Simulink blocks are used to model a data source which generates random binary data with the uniform distribution. The PLCP preamble and header is appended to convert the MAC sub-layer protocol data unit (MPDU) into a PPDU. *Modulate and Spread* is a configurable subsystem which implements CCK modulation where the PLCP preamble and header are modulated using DBPSK and the MPDU is modulated using CCK. A root raised cosine filter is used for pulse shaping before passing the modulated MPDU to the AWGN channel block. .

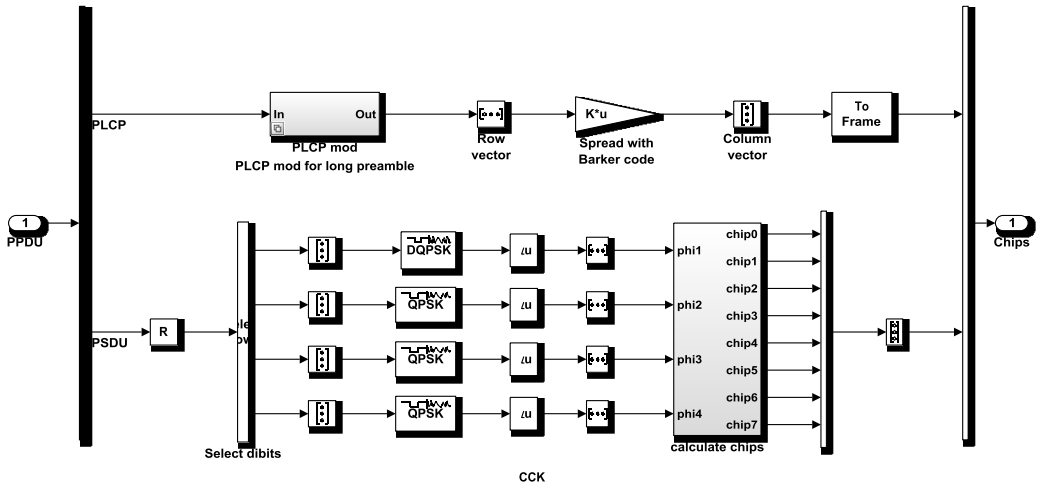

Figure 5.10: Implementation of CCK

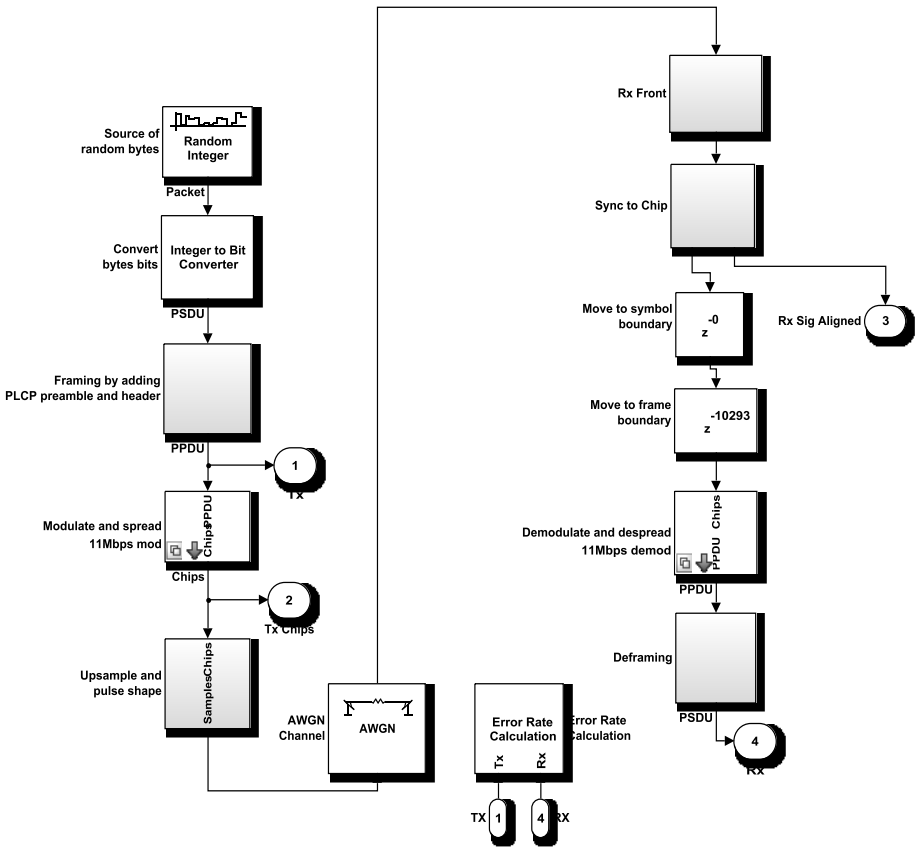

Figure 5.11: Simulation of WLAN High Rate DSSS PHY

5.2.6.4 Validation

The validation of PHY layer simulations is carried out by the comparison of simulated and theoretical BER. There is no analytical method available to compute the BER for CCK and thus validation is carried out by comparison of simulated BER with theoretical BER of DPSK [108]. CCK reduces the spreading rate to support high data rates in DSSS PHY. This spreading rate reduction, however, makes it more susceptible to narrowband interference and reduces the range. The spreading rate has no impact on the BER performance in AWGN and thus the AWGN BER performance of the PSK and CCK is the same.

The theoretical BER for DPSK is computed using the relationship in Equation 5.18 [99].

$$P_b = \frac{1}{2}\, exp^{\left(-\frac{E_b}{N_0}\right)} \qquad \text{(Equation 5.18)}$$

The BER comparison of the both HR-DSSS PHY modes is shown in Figure 5.12. A close match between the theoretical and the simulated BER validates the simulation.

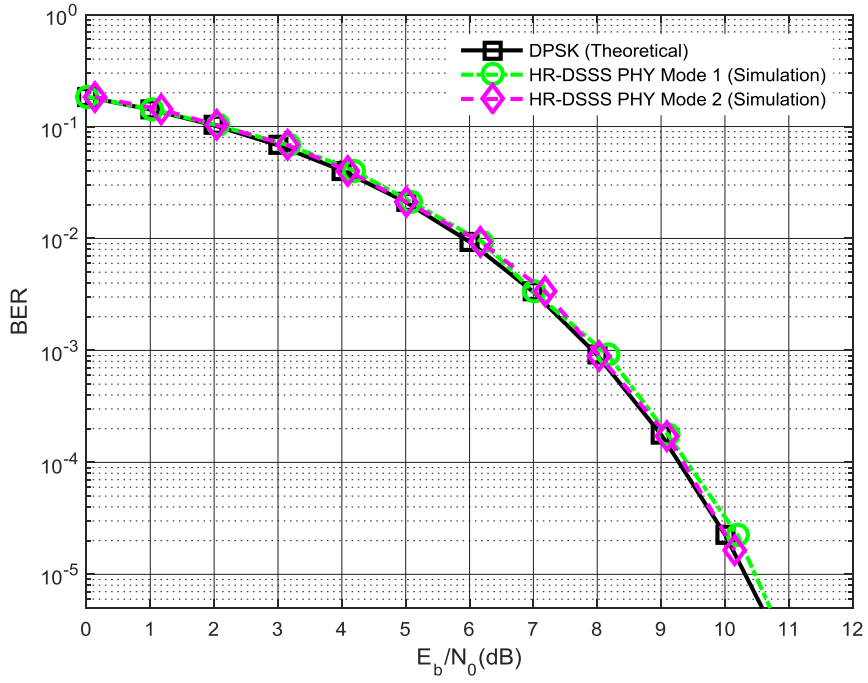

Figure 5.12: Validation of WLAN HR DSSS PHY

5.3 Bluetooth

Bluetooth is a standard for the wireless Personal Area Network (PAN) and is based on the technology developed by the Bluetooth Special Interest Group (SIG) which was later standardized by IEEE as IEEE 802.15.1 standard for WLAN PANs. [109]. The operating range of Bluetooth depends on the transmit power and range, varying between 1m (transmit power of 1 mW) and 100m (transmit power of 100 mW). The most commonly used Bluetooth devices have a nominal range of up to 10m and have a transmit power of 2.5 mW.

5.3.1 Modulation and Spreading

Bluetooth transceivers operate in the unlicensed Industrial Scientific and Medical (ISM) 2.4 – 2.483 GHz band using FHSS. To combat interference and fading from

co-existing WLAN transceivers, it hops among 1 MHz spaced 79 frequencies at a rate of 1600 hops/s.

The modulation used is Gaussian Minimum Shift Keying (GMSK) with bandwidth-time (BT) product of 0.5 and modulation index of ~0.3. The transmitted symbol rate is 1 Msymbol/s and a 2/3 Hamming FEC code is used for the error coding. In FHSS, the position of an M-ary signal set is shifted by a pseudo-randomly selected frequency over the hopping bandwidth.

FH-MSK modulation is a two-step process. In the first step, the data symbol is modulated using GMSK. In the second step, the data symbol is modulated using a randomly selected frequency. Transmission bandwidth for one hop is the same as conventional M-ary FSK but, when averaged over a number of hops, is equal to the entire spread-spectrum bandwidth. Frequency Hopping (FH) technologies can provide potentially much higher processing gains compared to DSSS as they allow hoping bandwidths of the order of GHz. The processing gain in an FH system is the ratio of hoping bandwidth and data rate [110].

In GMSK, the modulating signal is filtered using a Gaussian filter and modulated using a Minimum Shift Keying (MSK) where the MSK technique belongs to the class of Continuous Phase Modulations (CPM) and can be described either as O-QPSK with sinusoidal symbol weighting or as a special case of CPM. O-QPSK suppresses the out-of-band interference and MSK avoids the phase discontinuities. The MSK waveform is described by Equation 5.19; considering MSK as a special case of CPM [102].

$$s(t) = cos\left[2\pi\left(f_0 + \frac{d_k}{4T}\right)t + x_k\right] \qquad kT < t < (k+1)T \qquad \text{(Equation 5.19)}$$

where f_0 is the carrier frequency, d_k is either +1 or -1 (represents bipolar data) and x_k is a phase constant for k^{th} binary data interval. It can be observed from Equation 5.19 that the transmitted tones are (f_0+ $^1/_4$ T) and (f_0+ $^1/_4T$) when d_k = +1 and d_k = -1 respectively. The tone spacing is half of that required by orthogonal FSK, hence the name minimum shift keying.

A block diagram of the Simulink implementation of the Bluetooth PHY is shown in

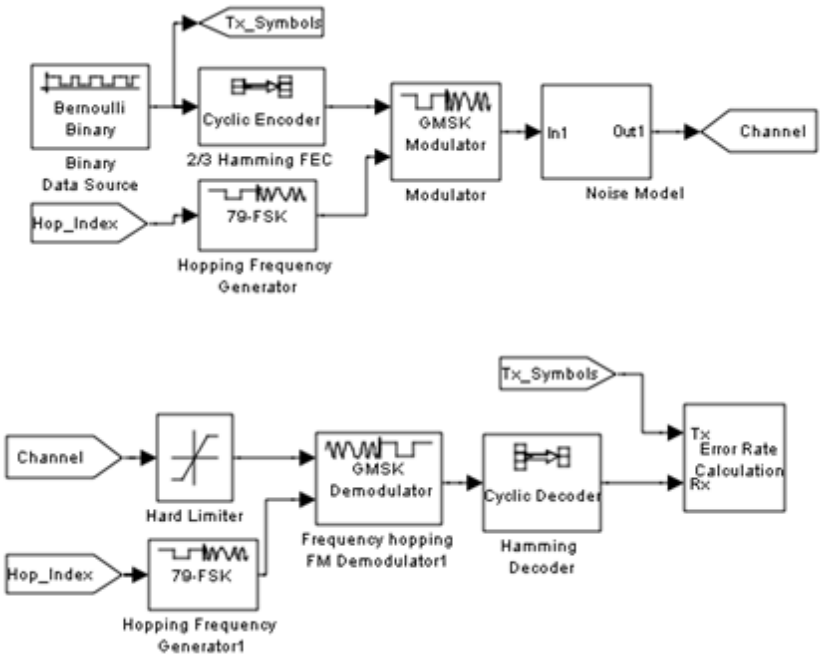

Figure 5.13: Simulation of Bluetooth PHY

5.3.2 Validation

The theoretical BER of a coherently detected MSK is the same as is that for BPSK/QPSK (Equation 5.13). However, GMSKemploys a Gaussian shaping filter

prior to modulation and thus the BER is a function of the Time-Bandwidth (TB)[11] product of the filter, which is shown in Equation 5.19.

$$BER = \frac{1}{2} erfc\left(\sqrt{\frac{kE_b}{N_0}}\right) \qquad \text{(Equation 5.19)}$$

In Equation 5.19, k is a constant derived from the TB of the shaping filter and the performance degradation due to Intersymbol Interference (ISI). The ISI introduced by the shaping filter, is $10\log_{10}(k/2)$. The value of k ranges from 0.6 to 0.85 for the values of TB ranging from 0.3 to ∞ and the BER degradation is minimal for BT = 0.5.

The simulation of the Bluetooth PHY has been validated by comparing its simulated performance in the presence of AWGN channel, with the theoretically expected performance. Figure 5.14 shows the results of the validation.

[11] Time-Bandwidth (TB) is a product of the symbol length (T) and the 3dB bandwidth (B) of the shaping filter and has typical values of 0.3-0.5. It is equivalent of the excess bandwidth term used in the context of raised cosine shaping filter, however the excess bandwidth of the Gaussian filter can-not be stated in terms of TB, given that its frequency response is not symmetrical around zero.

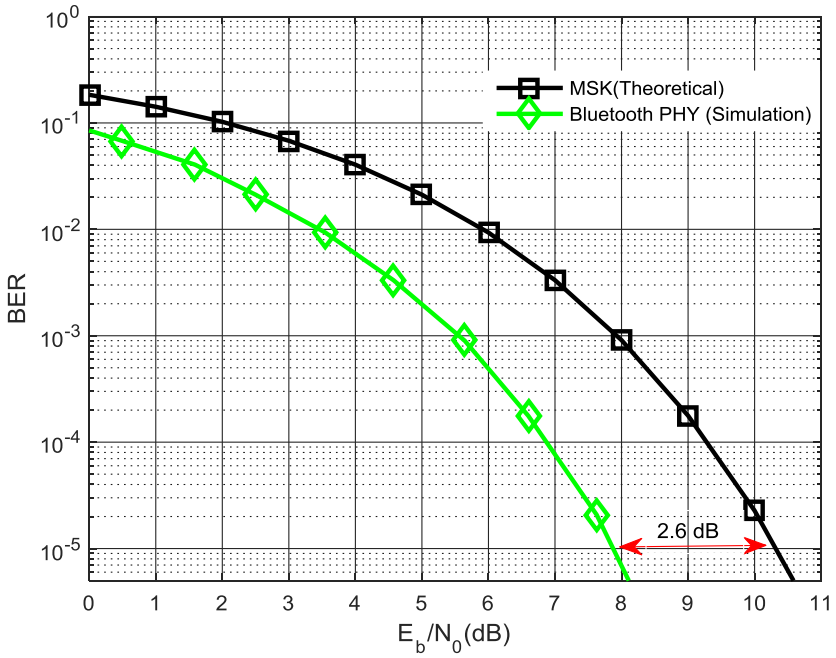

Figure 5.14: Validation of Bluetooth physical layer simulation

The difference between the two curves is as expected due to the (15, 10) Hamming code included in the simulation. The minimum distance of the (15, 10) Hamming code is 4 and thus (using the relationship in Equation 5.14) the coding gain is 2.67 dB [111, 112].

5.4 ZigBee

Zigbee is a standard for low power, low data-rate wireless communications and has a wide range of applications in home and industrial automation. The application of interest here is in the substation segment of smart grids. The standard was originally developed by the ZigBee Alliance and then standardized by the IEEE as IEEE 802.15.4 which has specifications for MAC and PHY layers.

5.4.1 PHY Modulation and Spreading

The IEEE standard 802.15.4 defines four PHYs which operate in 868/915 MHz and 2450 MHz frequency band. Of the four PHYs, two are optional. The specifications of the two mandatory PHYs are given below.

The first mandatory PHY operates in the 868/915 MHz frequency bands and supports data rates of 20 kbps and 40 kbps with chip rates of 300 kchip/s and 600 kchip/s respectively. It employs BPSK.

Modulation and spreading is a three-step process which includes differential encoding, bit-to-chip mapping and BPSK modulation. Differential encoding is the modulo-2 addition of the data bit with the previous encoded bit. The bit-to-chip block maps the data bit to a 15 chip PN sequence as shown in Table 5.6.

Table 5.6 Zigbee PHY bit-to-chip mapping for PHY-1

Input bit	Chip values (c_0, c_1 …c_{14})
0	1 1 1 1 0 1 0 1 1 0 0 1 0 0 0
1	0 0 0 0 1 0 1 0 0 1 1 0 1 1 1

The second mandatory PHY operates in the 2.4 GHz frequency band and supports data rates of 250 kbps with a chip rate of 2000 kchips/s. The PHY employs 16-ary orthogonal QPSK (O-QPSK). Again the modulation and spreading is a three-step process which includes bit-to-symbol, symbol-to-chips and O-QPSK modulation. Bit-to-symbol converts the 4 data bits into a symbol. Symbol-to-chips maps each symbol to a 32 chip PN sequence as shown in Table 5.7.

Table 5.7 Zigbee PHY bit-to-chip mapping for PHY-2

Data symbol (binary)	Chip values (c_0,c_1, c_3 … c_{31})
0 0 0 0	1 1 0 1 1 0 0 1 1 1 0 0 0 0 1 1 0 1 0 1 0 0 1 0 0 0 1 0 1 1 1 0
1 0 0 0	1 1 1 0 1 1 0 1 1 0 0 1 1 1 0 0 0 0 1 1 0 1 0 1 0 0 1 0 0 0 1 0
0 1 0 0	0 0 1 0 1 1 1 0 1 1 0 1 1 0 0 1 1 1 0 0 0 0 1 1 0 1 0 1 0 0 1 0
1 1 0 0	0 0 1 0 0 0 1 0 1 1 1 0 1 1 0 1 1 0 0 1 1 1 0 0 0 0 1 1 0 1 0 1
0 0 1 0	0 1 0 1 0 0 1 0 0 0 1 0 1 1 1 0 1 1 0 1 1 0 0 1 1 1 0 0 0 0 1 1
1 0 1 0	0 0 1 1 0 1 0 1 0 0 1 0 0 0 1 0 1 1 1 0 1 1 0 1 1 0 0 1 1 1 0 0
0 1 1 0	1 1 0 0 0 0 1 1 0 1 0 1 0 0 1 0 0 0 1 0 1 1 1 0 1 1 0 1 1 0 0 1
1 1 1 0	1 0 0 1 1 1 0 0 0 0 1 1 0 1 0 1 0 0 1 0 0 0 1 0 1 1 1 0 1 1 0 1
0 0 0 1	1 0 0 0 1 1 0 0 1 0 0 1 0 1 1 0 0 0 0 0 0 1 1 1 0 1 1 1 1 0 1 1
1 0 0 1	1 0 1 1 1 0 0 0 1 1 0 0 1 0 0 1 0 1 1 0 0 0 0 0 0 0 1 1 1 0 1 1
0 1 0 1	0 1 1 1 1 0 1 1 1 0 0 0 1 1 0 0 1 0 0 1 0 1 1 0 0 0 0 0 0 1 1 1
1 1 0 1	0 1 1 1 0 1 1 1 1 0 1 1 1 0 0 0 1 1 0 0 1 0 0 1 0 1 1 0 0 0 0 0
0 0 1 1	0 0 0 0 0 1 1 1 0 1 1 1 1 0 1 1 1 0 0 0 1 1 0 0 1 0 0 1 0 1 1 0
1 0 1 1	0 1 1 0 0 0 0 0 0 1 1 1 0 1 1 1 1 0 1 1 1 0 0 0 1 1 0 0 1 0 0 1
0 1 1 1	1 0 0 1 0 1 1 0 0 0 0 0 0 0 1 1 1 0 1 1 1 1 0 1 1 1 0 0 0 1 1 0 0
1 1 1 1	1 1 0 0 1 0 0 1 0 1 1 0 0 0 0 0 0 0 1 1 1 0 1 1 1 1 0 1 1 1 0 0 0

A Simulink block diagram of the implementation of the Zigbee PHY is shown in Figure 5.15.

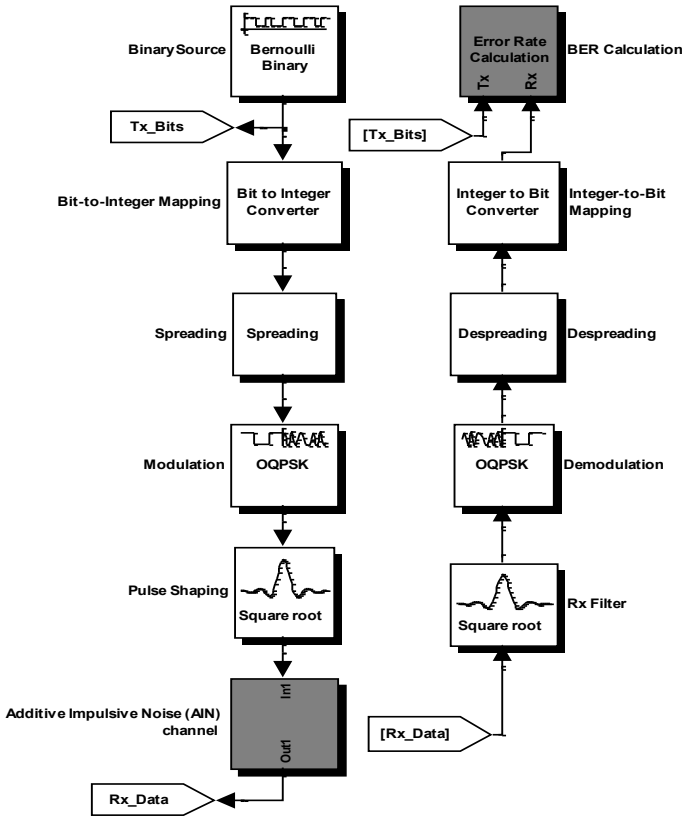

Figure 5.15 Simulation of Zigbee PHY

5.4.2 Validation

The PHY of a Zigbee transceiver has been implemented using MATLAB/Simulink. The validation of the simulation has been carried out by comparing the simulated BER with the theoretically expected BER of the underlying modulations, in the presence of AWGN channel. Figure 5.16 shows the validation results for both 868 MHz BPSK (Zigbee PHY 1) and 2.45 GHz OQPSK (Zigbee PHY-2) modes. The agreement between the simulated BER curves and the BPSK/O-QPSK BER curves validates the simulation.

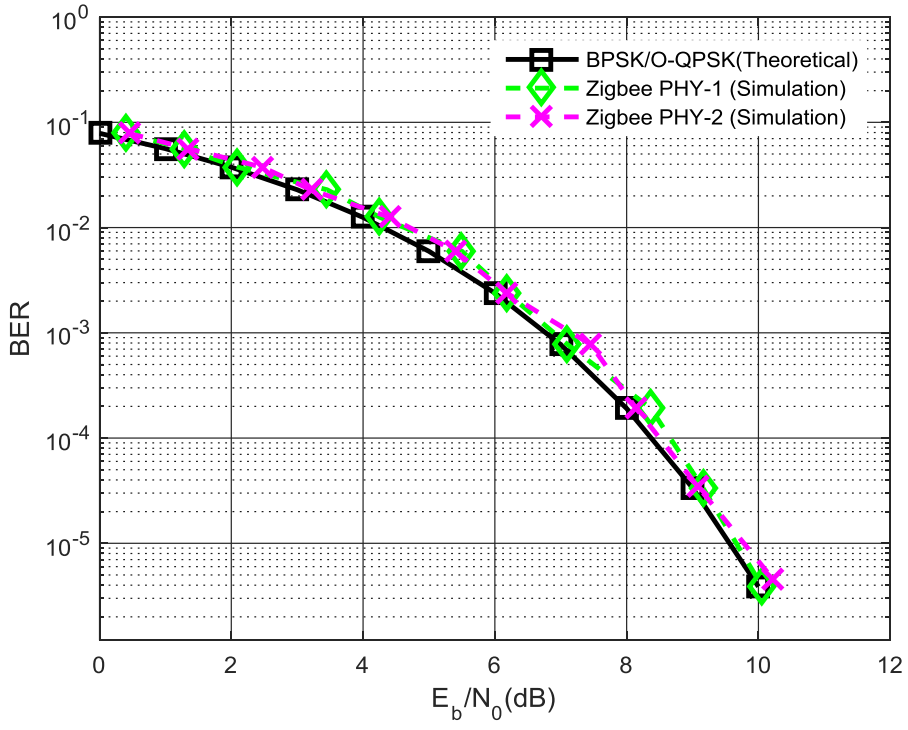

Figure 5.16: Validation of the Zigbee PHY simulation

5.5 Summary

This chapter describes simulation models for the PHYs of WLAN, Bluetooth and Zigbee short range wireless technologies. The simulation parameters are derived from the IEEE standard documents for the PHYs and MATLAB/Simulink is used to implement the signal processing tasks to realise the transmitters and receivers. The simulations are validated by comparing the simulation-computed and the theoretical BERs for an AWGN channel. The models presented in this chapter are used in Chapter 6 to evaluate the physical layer performance of the wireless technologies in the presence of impulsive noise.

CHAPTER 6

PERFORMANCE ASSESSMENT

6.1 Introduction

This chapter presents a BER performance evaluation of the candidate short-range wireless technologies using the impulsive noise models (chapter 4) and the PHY simulations of the short-range wireless technologies (chapter 5).

The chapter is divided into two parts; part 1 addresses performance evaluation results in the presence of narrowband impulsive noise and part 2 addresses performance in the presence of broadband impulsive noise.

The Middleton Class-A noise model is used to generate the narrowband impulsive noise, the noise parameters were estimated using the methods described in chapter 4. The estimated parameters are used to generate the impulsive noise time series which is representative of noise found in substations.

The SαS distribution based model is used to generate the broadband impulsive noise. The model parameters are estimated for the substation noise.

6.2 Performance in Narrowband Impulsive Noise

The Middleton Class A based narrowband impulsive model has two parameters which control the characteristics of noise - impulsive index (A) and scale parameter (Γ). The three sets of values for these parameters are used to represent the following three impulsive noise cases.

1. Highly Impulsive (HI) - when the wireless equipment is deployed in close vicinity to high voltage equipment and where the impulsive noise originating from the PD and switching transients dominates the Gaussian component of the overall noise profile.
2. Moderately Impulsive (MI) - when the wireless communications equipment is deployed inside electricity substation but is not close to a major source of PD.
3. ETS – The model parameters are estimated from the measurements data. The details of the estimation of model parameters are given in Chapter 4.

The values of the model parameters for the three cases are given in Table 6.1. The parameters for cases 1 and 2 are selected using the assumption that the impulsive noise component is ~1000 and ~100 times stronger than the Gaussian component, for the highly and moderately impulsive noise cases respectively.

Table 6.1 Parameters of Narrowband Impulsive Noise Model

Case	Model parameter values	
	Impulsive Index (A)	Scale Parameter (Γ)
Moderately Impulsive Noise	0.10	0.05
Highly Impulsive Noise	0.10	0.005
ETS Noise	0.132	0.02408

6.2.1 WLAN

The BER performance evaluation of three WLAN PHYs in the presence of narrowband impulsive noise is presented in this section.

6.2.1.1 WLAN DSSS PHY

WLAN DSSS PHY supports two modes of operation with data rates of 1 and 2 Mbit/s and employs DSSS and DBPSK/DQPSK.

The BER performance evaluation is shown in Figure 6.1 for the three impulsive noise cases and two modes of operations. The reference for the evaluation is BER performance in AWGN. The BER is calculated for AWGN, Class A – HI, Class A– MI and ETS using the DSSS PHY model and plotted as E_b/N_0 (dB) vs. BER. It can be seen that:

1. In the presence of Class A – HI, modes 1 and 2 have a performance degradation of ~2dB and ~3dB respectively at BER = 10^{-5} and for E_b/N_0 > 7dB. For E_b/N_0 < 7dB the impact of the impulsive noise is less than AWGN.

2. In the presence of Class A – MI and ETS, there is no performance degradation and the impact of impulsive noise is less than AWGN.

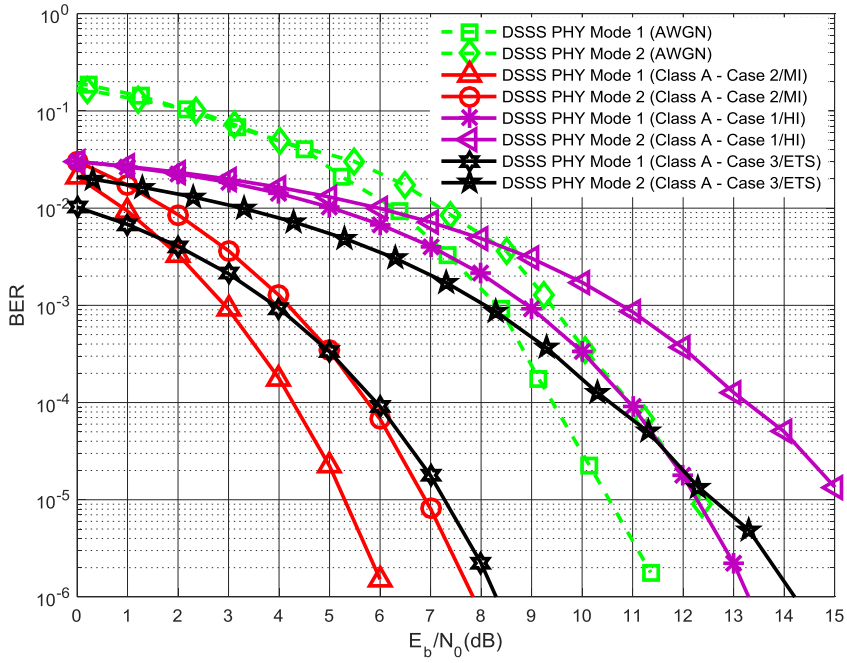

Figure 6.1: BER Performance evaluation of WLAN DSSS PHY in the presence of Narrowband Impulsive Noise

6.2.1.2 WLAN OFDM PHY

WLAN OFDM PHY supports 8 modes of operations with data rates ranging from 6Mbit/s to 54 Mbit/s and employs OFDM and convolutional FEC codes (Table 5.4). The BER performance of OFDM PHY (Modes 1, 3, 5, 7) in the presence of impulsive noise and AWGN is shown in Figures 6.2, 6.3 and 6.4. It can be seen that:

1. In the presence of Class A – HI, the performance of modes 1, 3, 5 and 7 degrades by ~1 dB, ~1dB, ~3dB and ~4dB respectively for at BER = 10^{-5}. There is an intersection between the AWGN and Class A – HI BER curves which shows the threshold for the $E_b/N_{0,}$ above which the impulsive noise has an impact on the BER greater than AWGN. The BER curves' intersection points for modes 1, 3, 5, and 7 are 3dB, 5dB, 7dB and 10dB and the corresponding BERs are ~10^{-3}, ~10-3, 0.0190 and 0.0280 (Figure 6.2).
2. In the presence of Class A – MI, there is no noticeable performance degradation for modes 1 and 3. For modes 5 and 7, however there a degradation of ~2dB (Figure 6.3).
3. In the presence of ETS, for modes 1 and 3, the performance degradation is <1dB whereas, for modes 5 and 7, it is ~3dB (Figure 6.4).

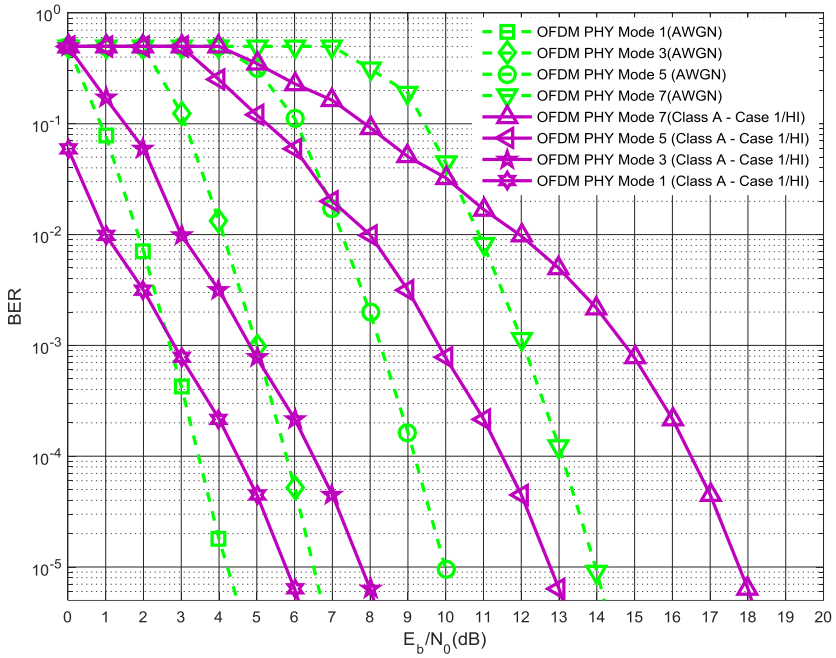

Figure 6.2: Performance of WLAN OFDM PHY in the presence of Class A - HI Noise.

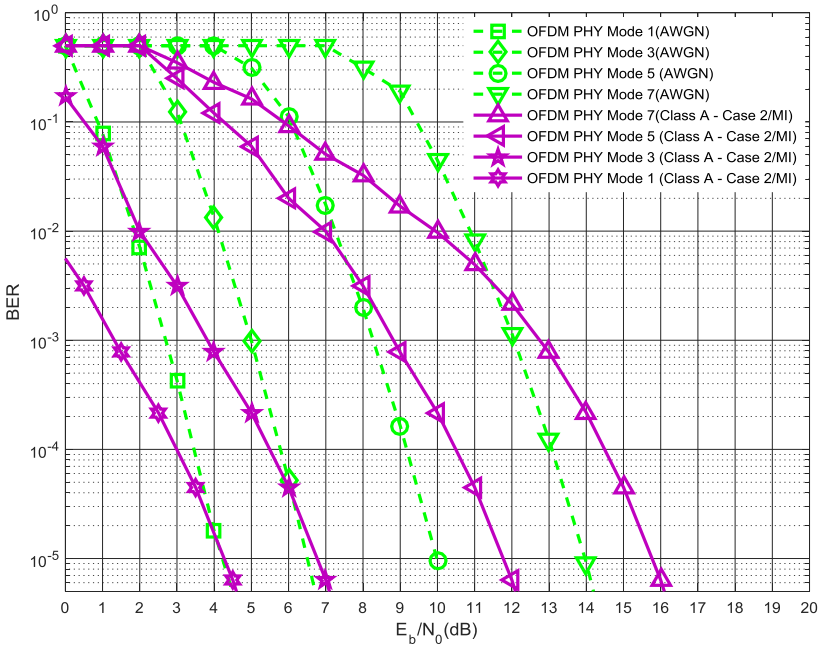

Figure 6.3: Performance of WLAN OFDM PHY in the presence of Class A – MI Noise

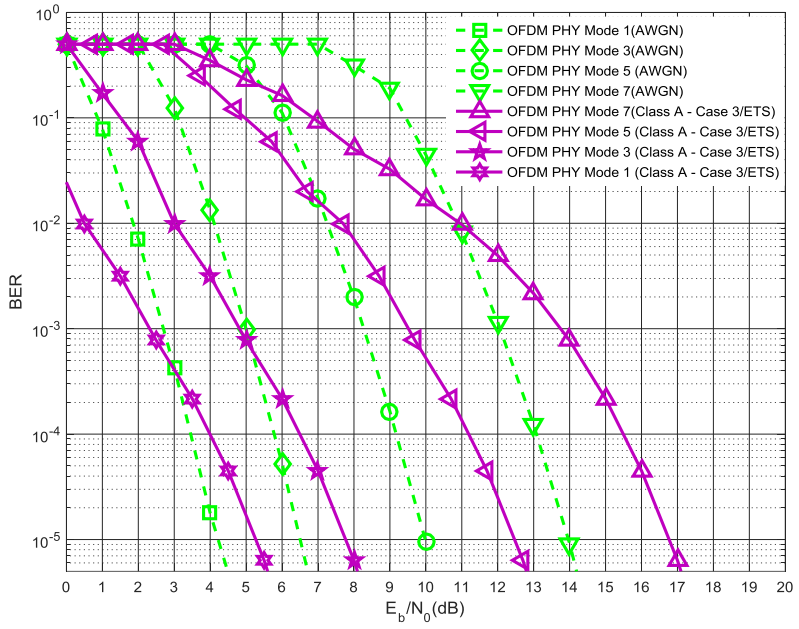

Figure 6.4: BER Performance of WLAN OFDM PHY in the presence of ETS Noise

6.2.1.3 WLAN HR DSSS PHY

WLAN HR DSSS PHY supports two modes of operations with data rates of 5.5 and 11Mbit/s and employs DSSS and CCK modulation. The BER performance in the presence of impulsive noise and AWGN is shown in Figure 6.5. It can be seen that:

1. In the presence of Class A – HI, the performance degradation for the modes 1 and 2 is 2dB and 5dB respectively for BER = 10^{-5}. The BER curves' intersection points are at 5 dB (mode 1) and 7 dB (mode 2) and the corresponding BER values are 0.005 and 0.05.
2. In the presence of Class A – MI and ETS, there is no noticeable performance degradation.

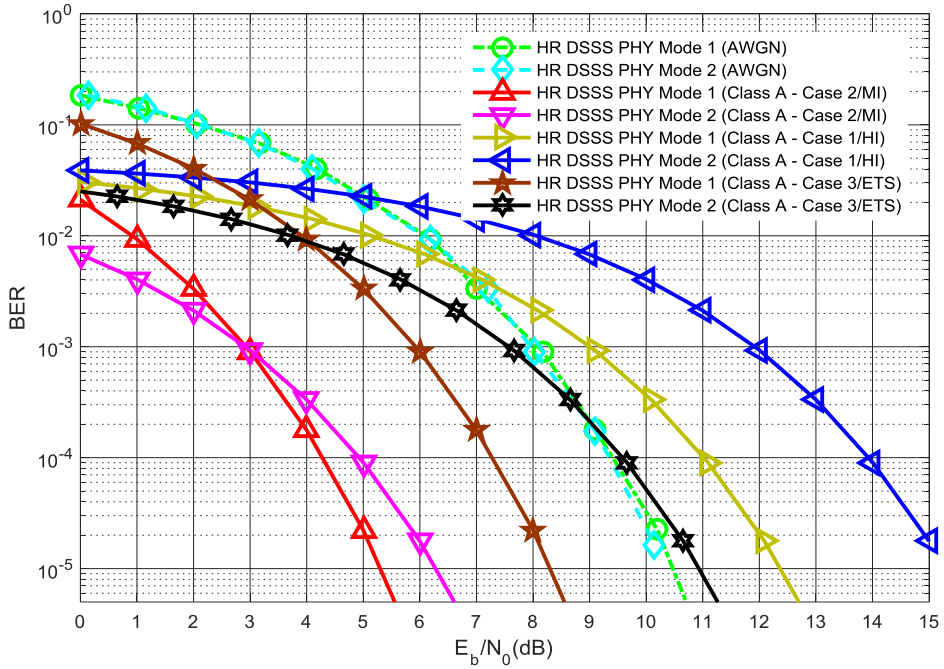

Figure 6.5: BER Performance of WLAN DSSS PHY in the presence of Narrowband Impulsive Noise.

6.2.2 Bluetooth

Bluetooth supports data rates of 1 Mbit/s and employs FHSS and GMSK. The BER performance comparison in the presence of impulsive noise and AWGN is shown in Figure 6.6.

It can be seen that, in the presence of Class A – HI, the performance degradation is ~3.5dB for BER = 10^{-5}. The BER curve intersection point is E_b/N_0 = 3dB and BER = 10^{-2}. In the presence of Class A – MI, the impact of impulsive noise is benign compared to the AWGN whereas the ETS noise degrades the performance by ~1dB at BER = 10^{-5}. The ETS BER curve intersects the AWGN BER curve at E_b/N_0. = 6.5dB and BER = ~10^{-4}.

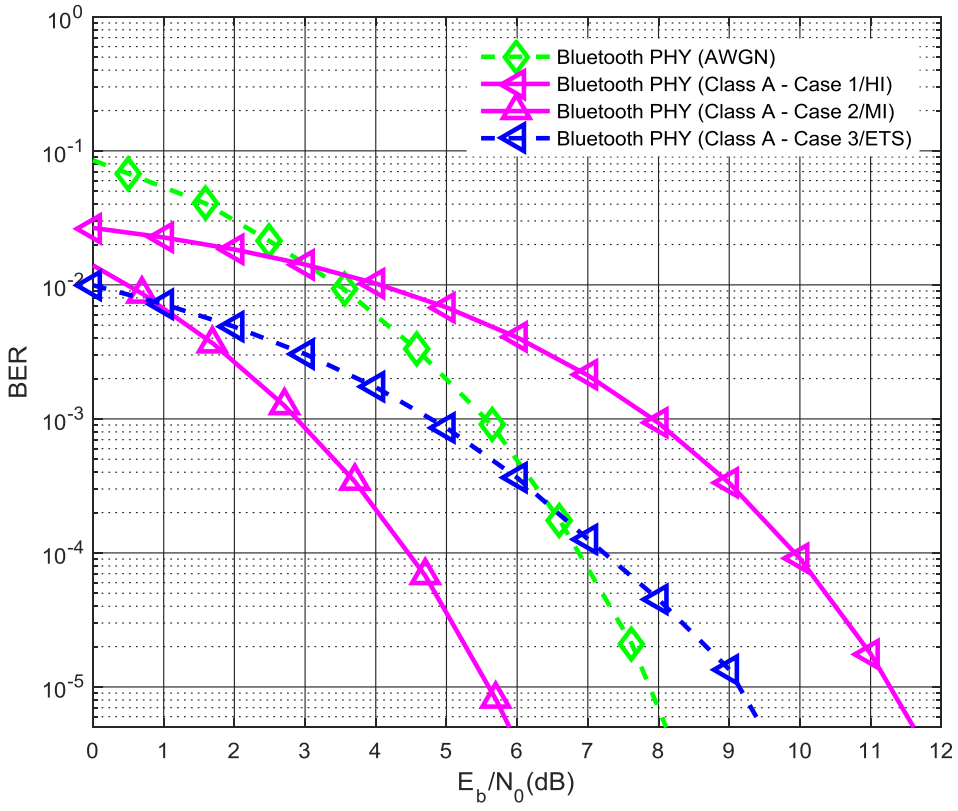

Figure 6.6: Performance of Bluetooth PHY in the presence of Narrowband Impulsive Noise

6.2.3 Zigbee

The BER performance evaluation of Zigbee PHY-1 is shown in Figure 6.7. The Zigbee PHY-1 supports a data rate of 20 kbps and employs DSSS and BPSK.

It can be seen that the BER performance in the presence of Class A - HI is comparable with that in AWGN and the performance degradation for BER = 10^{-5} is less than 1dB. In the presence of Class A – MI and ETS, the impact of impulsive noise is benign compared to AWGN.

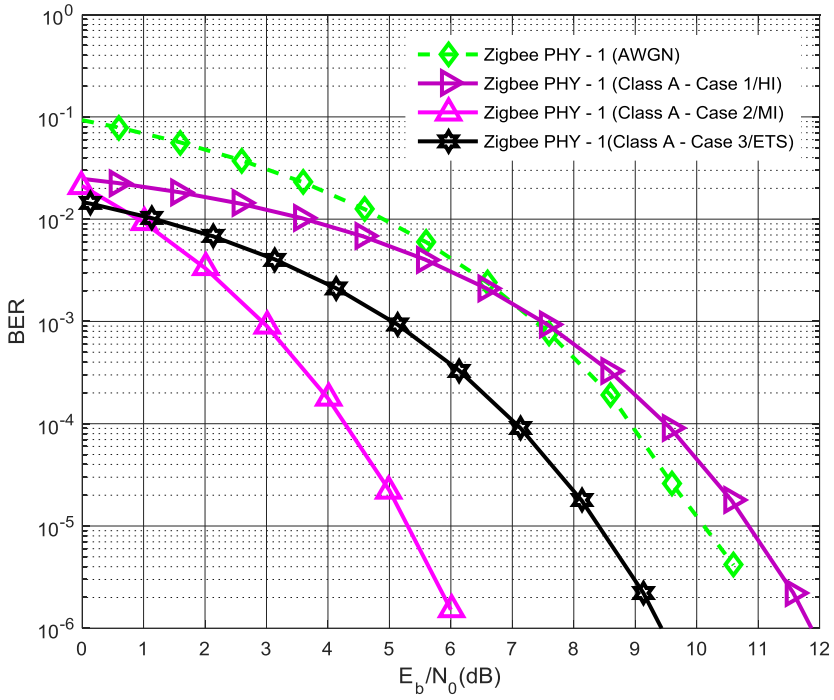

Figure 6.7: Performance of Zigbee PHY-1 in the presence of Narrowband Impulsive Noise

6.2.4 Comparison

In general, all candidate technologies perform poorly in the presence of highly impulsive noise at high E_b/N_0 and better at low E_b/N_0, compared to the performance in AWGN. However, in the presence of moderately impulsive and ETS noise, the BER performance, by and large, matches with the performance in the presence of Gaussian noise.

A BER performance comparison between WLAN, Bluetooth and Zigbee in the presence of narrowband impulsive noise is shown in Table 6.2. The performance is described in terms of the required E_b/N_0 to achieve a BER = 10^{-5} in the presence of impulsive noise. BER performance in the presence of AWGN is used as a reference.

The highest and lowest performance degradations are highlighted in red and green colours respectively.

Table 6.2: Performance comparison in the presence of Narrowband Impulsive Noise

Technology	Modulation	Spreading Gain	Coding Gain	Comparative Performance[12]		
				HI	MI	ETS
WLAN DSSS – Mode 1	DBPSK	10.4dB	No coding	- 2dB	5dB	3dB
WLAN DSSS - Mode 2	DQPSK	7.4dB	No coding	-3dB	5dB	4.5dB
WLAN OFDM - Mode 1	BPSK	No spreading	5dB	-1.5dB	0dB	-0.8dB
WLAN OFDM - Mode 3	QPSK	No spreading	3dB	-0.8dB	0dB	-1dB
WLAN OFDM - Mode 5	16 QAM	No spreading	3dB	-3dB	-1.5dB	-2.2dB
WLAN OFDM - Mode 7	64 QAM	No spreading	4dB	-4dB	-1.7dB	-2.5dB
WLAN HR DSSS - Mode 1	QPSK/CCK	3dB	No coding	-2dB	4dB	2dB
WLAN HR DSSS - Mode 2	QPSK/CCK	0dB	No coding	-5dB	3.7dB	2dB
Bluetooth	GMSK	80dB	2.6dB	-3.5dB	2.2dB	-1dB
Zigbee – PHY 1	BPSK	11.76dB	No coding	-0.8dB	4.7dB	1.7dB

6.3 Performance in Broadband Impulsive Noise

This section discusses performance evaluation of WLAN, Bluetooth and Zigbee in the presence of broadband impulsive noise, modelled as a SαS process. The broadband impulsive noise model has three parameters:

1. Shape parameter (α) controls the decay gradient of the PDF tails.
2. Dispersion parameter (γ) controls the spread of the distribution.
3. Location parameter (δ) is the point of symmetry of the SαS PDF.

[12] When BER = 10^{-5} and compared against BER for AWGN

The estimated parameters for the ETS noise are shown in Table 6.3.

Table 6.3 Parameters of SαS broadband noise model

Parameters	Estimated Value
Location Parameter (δ)	1.1805E-7
Characteristic Exponent (α)	1.4130
Dispersion (γ)	6.3422E-7

The SαS distribution does not have finite second-order moments and all SαS signal processing is therefore based on fractional lower order moments (FLOMs) [72]. Therefore, the use of a traditional signal-to-noise ratio (SNR) is not appropriate. BER performance can be characterized, however, as a function of dispersion (γ) and signal variance (*s)*. A generalized SNR (GSNR) is defined as [113]:

$$GSNR = 10log_{10}\left(\frac{s}{\gamma}\right) \qquad \text{Equation 6.1}$$

GSNR reduces to half (as a ratio, not decibels) of the SNR for Gaussian noise. The performance evaluation has been carried out as a function of GSNR and the PHY layer simulations (Chapter 5) are used to compute the BER.

6.3.1 WLAN

The BER performance evaluation of three WLAN PHYs in the presence of broadband impulsive noise is presented in this section.

6.3.1.1 WLAN DSSS PHY and WLAN HR DSSS PHY

The BER performance of DSSS and HR DSSS PHYs in the presence of ETS broadband impulsive noise is shown in Figure 6.8. The reference BER curves for the Gaussian case (SαS with $\alpha = 2$) are included for comparison. It can be seen that:

1. For DSSS PHY modes 1 and 2, there is a performance degradation of ~2dB and ~4.5dB respectively for BER = 10^{-5}.
2. For HR DSSS PHY modes 1 and 2, there is a performance degradation of 8.5 dB and 11 dB respectively for BER = 10^{-5}.

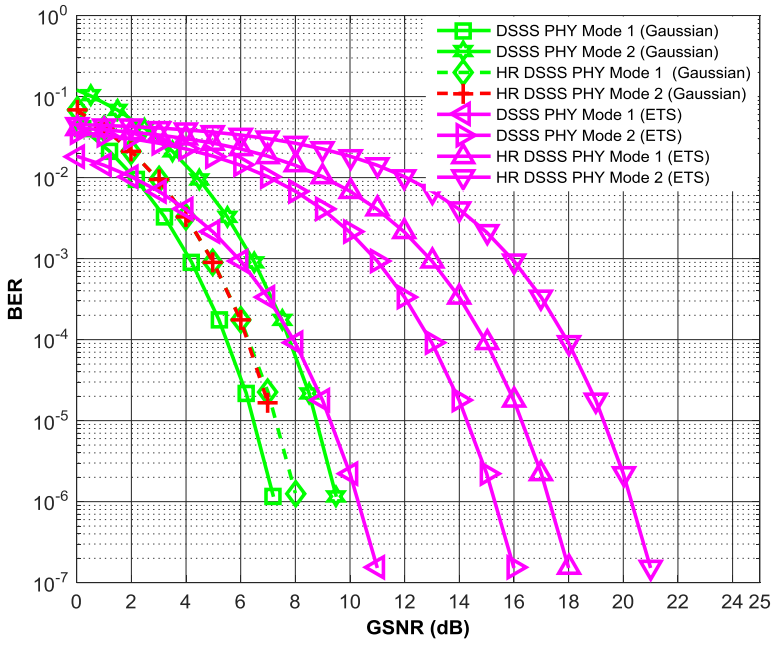

Figure 6.8 BER performance evaluation of DSSS PHY and HR DSSS PHY in the presence of broadband ETS noise

6.3.1.2 WLAN OFDM PHY

The BER performance of OFDM PHY (Modes 1, 3, 5 and 7) in the presence of ETS broadband impulsive noise is shown in Figure 6.9. It can be noticed that:

1. For mode 1, ETS noise has less effect on the BER performance compared with Gaussian noise, for low GSNR values. The required GSNR for achieving a BER = 10^{-5} is the same for the both Gaussian and ETS noise.
2. For mode 3, the BER performance has two distinct GSNR regions; low and high. In the low GSNR region ETS noise has less effect than Gaussian noise

whereas in the high GSNR region (GSNR > 7dB), ETS results in a performance degradation of ~ 2dB.

3. For mode 5 there is a performance degradation of ~1dB for BER = 10^{-5} when compared to Gaussian noise. For most of the practical GSNR operating range, the effect of the ETS noise is benign compared to Gaussian noise.
4. For mode 7, there is a performance degradation of ~4 dB when BER = 10^{-4} and it appears that the effect of an increase in the GSNR on the BER is low compared to modes 1, 3 and 5.

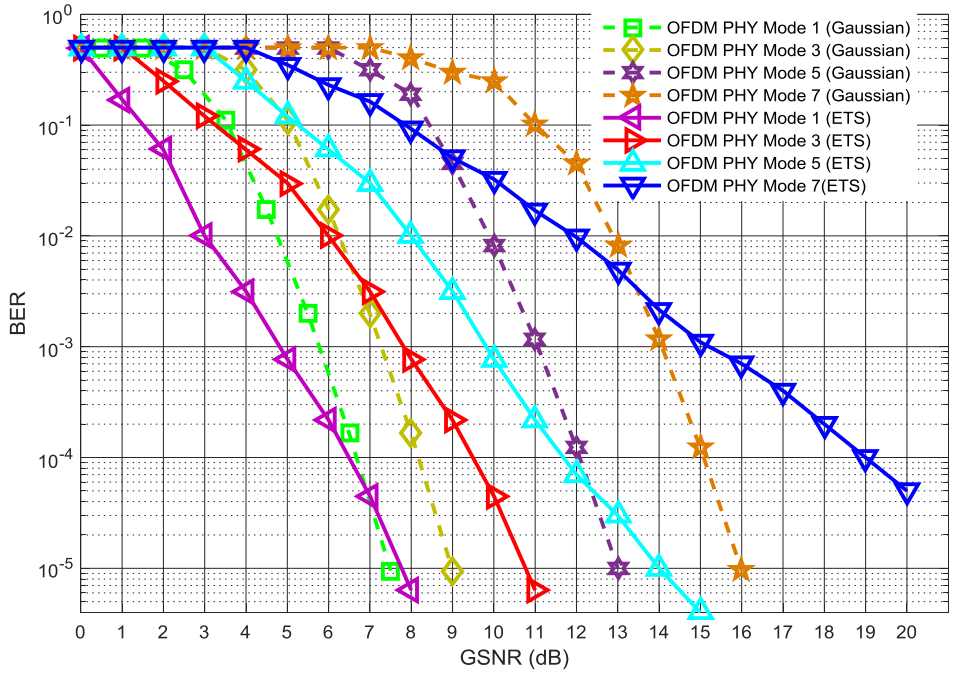

Figure 6.9: BER performance evaluation of OFDM PHY in the presence of broadband ETS noise

6.3.2 Bluetooth

BER performance of the Bluetooth PHY in the presence of broadband ETS noise is shown in Figure 6.10. It can be seen that for BER = 10^{-5}, there is a performance degradation of ~5dB when compared to performance in Gaussian noise.

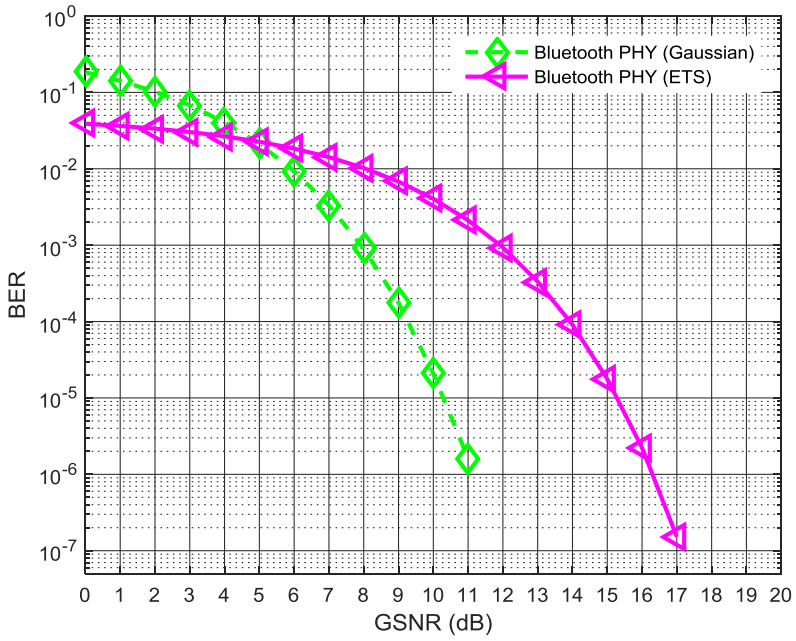

Figure 6.10: BER performance of Bluetooth receiver in the presence of broadband impulsive noise

6.3.3 Zigbee

The BER performance evaluation of the Zigbee PHY is split into two cases: (1) GSNR versus BER and (2) γ versus BER where γ is the dispersion parameter of the broadband impulsive noise model.

Figure 6.11 shows the results for the first case (for Zigbee PHY 1 and 2). It can be seen that the performance degradation due to broadband ETS is of the order of 1 dB and 2.5 dB worse than that due to Gaussian noise for PHY-1 and PHY-2

respectively. This is much less than the corresponding degradation in WLAN DSSS and HR DSSS PHYs. Zigbee supports a much lower maximum data-rate, however than that of WLAN PHYs.

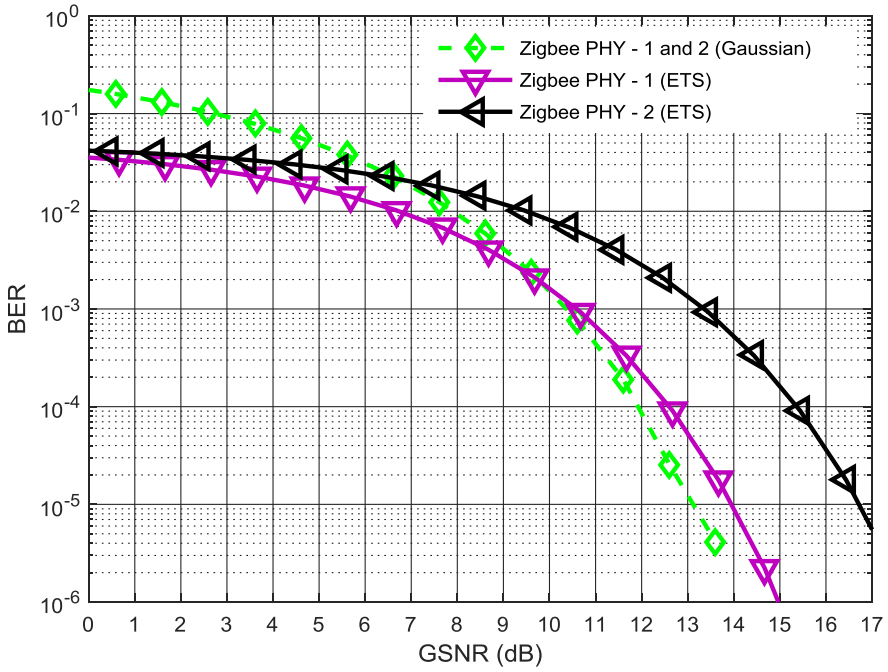

Figure 6.11 BER performance of Zigbee PHY in the presence of broadband ETS noise

The performance evaluation of case 2 is shown in Figures 13, where the BER is plotted against γ, for three values of α: 1 (corresponding to a Cauchy distribution), 1.40 (corresponding to broadband ETS noise) and 2 (corresponding to a Gaussian distribution). It can be seen that:

1. For $\gamma < 0.3$ the performance degradation with respect to the Gaussian case is negligible.

2. For $\gamma > 0.3$, the performance degradation is significant. Larger values of γ denote a greater dominance of impulsive noise power over Gaussian noise power. For example, for $\gamma = 0.4$, the BERs for the Gaussian and ETS noise are ~ 10^{-5} and 10^{-3} respectively. The Cauchy distribution represents noise that is more impulsive noise than ETS noise.

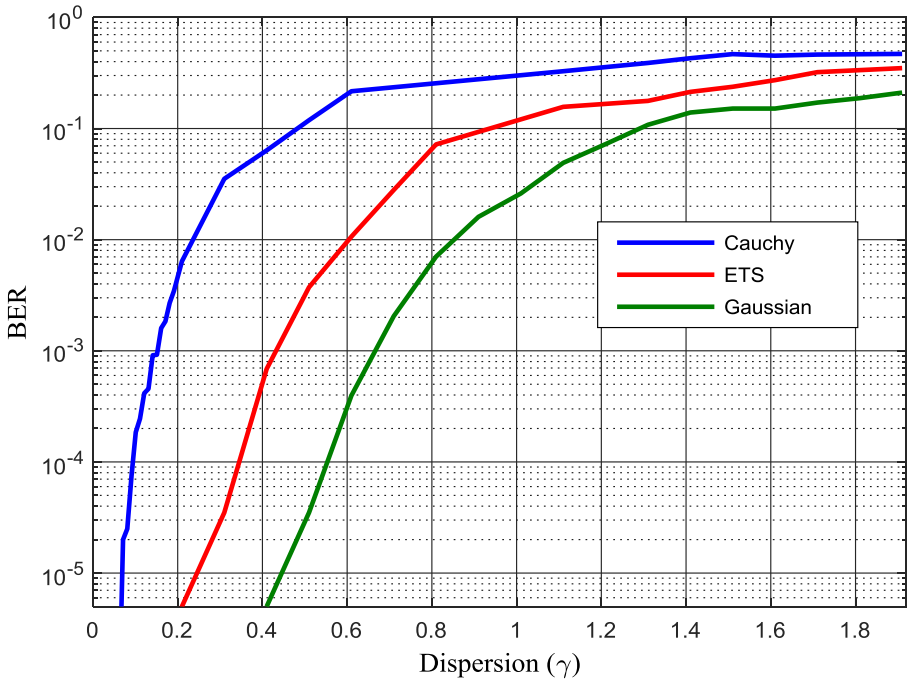

Figure 6.12 BER Performance of Zigbee PHY -1in the presence of broadband impulsive noise in term of γ.

6.3.4 Comparison

The performance comparison of WLAN, Bluetooth and Zigbee in the presence of the broadband ETS noise shows that the WLAN HR DSSS PHY - Mode 2, WLAN OFDM PHY Mode 7 and Bluetooth suffer a significant performance penalty whereas the other candidate technologies show either no, or little, performance penalty. A

comparison of the candidate technologies is given in Table 6.4 showing the degradation in terms of GSNR in the presence of ETS noise, with respect to AWGN for a BER = 10^{-5}.

Table 6.4: Performance comparison in the presence of narrowband and broadband ETS noise

Technology	Comparative Performance[13]	
	ETS (Broadband)	ETS (Narrowband)
WLAN DSSS – Mode 1	-2dB	3dB
WLAN DSSS - Mode 2	-4.5dB	4.5dB
WLAN OFDM - Mode 1	0 dB	-0.8dB
WLAN OFDM - Mode 3	-2 dB	-1dB
WLAN OFDM - Mode 5	-1 dB	-2.2dB
WLAN OFDM - Mode 7	> -5dB	-2.5dB
WLAN HR DSSS - Mode 1	-8.5dB	2dB
WLAN HR DSSS - Mode 2	-11dB	2dB
Bluetooth	-5dB	-1dB
Zigbee – PHY 1	-1 dB	1.7dB

6.4 Discussion

The results of the simulation-based performance evaluation, given in sections 6.2 and 6.3, cover a range of PHY layers which employ different modulation techniques, spreading codes/rates and error coding. It can be inferred from the results that:

1. The spreading rate has an explicit impact on the BER performance in the non-Gaussian noise environment. For example, the comparison of the WLAN

[13] When BER = 10^{-5} and compared against BER for AWGN

DSSS PHY, WLAN HR DSSS PHY and Zigbee PHY shows that PHYs with the higher spreading rate show less performance degradation. Zigbee has the highest spreading rate and lowest performance degradation whereas WLAN HR DSSS PHY has the lowest spreading rate and highest performance degradation. This is evident in both narrowband and broadband impulsive noise performance evaluation. (Table 6.2 and 6.4).

2. Two SNR regions can be seen in most of the performance results, low SNR region where AWGN dominates and a high SNR region where non-Gaussian impulsive component dominates the impact on the BER performance. There appears to be a noise floor which reduces the effect of an increase in SNR on the corresponding BER. In some cases, a clear plateau is visible in the BER curve.

6.5 Summary

BER performance of WLAN, Bluetooth and Zigbee in narrowband and broadband impulsive noise environments has been modelled, evaluated and compared against the expected performance in the presence of AWGN leading to a potential rank-ordering of the candidate technologies for electricity substation applications.

CHAPTER 7

CONCLUSIONS AND FUTURE WORK

The focus of research was to study and evaluate the PHY layer performance of candidate wireless technologies in the presence of impulsive noise found in electricity substations. The candidate technologies are WALN, Bluetooth and Zigbee.

7.1 Summary and Conclusions

The methodology adopted to carry out this research was to compile an impulsive noise database from substation RF noise measurements, characterize the noise using appropriate models, and perform computer simulations to evaluate the performance of candidate wireless technologies in terms of BER.

An impulsive noise database has been compiled from a seven-months-long substation noise measurements campaign. A WPT based de-noising algorithm was used to extract impulsive noise from the recorded time-series of substation noise. The characterization of substation noise has been defined by the electromagnetic substation noise sources, which are radiations from PD in electrical insulations and switching transients. It was established using a technical argument and an analysis of the recorded impulsive noise data that the substation noise profile is non-Gaussian and impulsive.

For building the substation representative noise models, the assumptions made in Middleton's work for modelling non-Gaussian noise have been objectively analysed

and their usability and relationship to the substation noise environment have been explored and positively exploited. Moreover, statistical analysis of the recorded time-series noise data has been used to determine that noise models based on Class A and SαS distributions could represent the substation noise.

The performance of candidate wireless technologies has been evaluated using computer simulations where PHY layer simulations of these technologies were implemented using MATLAB/Simulink and noise models were used to generate the impulsive noise. The parameters of noise models were estimated using the compiled impulsive noise database. Major conclusions drawn from this research work are listed below:

7.1.1 Substation Noise Modelling

The characteristics of Class A and SαS distributions make them a tool of choice for modelling of substation noise environment. A comparison of Class A (narrowband), SαS distributions (broadband), and statistical analysis of the recorded noise show that the SαS distributions represent a better approximation of substation noise. Based on the comparison of several parameter estimation methods, the EM-based method performs better for Class A and FLOM-EOS method performs better for SαS noise models.

7.1.2 Performance Evaluation

7.1.2.1 Performance in Highly Impulsive Class A noise

In the presence of highly impulsive Class A noise, all candidate technologies show significant performance degradation[14] for high E_b/N_0 region. In the low E_b/N_0 region, the impact of impulsive noise is less than AWGN. The E_b/N_0 values for the high and low region are different for each candidate technology.

7.1.2.2 Performance in Moderately Impulsive Class A Noise

In the presence of moderately impulsive Class A noise, the impact of impulsive noise is less than AWGN for all technologies, with the exception of WLAN OFDM PHY (modes 5 and 7), which shows a performance penalty of ~2 dB.

7.1.2.3 Performance in ETS Noise modelled as Class A (Narrowband)

There is no significant difference in terms of performance in the presence of moderately impulsive noise and ETS noise modelled as Class-A.

7.1.2.4 ETS Noise modelled as SαS (Broadband)

In the presence of ETS noise, all candidate technologies with the exception of WLAN OFDM PHY (mode 1) suffer a performance penalty[15]. Performance results for each technology are:

a. For WLAN DSSS PHY (modes 1 and 2) there is a performance degradation of ~2dB and ~4.5dB respectively.
b. For HR DSSS PHY (modes 1 and 2) there is a performance degradation of 8.5 dB and 11 dB respectively.

[14] The stated performance is with reference to AWGN, in terms of E_b/N_0 and for a BER = 10^{-5} (for narrowband case)
[15] The stated performance is with reference to AWGN, in terms of GSNR and for a BER = 10^{-5} (For broadband approximation)

c. For WLAN OFDM (mode 3), the BER performance has two distinct regions; in the low GSNR region, ETS noise has less effect than Gaussian noise whereas in the high GSNR region there is a performance degradation of ~ 2dB.
d. For WLAN OFDM (mode 5) there is a performance degradation of ~1dB for BER = 10^{-5}. For most of the practical GSNR operating range, the effect of the ETS noise is benign compared to Gaussian noise.
e. For Bluetooth, there is a performance degradation of ~5dB.
f. For Zigbee, there is a performance degradation of 1dB and 2.5dB for PHY-1 and PHY-2 respectively.

The WLAN OFDM PHY shows a better performance compared to other candidate technologies because of the application of the error coding. The performance difference between WLAN DSSS and HR DSSS PHY is due to different spreading rates. There is a noticeable pattern; the higher the spreading-rate is, the better the performance.

7.2 Thesis Contributions

Against the stated objective of research work to evaluate the performance of candidate short range wireless technologies for their deployment in electricity substation for control, protection and monitoring applications, following contributions have been made to the knowledge:

1. A framework has been proposed for the performance evaluation of candidate wireless technologies, which includes a compilation of impulsive noise

database, implementation of substation representative noise models and performance simulations.

2. Two representative models of substation noise have been developed with implementations of the corresponding parameter estimation methods. The developed models have been converted to Simulink blocks.
3. PHY layer simulations of three candidate wireless technologies have been implemented and validated.
4. A detailed performance assessment of these wireless technologies has been carried out which provides guidance for their deployment in an electricity substation. A rank ordering of these technologies has been proposed, based on the BER performance.

7.3 Limitations

The measurements data which is used to characterise the substation noise is recorded from one electricity substation whereas noise environment of different substations can vary and it would have been beneficial to record and use the data from a number of substations.

Given the benefits of using wireless receivers to support the functionalities needed to achieve the targets of true future smart grids, it is suggested to conduct the on-field trials of commercially available WLAN/WPAN transceivers including the ones, which have been recommended for communications in rugged industrial environments.

7.4 Scope for Further Research

7.4.1 Impact of Re-transmission

In addition to PHY performance, it is suggested to include the upper layers of OSI stack (particularly MAC) to study the impact of impulsive noise on re-transmission rate and delay. The IEC standard 61850-5 for substation automation specifies the time requirements of time-critical applications. The specified time requirements are 3 ms and 5 ms for transmission and distribution substations [114].

7.4.2 Robust Receiver Design

The performance evaluation carried out in this work is based on the matched filter detection at the receiver. It is suggested to further extend this work to include different receiver types and study their performance in the presence of impulsive noise.

7.4.3 BER based Fault Monitoring

A fault monitoring system based on BER or Packet Error Rate (PER) of sensor nodes is another possible extension of this work. It is evident that the performance of the candidate wireless technologies degrades significantly in the presence of highly impulsive noise (which is when the transceiver is in the close vicinity of a PD source). This trend can be used to design a fault monitoring system. A potential system would have a Wireless Sensor Network (WSN) setup in the substation and a smart system which would broadcast a known signal and ping all sensor nodes. A BER/PER would be computed by comparing the broadcasted and received signals.

REFERENCES

[1] A. Shapoury and M. Kezunovic, "Noise Profile of Wireless Channels in High Voltage Substations," in *Power Engineering Society General Meeting, 2007. IEEE*, 2007, pp. 1-8.

[2] A. Willig, K. Matheus, and A. Wolisz, "Wireless Technology in Industrial Networks," *Proceedings of the IEEE,* vol. 93, pp. 1130-1151, 2005.

[3] L. Chun-Hao and N. Ansari, "The Progressive Smart Grid System from Both Power and Communications Aspects," *Communications Surveys & Tutorials, IEEE,* vol. 14, pp. 799-821, 2012.

[4] T. Papallo, "Networks in a network, communications in electrical distribution," in *Petroleum and Chemical Industry Technical Conference (PCIC), 2013 Record of Conference Papers Industry Applications Society 60th Annual IEEE*, 2013, pp. 1-7.

[5] IEEE, "IEEE Standard C37.1, Definition, Specification, and Analysis of Systems Used for Supervisory Control, Data Acquisition, and Automatic Control," ed: IEEE, 1994.

[6] J. Bougie, "Engineering your substation network for protective relaying, automation and SCADA," in *Protective Relay Engineers, 2013 66th Annual Conference for*, 2013, pp. 292-298.

[7] M. K. Simon, J. K. Omura, R. A. Scholtz, and B. K. Levitt, *Spread Spectrum Communications Handbook*: McGraw-Hill, 2002.

[8] I. A. Glover, Q. Shan, P. J. Mooore, I. E. Portugues, and R. J. Watson, "An Investigation into the Vulnerability of WLAN and WPAN Technologies to Impulsive Noise in Electricity Transmission Substations," presented at the Ninth International Symposium on Communication Theory and Applications (ISCTA-07) Ambleside, Lake District, UK, 2007.

[9] M. G. Sanchez, I. Cuinas, and A. V. Alejos, "Interference and impairments in radio communication systems due to industrial shot noise," in *Industrial Electronics, 2007. ISIE 2007. IEEE International Symposium on*, 2007, pp. 1849-1854.

[10] D. Middleton, "Non-Gaussian noise models in signal processing for telecommunications: New methods and results for class A and class B noise models," *Ieee Transactions on Information Theory,* vol. 45, pp. 1129-1149, 1999.

[11] S. V. Vaseghi, *Advanced Digital Signal Processing and Noise Reduction*, Fourth ed.: John Wiley&Sons, Ltd, 2008.

[12] L.Breiman, *Probability Classics in Applied Mathematics*: SIAM: Society for Industrial and Applied Mathematics, 1968.

[13] W. Davenport and W. Root. (1987). *An introduction to the theory of random signals and noise*.

[14] S. V. Vaseeghi, "Advanced Digital Signal Processing and Noise Reduction, 4th Edition," 2008.

[15] R. Cristi, *Modern Digital Signal Processing*: Nelson Engineering, 2003.

[16] P. J. Moore, I. Portugues, and I. A. Glover, "Pollution of the radio spectrum from the generation of impulsive noise by high voltage equipment," in *IEE Conference – Getting the Most out of the Radio Spectrum*, 2002.

[17] R. J. Van Brunt, "Stochastic Properties of Partial-discharge Phenomena," *IEEE Transactions on Electrical Insulation,* vol. 26, pp. 902-948, 1991.

[18] B. L. Beers, V. W. Pine, and S. T. Ives, "Theoretical properties of streamers in solid dielectrics," in *Conference on Electrical Insulation & Dielectric Phenomena - Annual Report 1981*, 1981, pp. 390-397.
[19] J. Devins, "The 1984 J. B. Whitehead Memorial Lecture the Physics of Partial Discharges in Solid Dielectrics," *IEEE Transactions on Electrical Insulation,* vol. EI-19, pp. 475-495, 1984.
[20] R. V. Latham, "High-voltage Vacuum Insulation New Horizons," *IEEE Transactions on Electrical Insulation,* vol. 23, pp. 881-894, 1988.
[21] T. Kropp, "Technical Report: Wireless Connectivity for Electric Substations," EPRI Tech 2008.
[22] "P1777 Technical Report on Recommended Practices for Using Wireless Data Communications in Power System Operations," IEEE Power Engineering Society 2007.
[23] T. Kropp, "Tech Report : Assessment of WirelessTechnologies in Substation Functions (Part II: Substation Monitoring and Management)," EPRI Tech 2006.
[24] K. M. Abdel-Latif, M. M. Eissa, A. S. Ali, O. P. Malik, and M. E. Masoud, "Laboratory Investigation of Using Wi-Fi Protocol for Transmission Line Differential Protection," *IEEE Transactions on Power Delivery,* vol. 24, pp. 1087-1094, 2009.
[25] D. R. Brown, J. A. Slater, and A. E. Emanuel, "A wireless differential protection system for air-core inductors," *IEEE Transactions on Power Delivery,* vol. 20, pp. 579-587, 2005.
[26] G. Thonet and B. Deck, "A new wireless communication platform for medium-voltage protection and control," in *IEEE International Workshop on Factory Communication Systems, 2004. Proceedings.*, 2004, pp. 335-338.
[27] A. Timbus, M. Larsson, and C. Yuen, "Integration of wind energy resources in the utility control and information technology infrastructures," in *2008 IEEE International Symposium on Industrial Electronics*, 2008, pp. 2371-2376.
[28] P. Palensky and D. Dietrich, "Demand Side Management: Demand Response, Intelligent Energy Systems, and Smart Loads," *IEEE Transactions on Industrial Informatics,* vol. 7, pp. 381-388, 2011.
[29] L. K. Siow, P. L. So, H. B. Gooi, F. L. Luo, C. J. Gajanayake, and Q. N. Vo, "Wi-Fi based server in microgrid energy management system," in *TENCON 2009 - 2009 IEEE Region 10 Conference*, 2009, pp. 1-5.
[30] *RUGGEDCOM – Industrial Strength Network [Available Online at* http://www.ruggedcom.com/applications/smart-grid/*] 2011*.
[31] C. M. Wiggins, D. E. Thomas, F. S. Nickel, T. M. Salas, and S. E. Wright, "Transient electromagnetic interference in substations," *IEEE Transactions on Power Delivery,* vol. 9, pp. 1869-1884, 1994.
[32] W. H. Siew, Y. C. Liu, B. Musa, F. Mir, and Y. Wang, "Basis for a Wireless Network for EMC Measurements in Electric Substations," in *2007 IEEE International Symposium on Electromagnetic Compatibility*, 2007, pp. 1-5.
[33] I. Portuguds, P. J. Moore, and I. A. Glover, "Characterisation of radio frequency interference from high voltage electricity supply equipment," in *Twelfth International Conference on Antennas and Propagation, 2003 (ICAP 2003). (Conf. Publ. No. 491)*, 2003, pp. 820-823 vol.2.

[34] A. Shapoury and M. Kezunovic, "Field survey of wireless ISM-band channel properties for substation applications," in *2003 IEEE Power Engineering Society General Meeting (IEEE Cat. No.03CH37491)*, 2003, pp. 1-1074 Vol. 2.

[35] Q. Shan, I. A. Glover, R. Rutherford, S. Bhatti, R. Atkinson, I. E. Portugues, and P. J. Moore, "Detection of ultra-wide-band impulsive noise in a 400 kV air insulated electricity substation," in *Electricity Distribution - Part 1, 2009. CIRED 2009. 20th International Conference and Exhibition on*, 2009, pp. 1-4.

[36] Q. Shan, I. A. Glover, P. J. Moore, I. E. Portugues, M. Judd, R. Rutherford, and R. J. Watson, "TEM horn antenna for detection of impulsive noise," in *2008 International Symposium on Electromagnetic Compatibility - EMC Europe*, ed: IEEE, 2008, pp. 1-6.

[37] S. Miyamoto, M. Katayama, and N. Morinaga, "Performance analysis of QAM systems under class A impulsive noise environment," *Electromagnetic Compatibility, IEEE Transactions on,* vol. 37, pp. 260-267, 1995.

[38] S. Jong-Soo, S. J. Cho, and K. Feher, "Impact of non-Gaussian impulsive noise on the performance of high-level QAM," *Electromagnetic Compatibility, IEEE Transactions on,* vol. 31, pp. 177-180, 1989.

[39] W. Jianqing, O. Fujiwara, and T. Takagi, "Experimental evaluation of MSK and GMSK with differential detection in non-Gaussian impulsive noise environment," in *Electromagnetic Compatibility Proceedings, 1997 International Symposium on*, 1997, pp. 296-299.

[40] S. Ö. Tengstrand and P. Stenumgaard, "Performance estimation of DSSS wireless systems in impulsive interference," in *2015 IEEE International Symposium on Electromagnetic Compatibility (EMC)*, 2015, pp. 160-164.

[41] J. Jia and J. Meng, "Partial discharge impulsive noise in electricity substations and the impact on 2.4 GHz and 915 MHz ZigBee communications," in *2013 IEEE Power & Energy Society General Meeting*, 2013, pp. 1-5.

[42] A. Bo, Z. Weidong, C. Xiang, L. Jikun, S. Yingbin, and L. Shaoyu, "A study on immunity of wireless sensor unit in substation," in *International Symposium on Electromagnetic Compatibility - EMC EUROPE*, 2012, pp. 1-5.

[43] I. A. Glover, "Vulnerability of Wireless Network Technology to Impulsive Noise in Electricity Transmission Substations," ed. University of Strathclyde, Glasgow, UK: EPSRC, 2007.

[44] I. E. Portugues, P. J. Moore, and I. A. Glover, "An investigation into the effect of receiver bandwidth for the interpretation of partial discharge impulses using remote radio sensing," in *International University Power Engineering Conference*, ed, 2002, pp. 529-533.

[45] P. J. Moore, I. Portugues, and I. A. Glover, "A nonintrusive partial discharge measurement system based on RF technology," in *in Power Engineering Society General Meeting*, ed, 2003, p. 633.

[46] *UK OFCOM - United Kingdom table of radio frequency allocations*. Available: http://www.ofcom.org.uk/static/archive/ra/publication/ra_info/ra365.htm

[47] Q. Shan, S. Bhatti, I. A. Glover, R. Atkinson, I. E. Portugues, P. J. Moore, and R. Rutherford, "Extraction of impulsive noise from measurements in a

400 kV electricity substation," in *Proceedings of the 4th IASME/WSEAS international conference on Energy \& environment*, ed. Cambridge, UK: World Scientific and Engineering Academy and Society (WSEAS), 2009, pp. 135-139.

[48] S. Sriram, S. Nitin, K. M. M. Prabhu, and M. J. Bastiaans, "Signal denoising techniques for partial discharge measurements," *Dielectrics and Electrical Insulation, IEEE Transactions on,* vol. 12, pp. 1182-1191, 2005.

[49] L. Satish and B. Nazneen, "Wavelet-based denoising of partial discharge signals buried in excessive noise and interference," *Dielectrics and Electrical Insulation, IEEE Transactions on,* vol. 10, pp. 354-367, 2003.

[50] C. S. Chang, J. Jin, C. Chang, T. Hoshino, M. Hanai, and N. Kobayashi, "Separation of corona using wavelet packet transform and neural network for detection of partial discharge in gas-insulated substations," *IEEE Transactions on Power Delivery,* vol. 20, pp. 1363-1369, 2005.

[51] E. Hatzipantelis, A. Murray, and J. Penman, "Comparing hidden Markov models with artificial neural network architectures for condition monitoring applications," in *Artificial Neural Networks, 1995., Fourth International Conference on*, 1995, pp. 369-374.

[52] E. J. Wegman, S. C. Schwartz, and J. B. Thomas, *Topics in non-Gaussian signal processing*. New York: Springer-Verlag, 1989.

[53] M. Stojanovic and J. Preisig, "Underwater acoustic communication channels: Propagation models and statistical characterization," *Communications Magazine, IEEE,* vol. 47, pp. 84-89, 2009.

[54] J. D. Parsons, "Man-made Noise and Interference," in *The Mobile Radio Propagation Channel*, ed: John Wiley & Sons, Ltd, 2001, pp. 263-306.

[55] S. Banerjee and M. Agrawal, "Underwater acoustic communication in the presence of heavy-tailed impulsive noise with bi-parameter cauchy-Gaussian mixture model," in *Ocean Electronics (SYMPOL), 2013*, 2013, pp. 1-7.

[56] A. Kumar, R. Bahl, R. Gupta, and H. Choudhary, "Performance enhancement of GMSK and LDPC based VLF communication in atmospheric radio noise," in *Communications (NCC), 2013 National Conference on*, 2013, pp. 1-5.

[57] V. Algazi, "Binary detection in white non-gaussian noise," *Lincoln Laboratory Massachusetts Institute of Technology,* 1964.

[58] P. Mertz, "Model of Impulsive Noise for Data Transmission," *Communications Systems, IRE Transactions on,* vol. 9, pp. 130-137, 1961.

[59] G. Trunk, "Non-rayleigh sea clutter: properties and detection of targets," *Automatic Dectection and Radar Data Processing, D.C. Schleher, Ed., Artech House, Dedham,* 1980.

[60] W. Richter and T. Smits, "Signal Design and Error Rate of an Impulse Noise Channel," *IEEE Transactions on Communications,* vol. 19, pp. 446-458, 1971.

[61] S. O. Rice, "Mathematical analysis of random noise," *Bell Syst Tech J,* vol. 24, pp. 46-156, 1945.

[62] A. Spaulding and D. Middleton, "Optimum Reception in an Impulsive Interference Environment--Part I: Coherent Detection," *Communications, IEEE Transactions on,* vol. 25, pp. 910-923, 1977.

[63] M. S. Britton and M. L. Scholz, "Practical utilization of Middleton EMI models: Automated modelling, parameter estimation and optimization,"

Defence Science and Technology Organisation, Technical Report, DSTO-TR-02341995.
[64] K. Vastola, "Threshold Detection in Narrow-Band Non-Gaussian Noise," *IEEE Transactions on Communications,* vol. 32, pp. 134-139, 1984.
[65] L. Berry, "Understanding Middleton's Canonical Formula for Class a Noise," *IEEE Transactions on Electromagnetic Compatibility,* vol. EMC-23, pp. 337-344, 1981.
[66] H. Ishikawa, M. Itami, and K. Itoh, "A Study on Adaptive Modulation of OFDM under Middleton's Class-A Impulsive Noise Model," in *Consumer Electronics, 2007. ICCE 2007. Digest of Technical Papers. International Conference on*, 2007, pp. 1-2.
[67] K. M. Rabie and E. Alsusa, "Orthogonal poly-phase MC-CDMA over multipath power-line channels with Middleton class-A noise," in *Communications (ICC), 2015 IEEE International Conference on*, 2015, pp. 722-727.
[68] G. Yu, W. XuDong, H. Rongxi, and P. Fuwen, "Performance of space-time block coding under impulsive noise environment," in *Advanced Computer Control (ICACC), 2010 2nd International Conference on*, 2010, pp. 445-448.
[69] E. Alsusa and K. M. Rabie, "Dynamic Peak-Based Threshold Estimation Method for Mitigating Impulsive Noise in Power-Line Communication Systems," *Power Delivery, IEEE Transactions on,* vol. 28, pp. 2201-2208, 2013.
[70] R. Savoia and F. Verde, "Performance Analysis of Distributed Space–Time Block Coding Schemes in Middleton Class-A Noise," *Vehicular Technology, IEEE Transactions on,* vol. 62, pp. 2579-2595, 2013.
[71] G. T. Z. Yongsub Kim, "The Middleton Class B Model and Its Mixture Representation," in *Centre for Signal and Image processing, Technical Report No. CSIP TR-98-01*, 1998.
[72] M. Shao and C. L. Nikias, "Signal processing with fractional lower order moments: stable processes and their applications," *Proceedings of the IEEE,* vol. 81, pp. 986-1010, 1993.
[73] V. In, P. Longhini, and A. Palacios, *Applications of Nonlinear Dynamics: Model and Design of Complex Systems*: Springer Science & Business Media, 2009.
[74] J. Evans and A. Griffiths, "Design of a Sanguine Noise Processor Based Upon World-Wide Extremely Low Frequency (ELF) Recordings," *Communications, IEEE Transactions on,* vol. 22, pp. 528-539, 1974.
[75] B. K. W. Stuck, "A Statistical Analysis of Telephone Noise," *Bell Syst Tech J,* vol. 53, 1974.
[76] G. A. Tsihrintzis and C. L. Nikias, "Fast estimation of the parameters of alpha-stable impulsive interference," *Ieee Transactions on Signal Processing,* vol. 44, pp. 1492-1503, 1996.
[77] W. Henkel and T. Kessler, "Statistical description and modelling of impulsive noise on the German telephone network," *Electronics Letters,* vol. 30, pp. 935-936, 1994.
[78] L. F. Lind and N. A. Mufti, "Efficient method for modelling impulse noise in a communication system," *Electronics Letters,* vol. 32, pp. 1440-1441, 1996.

[79] J. H. Fennick, "Amplitude Distributions of Telephone Channel Noise and a Model for Impulse Noise," *Bell System Technical Journal,* vol. 48, pp. 3243-3263, 1969.
[80] K. Szechenyi, "On the NEXT and impulse noise properties of subscriber loops," in *Global Telecommunications Conference and Exhibition 'Communications Technology for the 1990s and Beyond' (GLOBECOM), 1989. IEEE*, 1989, pp. 1569-1573 vol.3.
[81] S. Qingshan, S. Bhatti, I. A. Glover, R. Atkinson, I. E. Portugues, P. J. Moore, and R. Rutherford, "Characteristics of impulsive noise in electricity substations," in *Signal Processing Conference, 2009 17th European*, 2009, pp. 2136-2140.
[82] D. Middleton, "Procedures for Determining the Parameters of the First-Order Canonical Models of Class A and Class B Electromagnetic Interference.," *Electromagnetic Compatibility, IEEE Transactions on,* vol. EMC-21, pp. 190-208, 1979.
[83] S. M. Zabin and H. V. Poor, "Parameter estimation for Middleton Class A interference processes," *Communications, IEEE Transactions on,* vol. 37, pp. 1042-1051, 1989.
[84] S. M. Zabin and H. V. Poor, "Efficient Estimation of Class-A noise via the EM Algorithm," *Ieee Transactions on Information Theory,* vol. 37, pp. 60-72, Jan 1991.
[85] J. Yu-Zhong, H. Xiu-lin, L. Wen-Lu, and Z. Shu-Xia, "Estimation of Two-dimensional Class A Noise Model Parameters By Markov Chain Monte Carlo," in *Computational Advances in Multi-Sensor Adaptive Processing, 2007. CAMPSAP 2007. 2nd IEEE International Workshop on*, 2007, pp. 249-252.
[86] Z. Shu-Xia and J. Yu-Zhong, "Identification of Class a Noise Parameters via Least Square Gradient Method," in *Image and Signal Processing, 2009. CISP '09. 2nd International Congress on*, 2009, pp. 1-3.
[87] E. F. Fama and R. Roll, "Parameter Estimates for Symmetric Stable Distributions," *Journal of the American Statistical Association,* vol. 66, pp. 331-338, 1971.
[88] J. H. McCulloch, "Simple consistent estimators of stable distribution parameters," *Communications in Statistics - Simulation and Computation,* vol. 15, pp. 1109-1136, 1986/01/01 1986.
[89] V. M. Zolotarev, "Mellin-Stieltjes Transforms in Probability Theory," *Theory of Probability & Its Applications,* vol. 2, pp. 433-460, 1957.
[90] M. Xinyu and C. L. Nikias, "Parameter estimation and blind channel identification in impulsive signal environments," *Ieee Transactions on Signal Processing,* vol. 43, pp. 2884-2897, 1995.
[91] M. Xinyu and C. L. Nikias, "On blind channel identification for impulsive signal environments," in *Acoustics, Speech, and Signal Processing, 1995. ICASSP-95., 1995 International Conference on*, 1995, pp. 1992-1995 vol.3.
[92] D. Silage, *Digital Communications Using MATLAB and Simulnk*: Bookstand Publishing, 2009.
[93] A. A. Giordano and A. H. Levesque, *Modeling of Digital Communication Systems Using SIMULINK*: Wiley-Blackwell, 2015.
[94] IEEE, "Standard for Information technology—Telecommunications and information exchange between systems— Local and metropolitan area

networks—Specific requirements: Wireless LAN Medium Access Control (MAC) and Physical Layer (PHY) specifications," ed: IEEE 802.11, 1997.
[95] H. T. William, P. T. Desmond, E. Z. Rodger, F. M. Nicholas, and W. M. Jon, "OSI Reference Model - The ISO Model of Architecture for Open Systems Interconnection," in *The Best of the Best:Fifty Years of Communications and Networking Research*, ed: Wiley-IEEE Press, 2007, pp. 599-606.
[96] IEEE, "Standard for Information technology—Telecommunications and information exchange between systems— Local and metropolitan area networks—Specific requirements— Part 11: Wireless LAN Medium Access Control (MAC) and Physical Layer (PHY) specifications," ed: IEEE 802.11-1999.
[97] H. Stern and S. Mahmoud, *Communication Systems Analysis and Design*: Prentice Hall, 2004.
[98] K. Ho Seop and L. Jong Kyu, "Optimal PN codes in a DS/SS wireless LAN system," in *Information Theory, 1994. Proceedings., 1994 IEEE International Symposium on*, 1994, p. 226.
[99] A. Yamakita, Y. Goto, and F. Maehara, "Simple series form formula of BER performance for DBPSK/OFDM signals in time selective nonlinear fading channels," in *Communications, Computers and Signal Processing, 2009. PacRim 2009. IEEE Pacific Rim Conference on*, 2009, pp. 205-210.
[100] J. G. Proakis, *Digital Communications*: McGraw-Hill, 2001.
[101] S. Haykin, *Communication Systems*, 4th ed.: John Wiley & Sons 2001
[102] B. Sklar, *Digital Communication: Fundamentals and Applications*, 2nd ed.: Prentice Hall, 2001.
[103] I. Jacobs, "Practical applications of coding," *Information Theory, IEEE Transactions on,* vol. 20, pp. 305-310, 1974.
[104] J. Heiskala and J. Terry, *OFDM Wireless LANs: A Theoretical and Practical Guide*, 1st ed.: Sams Publishing, 2001.
[105] M. K. Simon and M. S. Alouini, "A unified approach to the performance analysis of digital communication over generalized fading channels," *Proceedings of the IEEE,* vol. 86, pp. 1860-1877, 1998.
[106] C. Kyongkuk and Y. Dongweon, "On the general BER expression of one- and two-dimensional amplitude modulations," *Communications, IEEE Transactions on,* vol. 50, pp. 1074-1080, 2002.
[107] "ISO/IEC Standard for Information Technology - Telecommunications and Information Exchange Between Systems - Local and Metropolitan Area Networks - Specific Requirements Part 11: Wireless LAN Medium Access Control (MAC) and Physical Layer (PHY) Specifications (Includes IEEE Std 802.11, 1999 Edition; IEEE Std 802.11A.-1999; IEEE Std 802.11B.-1999; IEEE Std 802.11B.-1999/Cor 1-2001; and IEEE Std 802.11D.-2001)," *ISO/IEC 8802-11 IEEE Std 802.11 Second edition 2005-08-01 ISO/IEC 8802 11:2005(E) IEEE Std 802.11i-2003 Edition,* pp. 1-721, 2005.
[108] M. B. Pursley and T. C. Royster, "Properties and performance of the IEEE 802.11b complementary-code-key signal sets," *Communications, IEEE Transactions on,* vol. 57, pp. 440-449, 2009.
[109] IEEE, "IEEE 802.15.1 Standard for Information technology-Local and metropolitan area networks : Wireless Medium Access Control (MAC) and

Physical Layer (PHY) specifications for Wireless Personal Area Networks (WPAN)," ed: IEEE, 2005.
[110] S. Pasupathy, "Minimum shift keying: A spectrally efficient modulation," *Communications Magazine, IEEE,* vol. 17, pp. 14-22, 1979.
[111] L. Lampe, M. Jain, and R. Schober, "Improved decoding for Bluetooth systems," *IEEE Transactions on Communications,* vol. 53, pp. 1-4, 2005.
[112] J. R. Barry, E. A. Lee, and D. G. Messerschmitt, *Digital Communication*, 3rd ed., 2004.
[113] R. Adler, R. Feldman, and M. Taqqu, *A practical guide to heavy tails: statistical techniques and applications*: Birkhauser, 1998.
[114] IEC, "Communication Networks and Systems in Substations (Part 5: Communication Requirements for Functions and Device Models)," ed: IEC, 2003.